Tensile properties and fracture behaviour of Multipass Friction Stir Processed Al-7Si-0.3Mg cast alloy

by

Francis Abraham

A Thesis Submitted in Partial Fulfilment of the Degree of Master of Engineering

AUT
U N I V E R S I T Y
AUCKLAND, NEW ZEALAND

Auckland University of Technology
Auckland, New Zealand

July 2012

ACKNOWLEDGEMENT

ABSTRACT

Friction Stir Welding (FSW) is a solid state joining process using a rotating cylindrical shoulder and threaded pin which is plunged into the work piece to traverse along the join line. Friction Stir Processing (FSP) is a comparatively new process derived from FSW, which can be used to refine and modify as-cast microstructures for superior properties. In the last decade, several researchers have attempted to evaluate the microstructure and properties inside the stir zone. However, it is important to explain the features occurring outside the stir zone, in particular during multipass FSP (MP-FSP). The aim of this proposed research is to explain the MP-FSP process parameters and their relations to mechanical properties of the processed material, and hence to explain the fracture behaviour of the MP-FSPed material.

Experimentally, cast plates of A356 (Al-7Si- 0.3Mg) alloy were made. Initial set of experiments with a high tool rotation speed (ω rpm) was conducted to produce maximum stir zone area. However, on finding that this parameter was not suitable (as will be explained), lower ω range FSP experiments were conducted. First, single pass FSP experiments were carried out to understand the flow, particularly outside the stir zone followed by MP-FSP under varying process parameters. Tensile testing was conducted and factors/FS parameters relating to fracture strain, and thus the quality of MP-FSP stir zone were studied and fracture features were examined.

It was found that the use of high ω values resulted in the less deformed cast material wedging up into the stir zone of the previous pass. This wedging resulted in low tensile fracture strain. Explanation of Si particle alignment due to wedging and subsequently causing low fracture strain will be given. It will be shown that reducing ω reduces the degree of wedging, as the downward stir flow reduces. However, low ω values are shown to have a detrimental effect, incapable of completely disrupting / healing of tunnel wall oxide films, thus resulting in low fracture strain. It will be shown that with the current FS condition, ω=1000 rpm is the optimum value.

TABLE OF CONTENTS

LIST OF FIGURES

STATEMENT OF ORIGINALITY

I hereby declare that this submission is my own work and that, to the best of my knowledge and belief, it contains no material previously published or written by another person nor material which to a substantial extent has been accepted for the qualification of any other degree or diploma of a university or other institution of higher learning, except where due acknowledgement is made in the acknowledgements.

Signed:

Date: 17/11/2012

Chapter 1

INTRODUCTION

1.1 Cast light alloys

Weight reduction and fuel efficiency in automotive and aerospace industries have resulted in light (aluminium and magnesium) alloy castings increasingly being used. Aluminium alloy castings, particularly based on Al-7Si with Mg content ranged from 0.3 to 0.6%, (A356/A367) are widely and commonly used because it has good castability and can be strengthened by artificial aging. The other benefits include low specific gravity, excellent fluidity, high resistance to wear, reduced thermal expansion because of the presence of silicon, and adequate physical and mechanical properties at elevated temperatures.

It is well known that the structural defects (or concentration of defects) control the mechanical properties by giving rise to the largest stress concentration, i.e., the weakest link. In Al–Si alloy castings, tensile strength, elongation-to-fracture and fatigue life are properties related to fracture initiated at the weakest link. Therefore, the mechanical properties of cast Al–Si alloys are governed by the size distribution of defects, with the largest defects resulting in premature failure. The microstructure of A356 cast alloy is shown in Fig 1-1. A number of casting and solidification characteristics can usually result in unwanted microfeatures in castings. These include defects (shrinkage/hydrogen pores and oxide bifilms), formation/segregation/clustering of the brittle second phase particles to interdendritic regions and dendrites being coarse if the cooling rate during casting is low. Defects in various types and microstructures with brittle phases present in most as-cast forms reduce the fracture toughness significantly [1-5], resulting in difficulty of the castings to be used for automotive and particularly aerospace structures that are subject to critical loading.
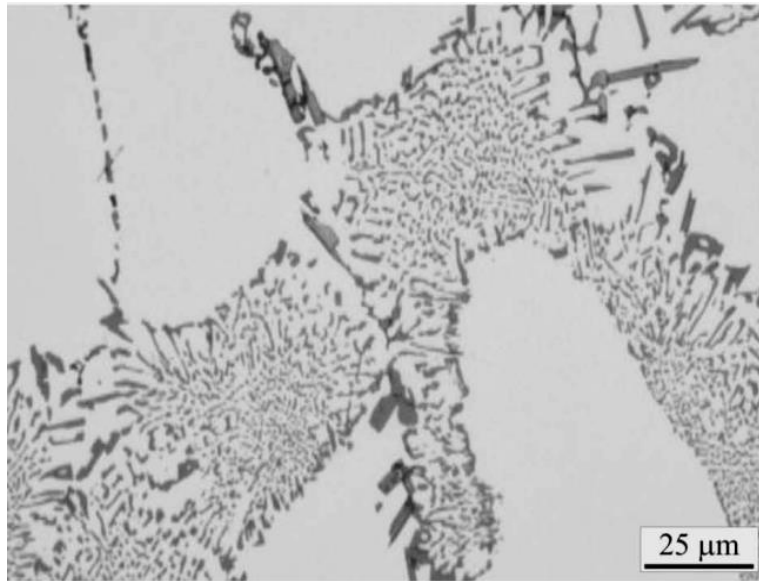
Figure 1-1   Microstruture of A356 showing the brittle needle like β phase particles and presence of porosities.

Eutectic modifiers and high temperature heat treatment are widely used to refine the Si particles in cast Al-7Si-0.3Mg alloy to enhance mechanical properties of the castings. In the past few years, various processing techniques such as thermomechanical treatment (TMT), equal channel angular pressing (ECAP), torsion under compression, multiaxial alternative forging (MAF), and accumulative roll bonding (ARB) have been used to produce the fine-grained materials for superplasticity [6]. They certainly can heal the casting porosity but cannot be used to heal porosity in parts/components.

1.2 Friction Stir Processing (FSP) and light alloys

Friction Stir Processing (FSP) is a comparatively new process derived from Friction Stir Welding (FSW), patent at The Welding Institute in 1991. FSW is considered to be the most significant development in metal joining in a decade and is a green technology. It is a solid state joining process that consists of a rotating cylindrical shoulder and threaded pin which is plunged into the work piece to traverse along the join line. The primary functions of tool are (a) heating of the work piece, and (b) flow of the material around the pin to produce joint. The frictional heat is generated, principally due to the high normal pressure and shearing action of the shoulder. FSW can be thought of as a process of constrained

extrusion under the action of the tool. The localized heating softens the material around the pin and combination of tool rotation and translation leads to the flow of material from the front of the pin to the back of the pin. The extruded material is deposited to form a solid phase joint behind the tool. Advancing side refers to the side where tool rotational motion and transverse motion are in same direction, where retreating side is defined as the side where these two motions have opposite directions (as shown in Fig 1-2).
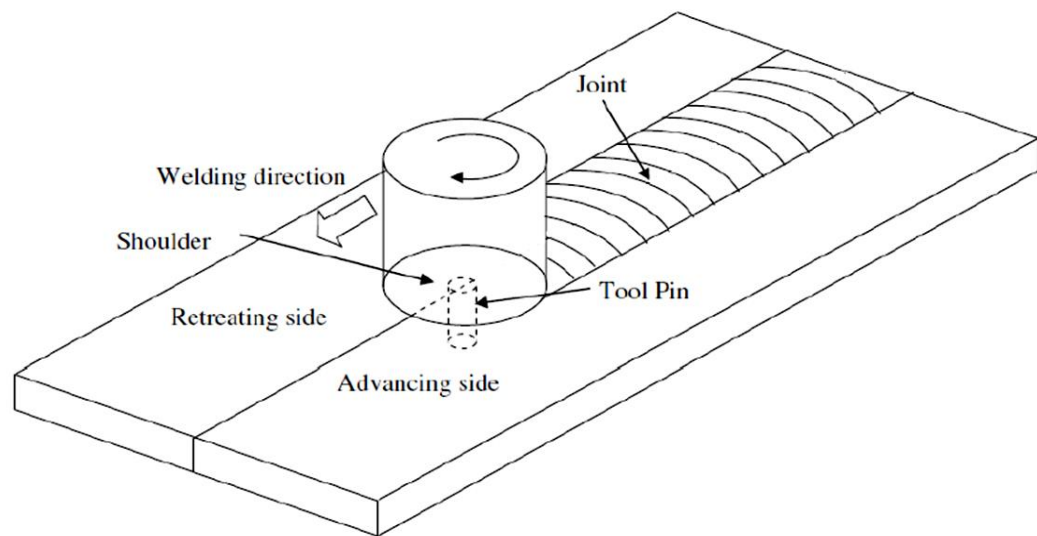
Figure 1-2   Schematic drawing of FSW

FSP, based on the same thermomechanical principle was developed by Mishra et al. [6] for localized microstructural modification and thus for enhancing desired material properties. The basic concept of FSP is as shown in Fig 1-3. A rotating tool with pin and shoulder is inserted in a single piece of material and traverse across the workpiece, resulting in significant microstructural changes in the processed zone due to intense plastic deformation, mixing, and thermal exposure of material. Many researchers have reported the formation of equiaxed recrystallized grains, where the grain size were approximately 10-100 times smaller than those in the original work piece material [7,8]. The fine-grained processed structure yields superior mechanical properties compared to that materials produced by traditional processes, such as higher UTS and creep resistance, and better corrosion resistance.
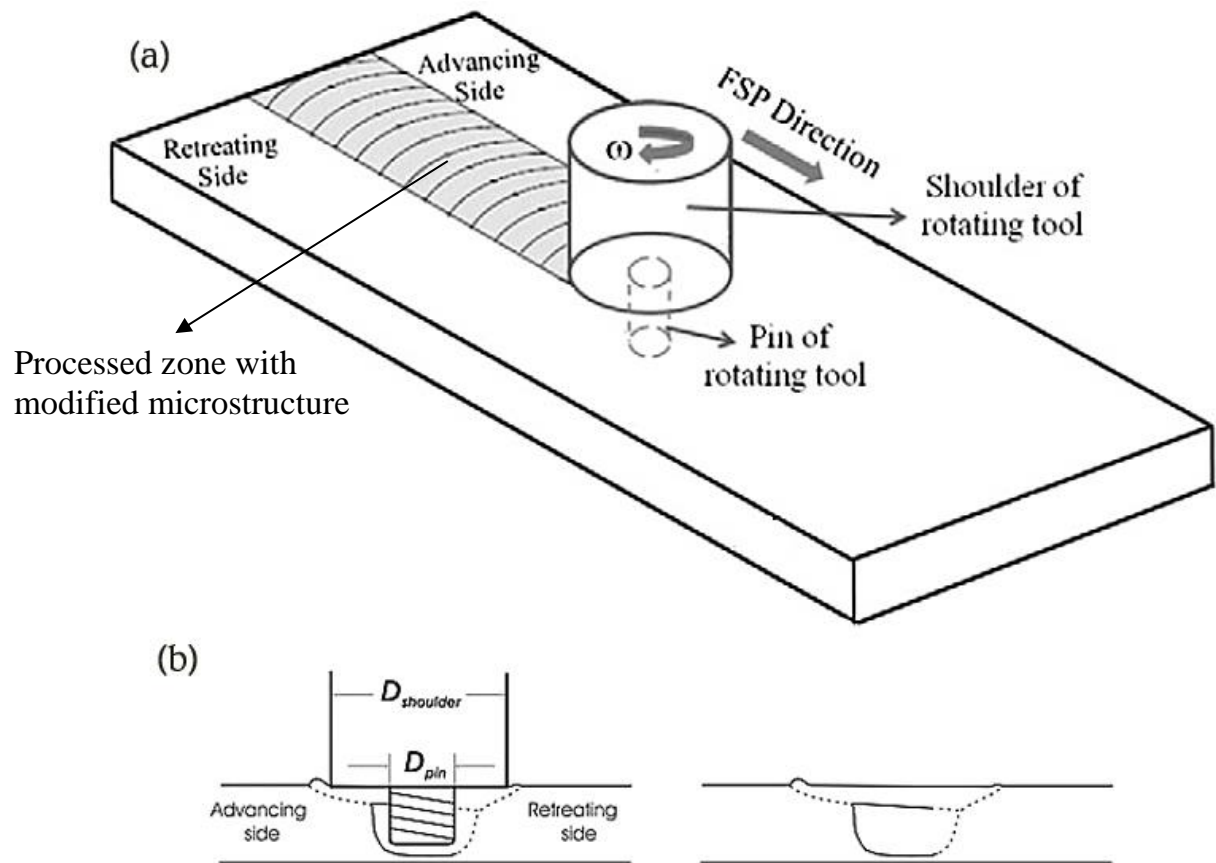
Figure 1-3   Schematic representation showing (a) the process of FSP, and (b)the crossection of a FSP plate and the shape of the FSPed zone.

The characteristics of FSP has led to several applications for microstructural modification in metallic materials, including superplasticity, surface composite homogenization of nanophase aluminium alloys and metal matrix composites, microstructural refinement of cast aluminium alloys [8]. An example of microstructure refinement can be seen in Fig 1-4, showing coarse α-Al dendrites and eutectic Al-Si in cast state and fine Si particles evenly distributed in α-Al matrix after FSP. However, the most important and potential application of FSP is in eliminating porosity, breaking up of oxide films and refinement of the microstructure of cast light alloys, such as Al, Mg, and Ti alloys, in order to improve the relatively poor as-cast mechanical properties.

| **Cast Microstructure** | **After FSP** |
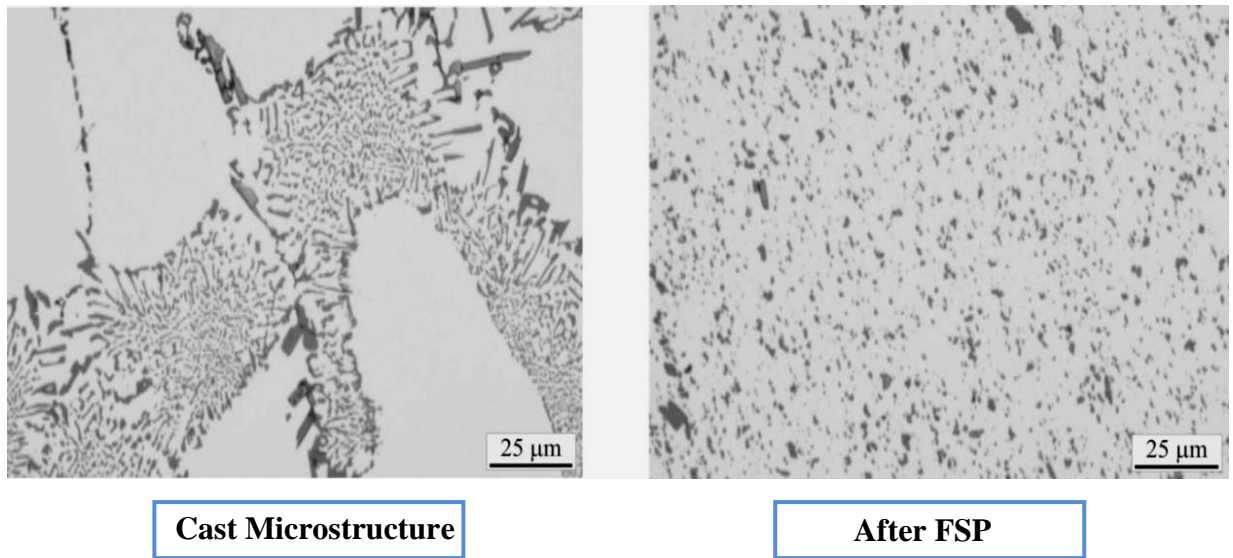
Figure 1-4   Micrograph (produced from FSP lab at AUT) showing the drastic improvement occurs before and after FSP

Mishra *et al* [6] has demonstrated FSP as tool for microstructural modification in metallic materials due to its distinct advantages.

1. FSP is a solid-state processing technique with one-step processing that achieves microstructural refinement, densification, and homogeneity.

2. The microstructure and mechanical properties of the processed zone can be accurately controlled by optimizing the tool design, FSP parameters, and active cooling/heating.

3. The depth of the processed zone can be optionally adjusted by changing the length of the tool pin, with the depth being between several hundred micrometers and tens of millimetres; it is difficult to achieve an optionally adjusted processed depth using other metalworking techniques.

4. FSP is a versatile technique with a comprehensive function for the fabrication, processing, and synthesis of materials.

5. The heat input during FSP comes from friction and plastic deformation, which means FSP is a green and energy-efficient technique without

deleterious gas, eradiation, and noise. Sixth, FSP does not change the shape and size of the processed components.

1.3 Process Parameters:

In this section, the major factors affecting FSW/FSP materials, such as tool geometry and process parameters are explained.

1. Tool Geometry

One of the most influential factors of FSP process is tool geometry. It has a major influence and plays a critical role in material flow and hence the macro and microstructure of the processed zones. A FSP tool consists of a shoulder and a pin as shown schematically in Fig. 1-5. As mentioned earlier, the tool has two primary functions:

(a) localized heating

(b) stirring the heated and plasticized material

In the initial stage of tool plunge, the heating results primarily from the friction between pin and workpiece. The tool is plunged till the shoulder touches the workpiece. The friction between the shoulder and workpiece results in the biggest component of heating. Considering heating, the relative size of pin and shoulder is important, and the other design features are not critical. The shoulder also provides confinement for the heated volume of material. The second function of the tool is to stir and move the material. The uniformity of microstructure and properties as well as process loads is governed by the tool design. Generally a concave shoulder and threaded cylindrical pins are used. With increasing experience and some improvement in understanding of material flow, the tool geometry has evolved significantly.

Featureless Shoulder   Scrolled Shoulder
(viewed from underneath)

Threaded Pin   Threaded Pin with Flutes

Shoulder
Pin
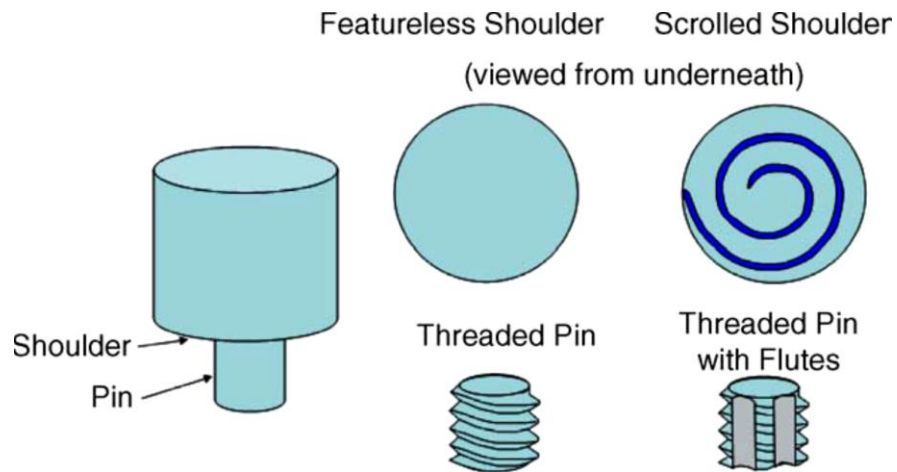
Figure 1-5   Drawing of the most commonly used FSP tool pin – cylindrical threaded pin

The other parameters, which contribute more towards the macro/micro features, are listed below and also illustrated in Fig 1-6.

2. Tool rotation speedj ω (rpm)
3. Tool traverse speed v (mm/min)
4. Tilt angle θ º
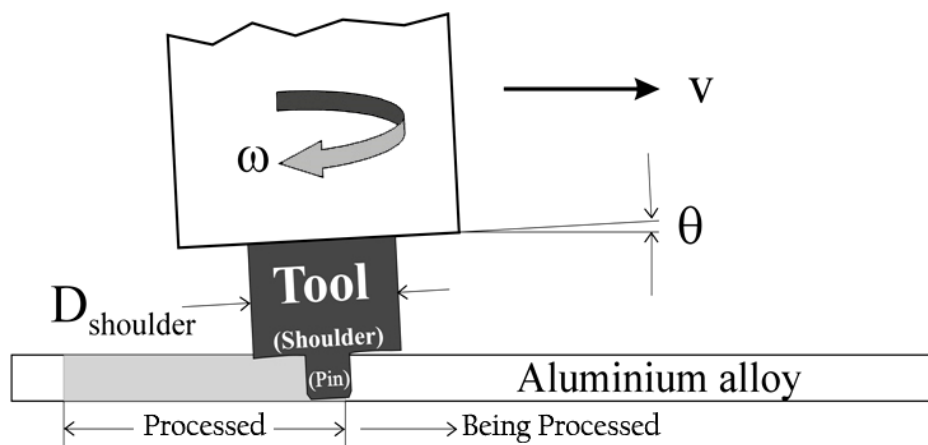
Figure 1-6   Tool position and process parameters as the tool traverses along the   work piece

Changes in any of these parameters will result in different mechanical and metallurgical properties of the processed material. Hence these parameters must be taken in careful consideration while running FSP, in particular multipass conditions.

1.4   Single pass FSP to Multipass FSP

Multipass FSP (MP-FSP) is demonstrated as a prime tool in processing large areas composed by several overlapped passes as illustrated in Fig 1-7. Here, the FSPed region is been overlapped by subsequent FSP passes. Since the depth of processing can be controlled by the length of the tool pin, FS can be called as a processing technique to process almost the entire thickness. And overlapping of each FSP passes makes it able to process the entire workpiece, both in longitude and transverse directions. From an engineering point of view, the properties along the entire MP-FSPed workpiece vary with macro and micro features. On a metallurgical aspect; shape, size, orientation and aspect ratio of the Si particles within the A356 samples varies across the sample. In between the subsequent passes, a region of partially deformed material remains. The size of this area depends on the level of overlap of FSP passes. As will be detailed in literature review, there have been a number of reports on MP-FSP conditions, the formation of wedged upflow, its adverse mechanical effects and its relations with process parameters are unknown.
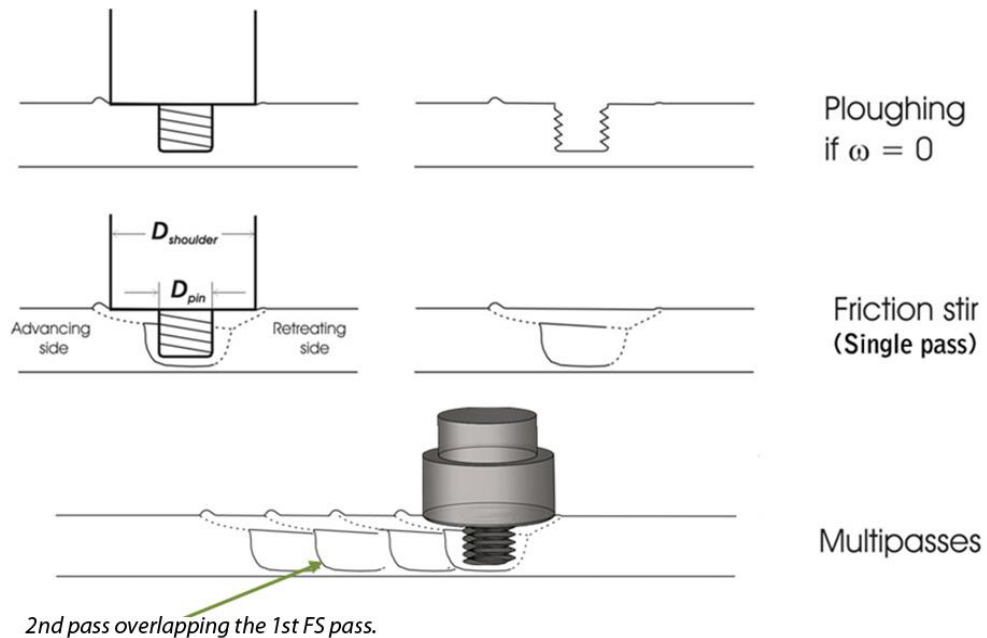
Figure 1-7   Illustration of the single and MP-FSP

Though the process and tool parameters for MP-FSP is same as of single pass FSP, two additional process parameters should explained as below.

1. Overlap distance:

The overlap distance plays a vital role in defining the microstructure and hence the mechanical properties in a wider scale. It defines how much the subsequent pass overlaps the previous pass. In Fig 1-8, the tool positions and the resultant SZ is been schematically shown, where the tool pin for the second pass has overlapped, say 1mm over the position of first pass. The basic idea is to create well overlap of the passes, so that all as-cast microstructural features can be completely modified and refined.
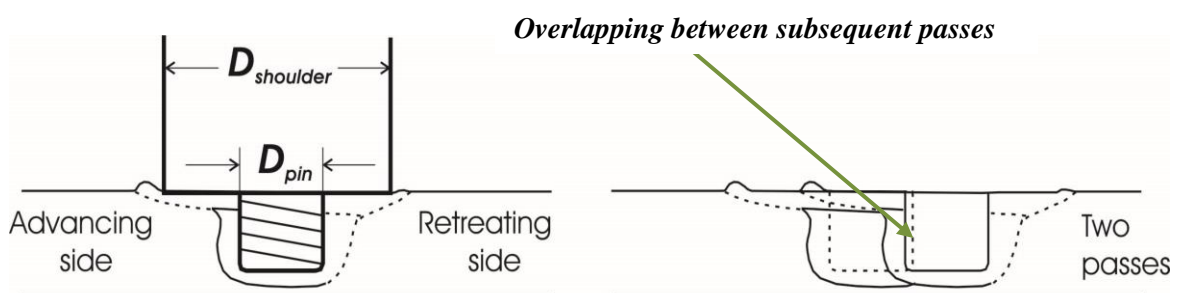
Figure 1-8   Illustrates two subsequent passes and how it's done

2. Multipass direction (Overlap direction)

As stated previously, the macro/micro features varies along the entire FSP zone. The advancing and retreating side of the SZ are experiencing different material deformation. Thus the flow path of material arriving and depositing in each region is likely to be different from one to the other. On this context, considering the overlap direction is so crucial. One such practice is overlapping advancing side of the next pass with the retreating side of the previous pass (as shown in Fig 1-9a). Other technique involves overlapping the retreating side of the pass with the advancing side of the previous pass. (Fig 1-9b)
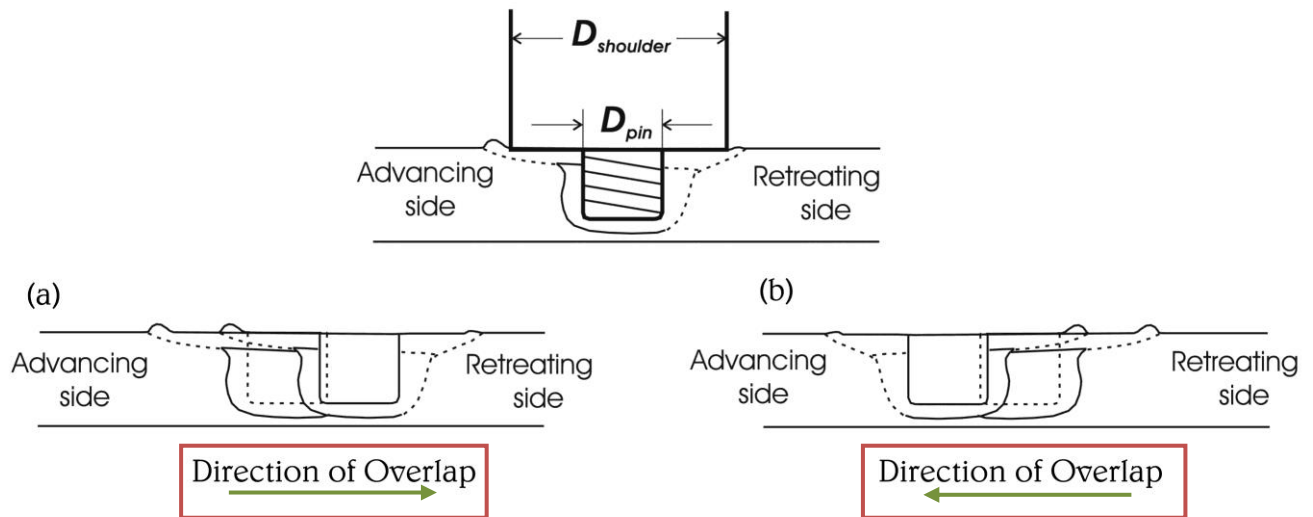
Figure 1-9   MP-FSP with; (a) overlapping advancing side of the next pass with the retreating side of the previous pass, (b) overlapping the retreating side of the pass with the advancing side of the previous pass.

1.5 Current understanding: *an overview*

The researches associated with FSW have paved way for FSP, developed by Mishra et.al [6]. Since the review work done by Ma et.al [8] in 2008, various efforts has been carried out in the research field to develop FSP as an attempt to solve many of the metallurgical problems. The aforementioned disadvantages reduce the potentials of the cast alloys being used more extensively as structural components which are subject to critical loadings (both static and cyclic). The use of FSP to achieve local/global refinement of the intrinsic coarse microstructures of cast alloys has been proven to be effective. This has paved way for FSP, which is effective and economical. In general, the current understanding on FSP as a processing technique to modify and refine Al-Si cast structure is mainly focussed on the following metallographic features.

1. to break-up the coarse Si particles, and re-distribute them evenly within the matrix of Al alloys

2. to refine the coarse aluminium dendrites and resulting in recrystallized (equiaxed) grains.

3. to break-up the coarse precipitates and dissolve part or most of them into the matrix;

4. to eliminate the casting porosity.

In order to achieve the above mentioned properties, a systematic approach towards reporting the process parameters is vital. Efforts are carried out towards the investigation of mechanical properties of single pass FSP and MP-FSP and its relation to the process parameters such as:

- Tool rotation speed ω (rpm)
- Tool traverse speed v (mm/min)
- Tilt angle θ ^{o}
- Overlap distance (mm)
- Overlap direction

Despite of all these attempts, since it has been a new technology, a complete scientific understanding of FSP has a long way to reach. No attempts are taken to study the behaviour of processed zone, as a function of process parameters and its adverse effects, in particular, at the interpass locations of MP-FSP. The, lack of clarity is visible in the approach towards fracture mechanism, and other features which catalyst the cracking mechanism. Hence, the process parameters will be carefully reviewed in the next chapter. In this proposed study, the various tool rotation speed will be analysed on the basis of how it affects the flow features.

Chapter 2

LITERATURE REVIEW AND RESEARCH OBJECTIVE

This chapter reviews the literature on FSP in the aspect of material flow patterns, relationship between process parameters and mechanical properties, current experiment and analysis techniques. The review also served to identify the knowledge gap that has been incorporated into the research objectives.

2.1 As-cast and FS processed Al-Si alloy

2.1.1 Porosity

Over the last decade, a number of studies were carried out to describe FSP as means to eliminate casting porosities. Porosity in the cast is the prime point of crack initiation and also paves way for crack propagation, leading to poor mechanical properties in particular tensile and fatigue properties. Sharma *et al.* [9] found that modifying Al castings with FSP leads to the elimination of porosity. A study on the relationship between porosity and fatigue strength on aluminium alloys has reported by Dabayeh *et al.* [10] shows that fatigue cracks initiated and propagated from casting pores. Since Mishra *et al.* [6] has reported FSP as a prime machining tool for many mechanical and metallurgical problems, the major point of interest has reported more on the refinement and elimination of porosity. The review work done by Ma *et al.* [8] has aimed at reporting the elimination of casting porosity by increasing tool rotation speeds. Fig 2-1 displays the micro porosities within the cast A356.
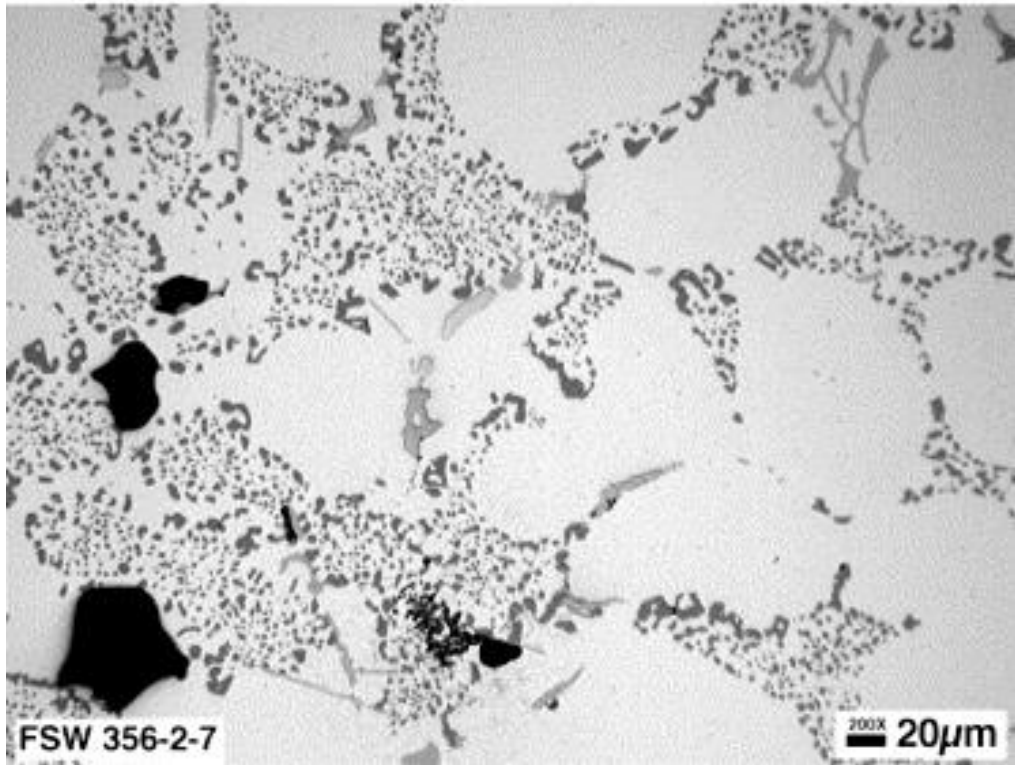
Figure 2-1   Optical micrographs showing as-cast microstructures of A356 sand castings.

Paris equation leads to better illustration of how the presence of defect in the cast results in poor fatigue properties.

$$\frac{da}{dN} = A(Y\,\Delta\sigma\sqrt{\pi a})^m \qquad\qquad\qquad \textit{Equation 2-1}$$

Where a is the crack length, N is the number or cycles, K the range of stress intensity factor, σ the range of stress applied, Y the geometrical constant and A and m material constants. Thus the following is found.

$$N_f = \int_{a_o}^{a_c} \frac{da}{\text{A}(Y\Delta\sigma\sqrt{\pi a})^m} = \frac{2}{(m-2)AY^m\Delta\sigma^m\pi^{m/2}}\left(\frac{1}{a_0^{m-2/2}} - \frac{1}{a_c^{m-2/2}}\right) \;\textit{Equation 2-2}$$

Here, N_f is the total number of cycles and a_c and a_o are the critical and initial crack lengths respectively. It shows that the larger the defect size the less the number of fatigue cycles possible before failure, lowering fatigue resistance. There have been

13

a large number of studies, investigating the effect on the mechanical properties of A356 castings. For example, Sabau *et al* [11] has investigated on the substantial reduction in ductility as a result of porosity. Overall, it can be concluded porosity aids crack nucleation, and propagation, thereby weakening the microstructure of cast A356.

2.1.2 Coarse Acicular Si particles

From a metallurgical point of view, it is important to explain the size, shape, orientation and distribution of Si particles along the primary α-Al matrix. The size is so important that the large elongated Si particles will break early during tensile deformation, which is a clear indication of poor fracture toughness. It reveals the brittle character of silicon particles in comparison with the surrounding aluminium matrix. Chances for crack initiation/ propagation are very low, when uniformly distributed fine Si particles with improved Aspect ratio are present within the Al matrix. However, since eutectic Si particles present in the A356 alloys deteriorate strength, and fracture toughness, it is important to break up the eutectic particles and evenly distributed in the Al matrix. Apart from the size of the eutectic particles, distribution within the Al matrix also plays a major role in defining fracture toughness. Refined microstructure with reduced spacing between eutectic Si particles has been reported with low fracture toughness by Lee, K *et al* [15].

Attempts from Ma *et al* (2006) showed that the homogeneous distribution of Si particles through FSP provides improvement to strength and ductility. Other researchers [17] have correlated these improvements in mechanical properties to an increase in the pathway for crack propagation when silicon particles are broken up and uniformly distributed. Overall these studies have outlined improvements in ductility, fracture toughness and fatigue resistance as a result of FSP and breaking up and uniformly distributing Si particles. Fig 2-2 shows how drastically FSP can improve the metallographic features of the cast Al alloy.

(a)   (b)
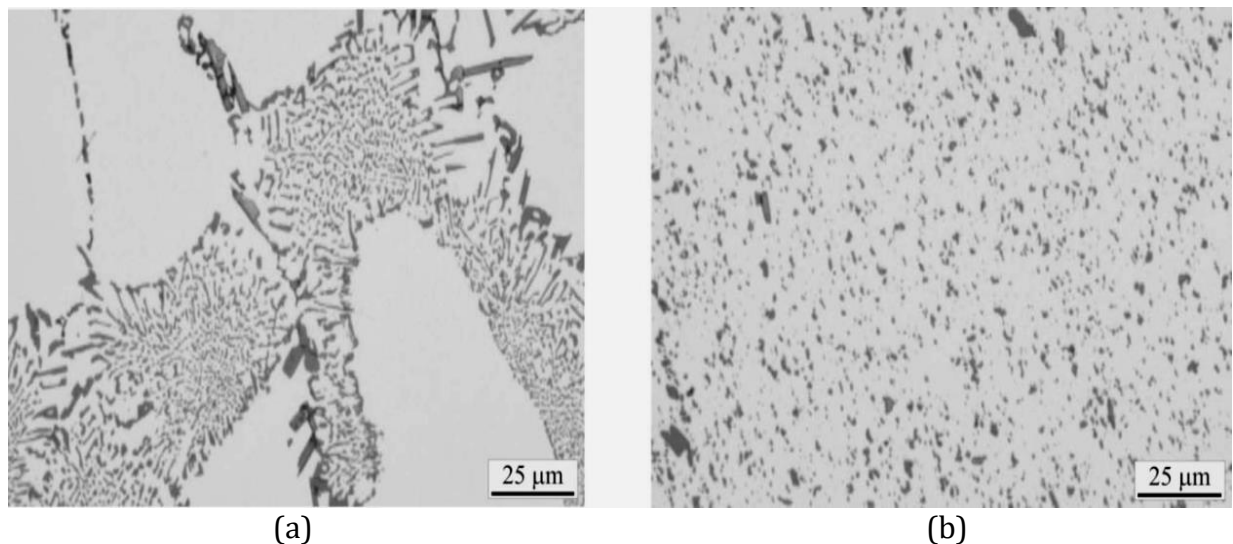
Figure 2-2   Micrograpgh showing: (a) As-cast A356 - Black and white areas the Al(α)-Si eutectic and surrounding area primary aluminium dendrites (b) FSPed A356 - Black areas are the silicon particles and white areas the aluminium matrix. [12]

Most common applications of FSP for in-volume processing are localized modification and microstructure control in thin surface layers of processed metallic components for specific property enhancement. It has been proven to be an effective treatment to achieve major microstructural refinement [16], densification and homogeneity of the processed zone, as well as, elimination of defects from manufacturing processes. Processed surface regions have shown an improvement of mechanical properties, such as hardness, tensile strength, fatigue, corrosion and wear resistance [17&18]. Significant improvement in mechanical properties of aluminium and magnesium cast alloys after single pass FSP has further reported [14, 18-19].

In short, hot deformation and dynamic recrystallization during FSP refine the matrix grains. Studies of FSP Al-Si cast alloys by Cui [24] at AUT, has reported dynamic recrystallisation during FS, resulting in the final grain sizes of 2-4 μm. The intense plastic strain during FS, through transferring large stresses from the deforming matrix to and thus fracturing the undissolving and nondeforming particles, causes a considerable reduction in sizes of the particles. The example shown in Fig. 2-2 shows that the deforming dendrites and eutectic can merge

15

together resulting in the refined   (2-3 μm in sizes) Si particles considerably more evenly distributed in the recrystallized α(Al) matrix in certain locations for single pass. The refinement of Si particles and an even distribution of the particles can be achieved in the whole nugget of a single pass using high tool rotation speed (rpm) and low travel speed v (mm/min). Hence it is so important to understand the phenomenon of material flow and how it is connected to process and tool parameters.

2.2 Material flow and Process Parameters

Material flow around the tool pin during FSP is considered as material being forced and displaced from the leading side of the pin to the trailing side of the pin under the rotational and translational action of the tool. This results in a non-symmetrical flow field where three flow regions have been found. Thus, explaining the macro/microstructure distributed in the SZ is highly relevant.

2.2.1 Characterization of SZ

Intense plastic deformation and frictional heating during FSW/FSP result in generation of a recrystallized fine-grained microstructure within stirred zone. As will be explained the forging action of the tool shoulder is the main reason for the material flow at the top of the work piece, leaving a shear layer between the tool shoulder and the top surface of the work piece. While on the mid region, the deformation zone consists of rotational and transitional zone as shown in Fig 2-3. And due to the interaction between the bottom of the tool pin and the backing plate, a swirl zone is formed at the bottom of the SZ. A typical cross section of a FSP-A356 sample produced using a cylindrical threaded tool is shown in Fig 2-3.
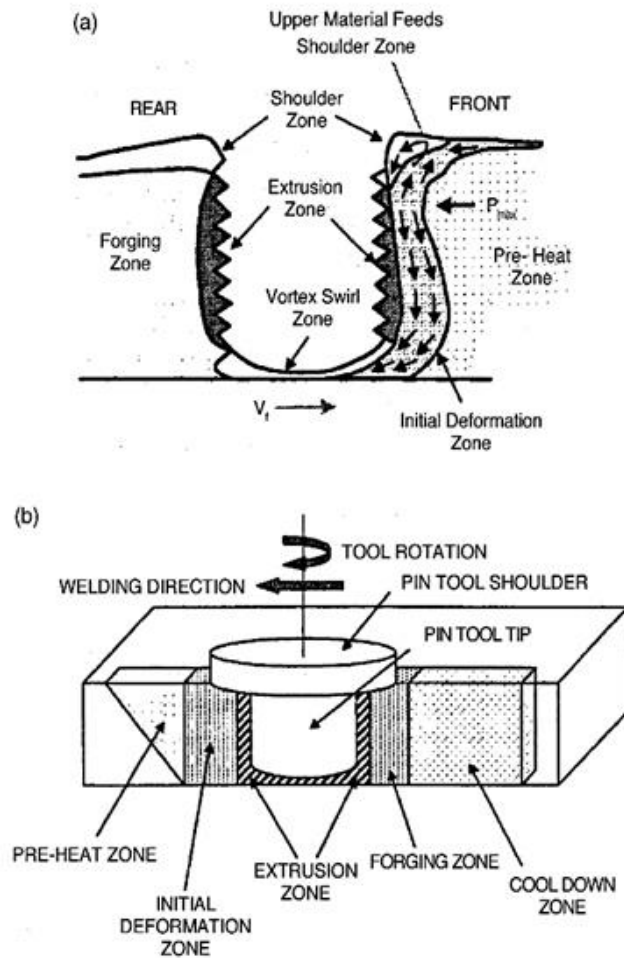
Figure 2-3   Schematical illustration: (a) Showing how the material flows around the tool pin from front to rear during FSP. (b) The development of FSP processing zones around the tool. [6]

Based on microstructural characterization of grains and precipitates, three distinct zones: total SZ (SZ), thermo-mechanically affected zone (TMAZ), and heat affected zone (HAZ) can be identified. This is better illustrated in Figure 2-4. The total SZ contains shoulder flow zone and nugget flow zone which are induced by the shoulder and pin respectively. Intensive high temperature deformation results in recrystallized fine-grained microstructure within the SZ. Unique to the FS process is the formation of a transition zone – TMAZ between HAZ and SZ. The TMAZ also experiences high temperature deformation, however not as intensive as in the SZ so that generally no recrystallization occurs. On the other hand, dissolution of some precipitates can occur, and grains in TMAZ usually contain a high density of

sub-boundaries. Beyond the TMAZ there is a HAZ, which experiences a thermal cycle but does not undergo any plastic deformation. The HAZ retains the same grain structure as the parent material. However, coarsening of precipitates and the widening of precipitate free zone (PFZ) can occur.
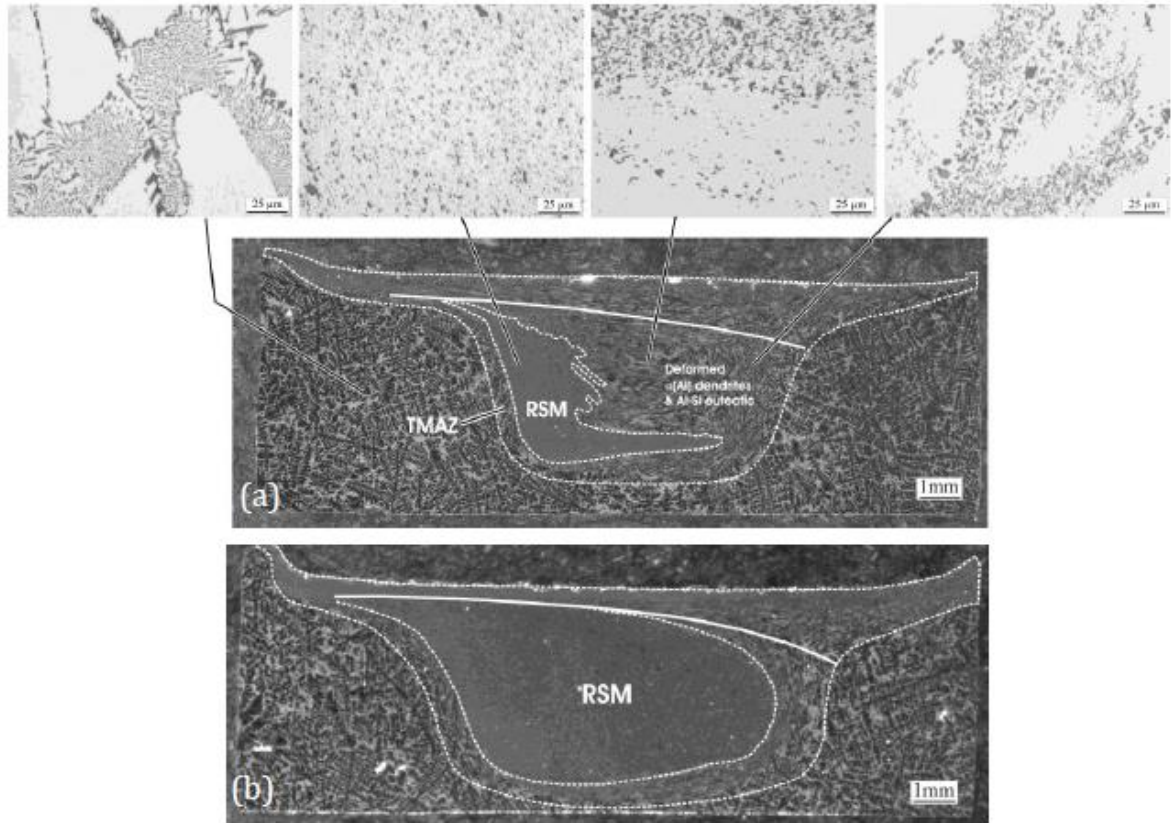
Figure 2-4   Macro/Micrographs showing: (a) Cross sections (advancing side on the left) of a single pass FSP samples made using θ = 2.5°, ω = 710 rpm and v = 224 mm/s. The total SZ has been outlined. The solid line marks the division of shoulder induced (above) zone and pin induced (below) flow zone. RSM denotes rotational shear material in the nugget. (b) Improved RSM area in the nugget obtained with ω = 710 rpm and low travel speed v=28mm/min. [AUT FSP labs]

Under normal FS conditions, the nugget zone usually occupies a very large portion of the SZ. In Figure 2-4a, the micro/macro distribution and formation of α-Al dendrites and Al-Si eutectic at higher tool traverse speed (v mm/min) is shown. The as-cast region, outside the SZ has a coarse microstructure, whereas the SZ (SZ) has several regions according to the deformation and distribution. A rotation shear

material (RSM), comprising of refined eutectic Si particles within the Al matrix with homogeneous distribution along the matrix is visible on the advancing side (left) of the nugget and this RSM region extends but tails off toward the retreating side (right) in the mid-to-lower region (but not the bottom) of the nugget zone. And a less extensive deformed region, which resembles to the normal as-cast microstructure, is visible along the rest of the nugget (towards the retreating side). These 2 regions are differentiated in Figure 2-4a with the dotted curve. However, reducing v from 224 to 28 mm/min has produced an increase in the portion of RSM region in the nugget (Figure 2-4b). RSM extends to the retreating side, occupying almost fully the nugget. Hence, it is clear how the area of RSM region changes with changing tool traverse speed.

2.2.2 Effect of Process Parameters on Material flow

A large number of researches have focussed on the formation of onion ring structure (figure 2-5) [20-23]. The material flow during FSP is quite complex and varies depending on the material to be processed. It is of practical importance to understand the material flow characteristics for optimal tool design and obtain high structural efficient processed zone. This has led to numerous investigations on material flow behavior during FSP. It is important to point out that there are many factors that can influence the material flow during FSP. These factors include tool geometry (pin and shoulder design, relative dimensions of pin and shoulder), processing parameters (tool rotation rate and direction, i.e., clockwise or counterclockwise, traverse speed, plunge depth, tool tilt angle), material types, workpiece temperature, etc. It is very likely that the material flow within the nugget during FSP consists of several independent deformation processes.

Various shapes of nugget zone have been observed depending on processing parameter, tool geometry, temperature of workpiece, and thermal conductivity of the material. Basically, nugget zone can be classified into two types, basin-shaped nugget that widens near the upper surface and elliptical nugget as shown in Fig 2-5 [6]. The formation of basin-shaped nugget on FSW of 6063Al-T5 plate was reported by Sato *et al.* [20]. They suggested that the extreme deformation and

frictional heating experiencing at the upper surface, by contact with a cylindrical-tool shoulder is the major reason in generation of basin-shaped nugget zone. On the other hand, *Mahoney et al.* [21] reported elliptical nugget zone in the weld of 7075Al-T651.
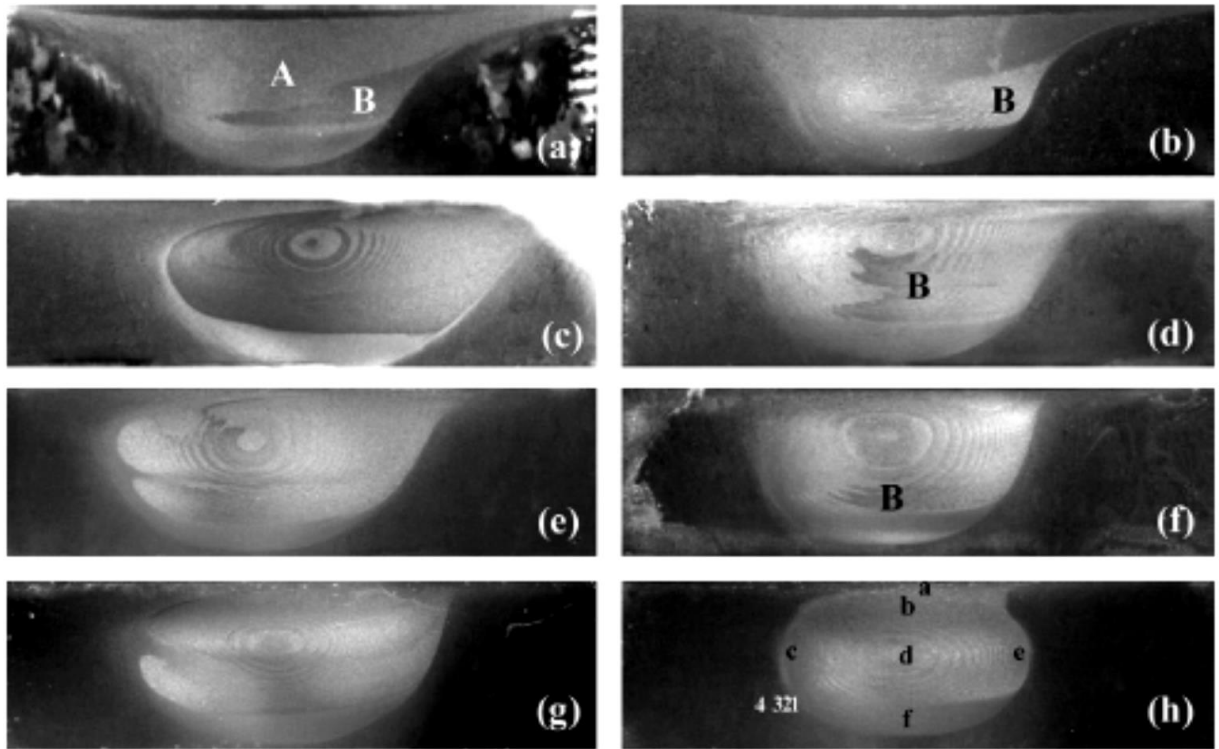
Figure 2-5   Macrographs showing variation in the processed zone in FSP A356 samples with processing parameter combinations of (a) 300 rpm, 51 mm/min; (b) 300 rpm, 102 mm/min; (c) 500 rpm, 51 mm/min; (d) 500 rpm, 102 mm/min; (e) 700 rpm, 102 mm/min; (f) 700 rpm, 203 mm/min; (g) 900 rpm, 102 mm/min; (h) 900 rpm, 203 mm/min. The advancing side of the nugget is on the right in all macrographs. [6]

Recently, an investigation was conducted on the effect of FSP parameter on the microstructure and properties of cast A356 [22]. The results indicated that lower tool rotation rate of 300–500 rpm resulted in generation of basin-shaped nugget zone, whereas elliptical nugget zone was observed by FSP at higher tool rotation of >700 rpm (Fig. 2-6). This indicates that with same tool geometry, different nugget shapes can be produced by changing processing parameters. Reynolds [23] investigated the relationship between nugget size and pin size. It was reported that

the nugget zone was slightly larger than the pin diameter, except at the bottom of the weld where the pin tapered to a hemispherical termination. Further, it was revealed that as the pin diameter increases, the nugget acquired a more rounded shape with a maximum diameter in the middle of the SZ.

Apart from the size and shape of nugget, on referring back to Fig 2-4, the various regions within the SZ can be seen changing as the tool rotation speed (rpm) changes. Fig 2-4a reveals regions of high eutectic refinement (RSM) and less extensive deformation within the SZ. However, the SZ is totally dominated by RSM, on higher tool rotation speed. This change in flow regions, and distribution of highly refined matrix was investigated by Cui [24]. Thus on a constant traverse speed (*V mm/*min) and tilt angle, a highly refined microstructure was produced by increasing tool rotation speed.

2.3 Multipass-FSP

Although the factors governing the mechanical properties of multipass FSP (MP-FSP) is much similar to those of single pass FSP, there are a number of additional features relating to the effects of overlap distance and its direction. The microsctructural evolution at the overlapping region plays a vital role in demonstrating the different mechanical properties. Full or partial nugget interpenetration and similar technological conditions for each track are crucial to assure property homogenization and uniform thickness layers. To produce fine grained microstructures at full thickness along the cast plates, Sun *et al.* [25] concluded that it was possible to process any desired size in thin sheets by running multiple overlapping passes to a uniform ultrafine grained microstructure, as grain size was found to be similar for various regions. Johannes *et al.* [26] investigated the influence of overlap in the FSP using a 42% overlapping between consecutive passes. These authors concluded that hardness and grain size remained approximately constant without variation between passes. However, multipass surfaces often presented a slightly lower ductility than single pass samples. Fig 2-6 illustrates the MP-FSP.
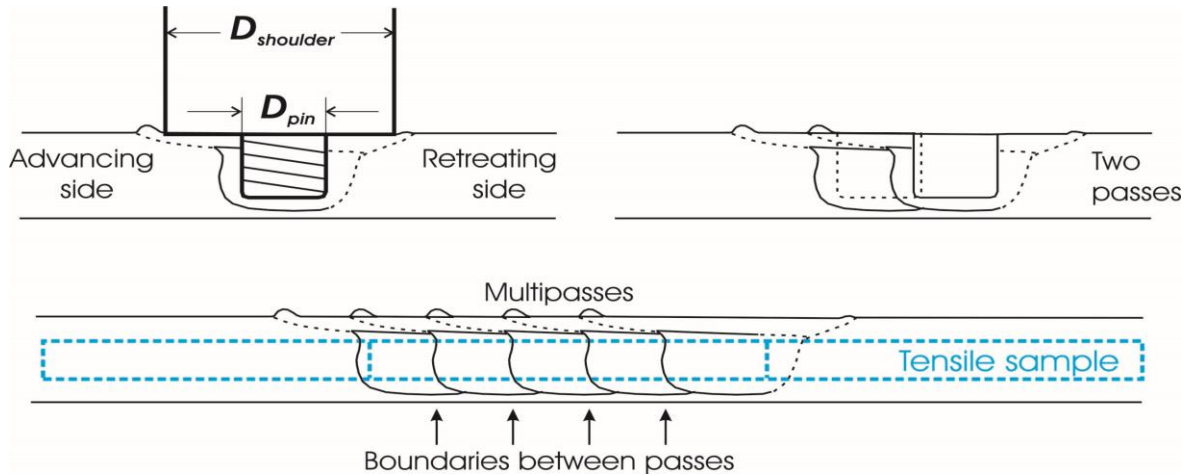
Figure 2-6   Illustration of the MP-FSP showing plunging, overlapping and how tensile sampling has done.

As will be shown later, the sufficient overlapping between the subsequent passes, an appearance of insufficient overlap is visible in the microstructures, which results in crack nucleation and its propagation. This is observed as a region of nugget, composed of coarse and less deformed particiles. This insufficient overlap is visible in all the above mentioned literatures and no reasonable study has done so far to reveal the uncertainity of those features. In a MP-FSP study done at AUT, we have observed that the tensile crack initiates and propagates on aid of these features at the locations of overlapping between subsequent passes. From a scientific point of view, these various local and global thermomechanical and metallurgical phenomena during MP-FSP and a quantitative micro-analysis of the common aluminium cast alloys need to be revealed and well understood.

From an engineering point of view, the properties along the entire multipass sample should be analysed and reported, owing to its importance. The major aim so far, attempts to demonstrate the mechanical behaviour of the MP-FSP samples, using mini-tensile sampling, where the samples were chosen from locations A-I in Fig 2-7a [27]. This attempt does not report the tensile behaviour of entire MP-FSP zone. This approach is not a good practice, while considering MP-FSP as a machining/modifying process for large surface areas.

We now briefly examine the overlap locations from the literatures which results in various macro/microstructural deformations. Between the subsequent passes, a region of coarse particles which is the extruded original dendritic cast material from the bottom of the pin at the advancing side of the next pass. Fig 2-7c highlights the bottom of the nugget (processed by overlapping the advancing side with the retreating side), demonstrating how the initial coarse microfeatures are extruded along the TMAZ of the Nth pass, thereby eliminating the advancing side micro/macro features of the $(N-1)^{th}$ pass. Along these locations, the Si particle distribution could be highly non-uniform with very small density of Si particles along the primary Al matrix.. Nascimento *et al.* [32] has formulated an equation to characterize the overlapping between passes. This was denominated overlap ratio (OR) and is defined in Eq. (2-3).

$$OR = 1 - \frac{l}{D\text{pin}} \hspace{4cm} \textit{Equation 2-3}$$

Where l is the distance between centres of each pass and Dpin is the maximum diameter of the pin. From this equation it is defined that fully overlapped passes have an OR= 1 and that the OR will decrease when increasing the distance between passes. (When OR< 0 no overlap of the nuggets exists)

Only a few has analysed the properties along the entire MP regions. Efforts from very few researchers like Nakata *et al* [30] (*Fig 2-7b*) and Santella *et al.* [31] aimed at the overall tensile property of MP-FSP sample and has briefly reported the improvement in the properties. Nakata *et al.* [30], has analysed the mechanical properties of the entire MP-FSP zone (Fig 2.7b). However, the rest of the MP-FSP researches were focussed on highlighting the local tensile properties, using mini tensile samples from particular locations. Here again, the aforementioned feature at the bottom of inerpass locations are visible, which the researchers have failed to report and analyse. Very recently, in 2011, Gandra *et al.* [33] has reported the changes in surface characteristics by changing overlapping directions (Fig 2-7c).
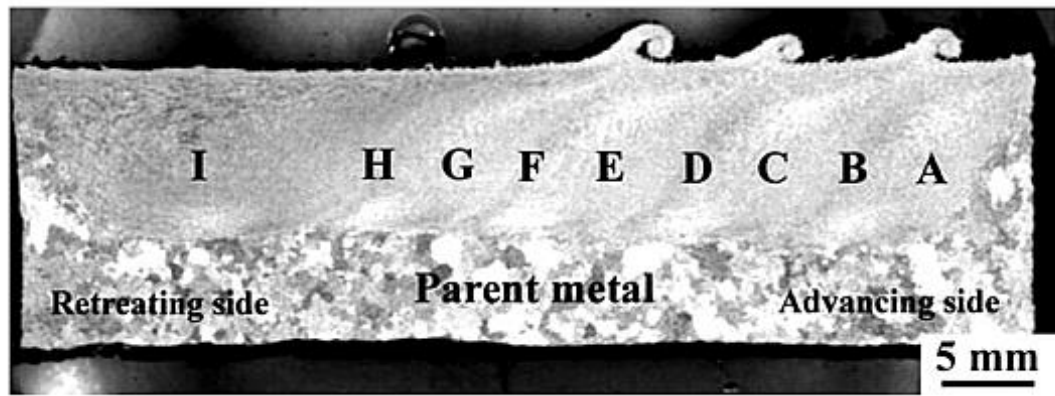
(a)
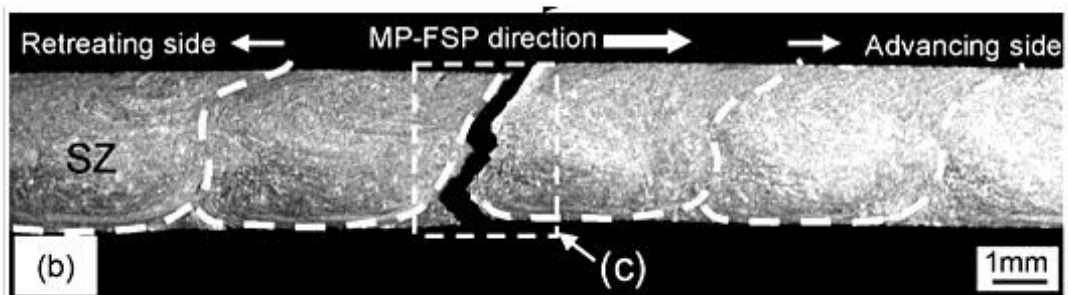
(b)
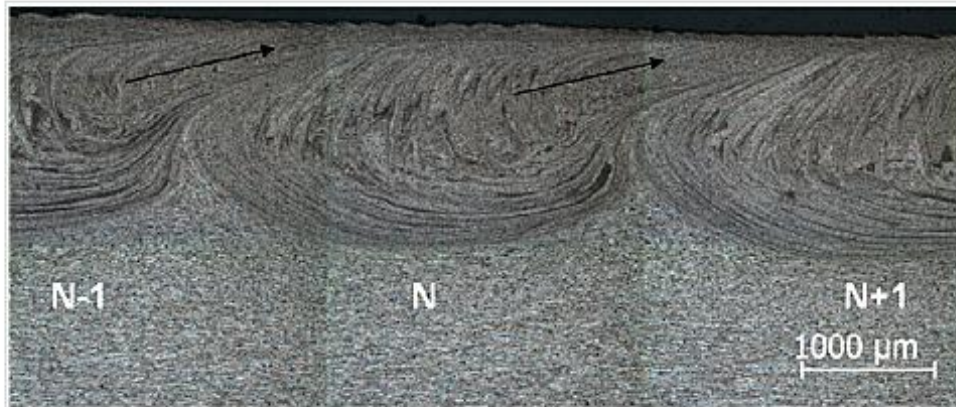
(c)

Figure 2-7   From the literatures: (a) Macrographs showing nugget and transitional
zones of 5-pass FSP on A356 and locations of mini tensile using ω=700
rpm (b) Tensile specimen view of a MP-FSP sample using ω=1250 rpm,
demonstrated by Nakata [30] *(c) Nugget interfaces with sufficient*
overlapping between subsequent passes, using ω=1000 rpm, reported by
Gandra [33].

Since the focus of these researches was to define and mechanical properties along the MP-FSP, none of these studies has reported the scientific and physical reason for the formation along the FSP passes and interpass regions. In Fig 2-7a, a sample processed under low tool rpm of 700 rpm is shown. And, a region of overlap is visible in Fig 2-7b, which was processed using high tool rpm (1250 rpm). These two studies have investigated on the mulitpass features using advancing side overlap technique. On a closer look, it can be observed that, the entire MP-FSP zone has varying macro features, especially at the interpass locations. However, the locations of overlap highlighted in Fig 2-7c are produced by overlapping by retreating side (reversed overlap direction). Again, a region of insufficient overlap is formed (despite of the 50% pin overlap provided) between the FSP passes.

In short, although these literatures have reported MP-FSP samples with sufficient overlap, the presence of appearance of insufficient overlap features are still evident and no systematic clarification is provided on any of these works. Studies by Cui [24], has focussed on the flow characteristics around the tool pin under single pass FSP conditions. However in this proposed study, more focus will be given to the bottom of the pin, and flow characteristics which leads to the formation of these regions and its effects on MP-FSP crossection as a function of FSP process parameters.

2.4 Objective of the proposed study

So far, the correlation between MP-FSP process parameters, which causes the microstructural distribution of fragmented Si particles in the α-Al matrix, and the tensile properties is unknown, particularly on overlap locations. Very few studies have attempted to improve the mechanical properties of MP-FSP through varying the process parameters, especially the overlap distance. And no validation is been done on how the various rotation speeds will respond to the wedging and macro/micro features, which results in poor mechanical behaviour. Hence, a systematic approach is required as illustrated in Fig 2-8. The following are the objectives designed for this proposed research.
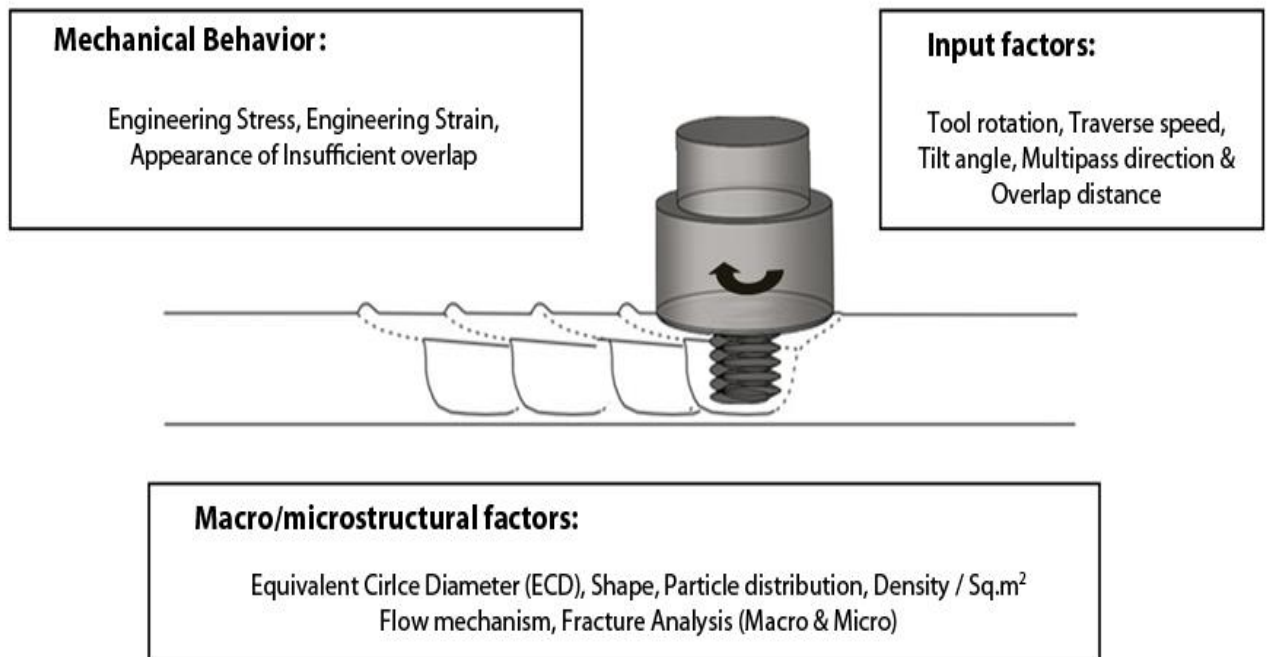
Figure 2-8   Schematic representation of a MP-FSP. The physical quantities
addressed in this proposed project are illustrated in 3 major factors.

1. *MP-FSP process parameters*
   – MP-FSP under various tool rotation speeds 500,710 & 1000rpm.
   – Investigate on with 2 overlap directions.

2. *Static strength determination and failure analysis*
   – Establish how various MP-FSP conditions affect tensile properties.
   – Determine the various fracturing processes of the FS processed material under tensile loading, relating to the various combinations of FS microstructures.

3. *Determination of particle deformation/fracture mechanisms*
   – From the thermomechanical and microstructural data gained, explain:
      a. Appearance of insufficient overlap
      b. Any other features which affects the fracture mechanism.
   – Changes in fracture mechanism towards change in overlap direction.

A clear understanding of these properties will make FSP a more viable process in the future as a microstructural modification technique and thereby overcoming the limitations of light weight alloys, especially in the development of critical components in structures. This study will provide a clear picture in the metallographic design and hence the applications of A356 in a wider scale for automotive and aerospace industries.

Chapter 3

METHODOLOGY AND PROCEDURE

The previous chapter has outlined the knowledge gap and the objective of this research. In this chapter, the experimental procedures of the current ME study will be illustrated in detail. An overview on the experiments designed to investigate each of the subjects (as summarized in chapter 1 & 2) will be outlined followed by, machine setup, FSP experimental conditions, metallurgical examinations, and other quantitative analysis will be detailed in Section 3.1 – 3.5 respectively on;

1. Preparation
   a. of A356 plates
   b. FSP tools
2. FSP
3. Heat treatment
4. Tensile Test
5. Metallographic Analysis

3.1 Preparation of A356 plates and FSP tools

The processes of casting followed by machining to the correct dimensions were performed to produce the A356 plates. Castings of Al-7Si-0.3Mg alloy (Table 1) were carried out at AUTs casting laboratory. The molten Al-7Si-0.3Mg (A356) was created by melting the cast ingots in an induction furnace and was later poured into a permanent mould made from heat treated mild steel. Fig 3-1 shows the induction furnace, crucible and thermocouple stick used during casting.

Table 1. The composition of A356 ingots used.

Al	Si	Mg	Fe	Ti	Sr	Others
Bal.	7.1	0.33	0.1	0.05	0.01	<0.01

Figure 3-1   *Induction furnace, crucible and thermocouple stick used for the casting of Al-7Si-0.3Mg alloy*

3.1.1 Casting of plates

Fig 3-2 illustrates the permanent mould used for casting the plates. The two mould halves were bolted together to form the mold cavity.
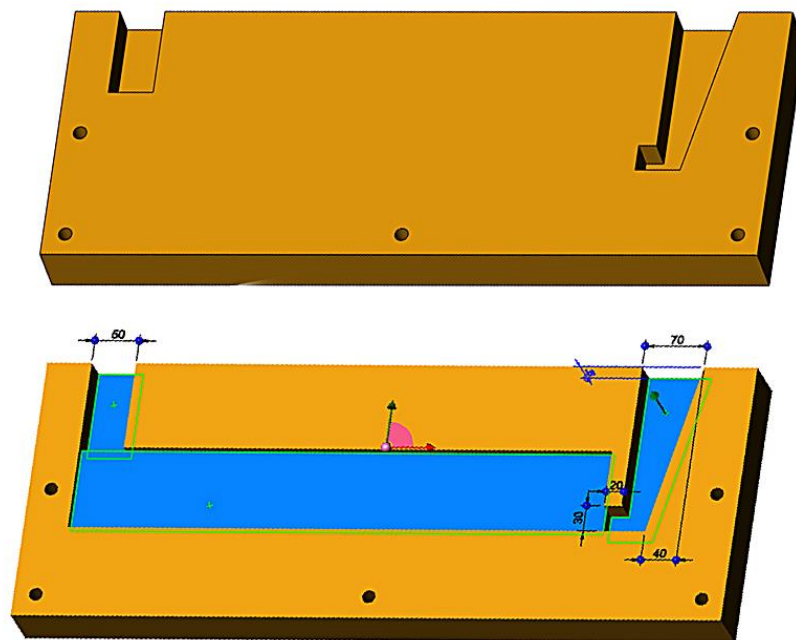
Figure 3-2   *Permanent mould made from heat treated mild steel*

The method for the casting process used was as follows:

1. Mould wash, which is an aqueous or alcoholic suspension or emulsion to coat the surfaces of a mould cavity, was applied to the inner surface of the mould to prevent the casting from sticking to the mould, rapid heat loss and consequential premature solidification. The mould wash used for casting was an Emulsion of Zircon based emulsion.

2. A356 ingots were heated to a liquid state in a crucible using the induction furnace. Simultaneously the mould was heated using an oxyacetylene torch. This heating of the mould was to help prevent premature solidification of the liquid metal when being poured into the mould. The mould was heated for 10 – 15mins to achieve a uniform mould temperature of 150°C.

3. When the molten A356 has attained the pouring temperature of 710°C (monitored with a thermocouple stick) and the mould had been sufficiently heated (for approximately half an hour) the liquid metal was poured into the mould.

4. After the metal had solidified and cooled the plates were removed from the mould.

3.1.2 Milling cast plates

The casted plates were then machined down to a required dimension (285x110x8mm) using a milling machine. For a better quality FSP, the following features must be obtained:

- Uniform thickness
- Fine surface finish

The cast plates which have uneven surface finish with shrinkage pores along the plate surface, were machined to make the smooth surface finish and uniform thickness to both sides of the plate. The milling operation was conducted on a Pacific FU125 universal milling machine as shown in figure 3-3. Uniform thickness

was carefully monitored and maintained, in order to produce a high quality FSPed surface. A finished A356 plate is shown in Fig 3-4.
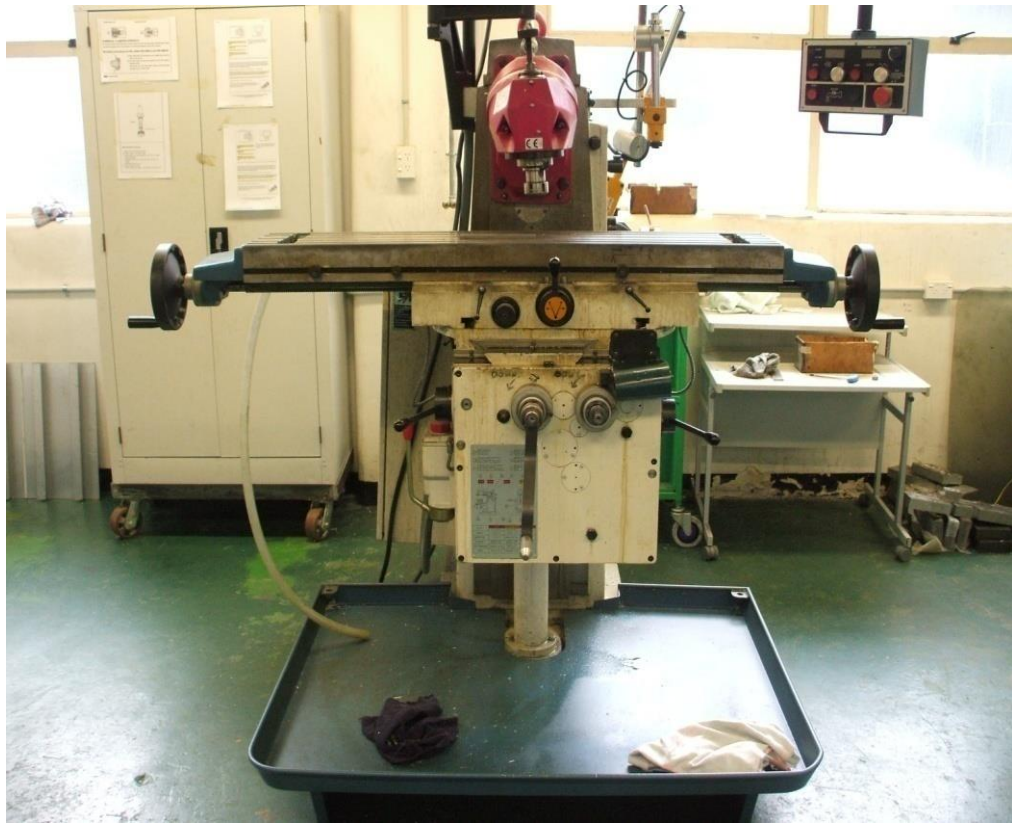
Figure 3-3.   Pacific FU125 universal milling machine

Figure 3-4.   Machined plate to a dimension of 285mm x 110mm x 8mm.

3.1.3 Welding of Additional plates

The minimum gauge length to fit in the extensometer was 25mm. The machined plate was not enough to produce a sufficient tensile sample, with enough surface to grip the sample tight. Hence, 2 A6060 side plates were then welded to A356 plate (of same thickness) on both sides (Fig 3-5). A6060 was chosen due to the ease of castability. We have used FSW to weld the plates and were conducted on the same TOS OLOMOUC FV20 universal milling machine used as shown in Fig 3-5. This machine was used to weld additional Aluminium 6060 plates on each side of the length of the A356 casting. A clamping system was designed prior to the welding to provide a better quality weld. Fig 3-5 demonstrates the plates clamped over the backing plate. For the ease of welding, A6060 plates were chosen to weld on either sides of A356 plate
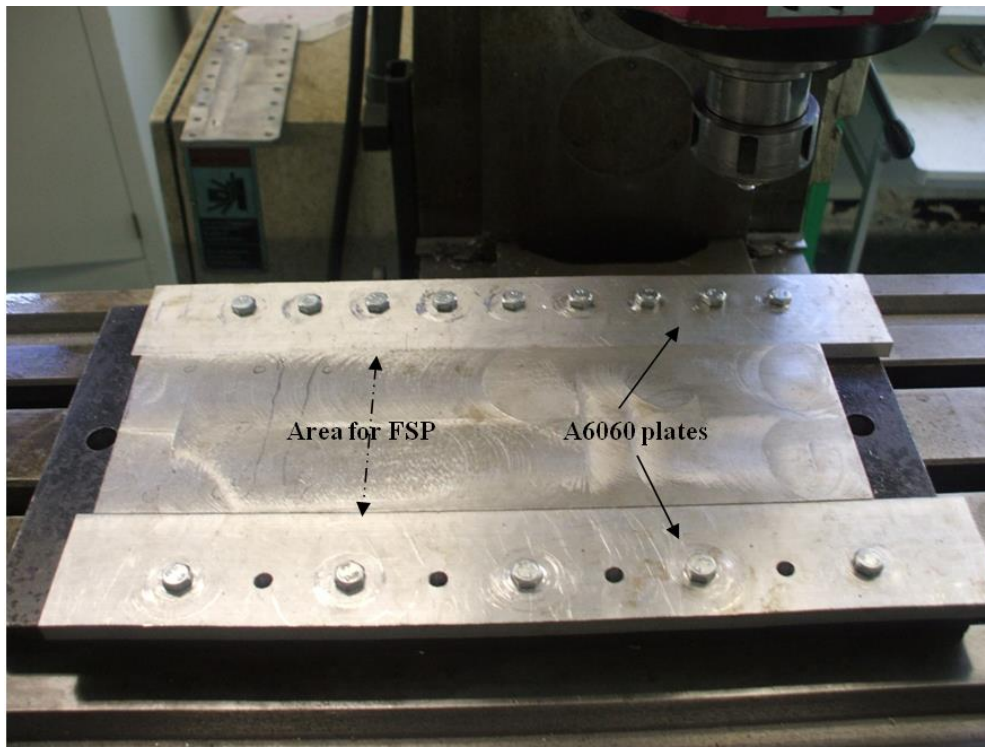
Figure 3-5.   FSP completed before the feed stalled

For the FSW operation the tool rotation, traverse speed and tilt angle of the tool was 1000rpm, 56mm/min and 2.5° respectively. A cylindrical threaded tool of 7mm diameter and effective 6.9mm pin length was used to weld the plates as shown in Fig 3-6. These parameters were selected owing to its good quality results

that we obtained through pre-weld trials. The final plate assembly for FSW can be seen in Fig 3-4.
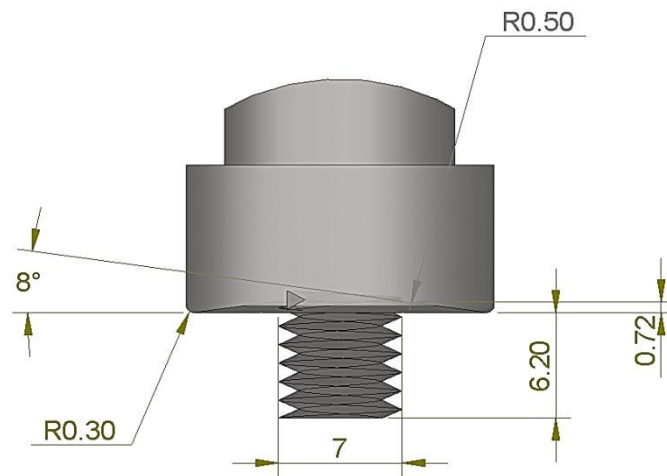
Figure 3-6.   Geometry of tool pin used to weld the additional plates to A356 plate

3.1.4 Clamping of plates for FSP

Clamping of the plates on to the milling bed is a vital feature in FSW/FSP, as an insufficient holding/clamping force will disrupt the material flow and may buckle the plates resulting in poor weld/processed zones. Because of the high forces involved in FSP and FSW there must be sufficient clamping of the work pieces which are being processed.   Fig 3-7 shows the clamping clearance holes were drilled, leaving sufficient space for the tool to traverse, in order to meet the required FSP area on A356 plate.
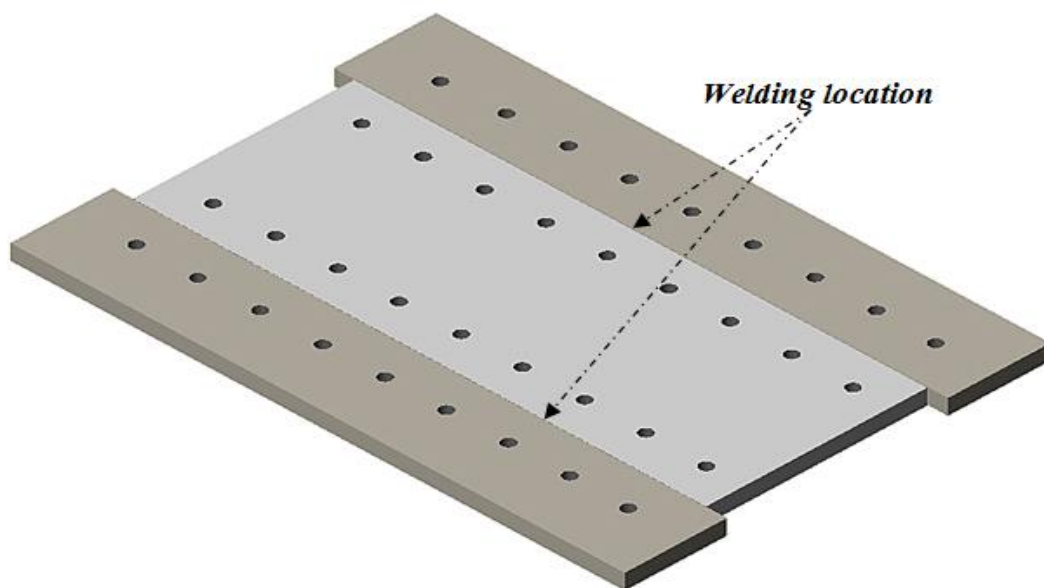
Figure 3-7.   Clamping clearance holes drilled on the plates.

A backing plate was used to protect the milling bed from any damage that could occur during the FS process (can be seen in Fig 3-8a and engineering drawings can be found in Appendix B). The final clamping setup can be seen in Fig 3-8b.

(a)

(b)
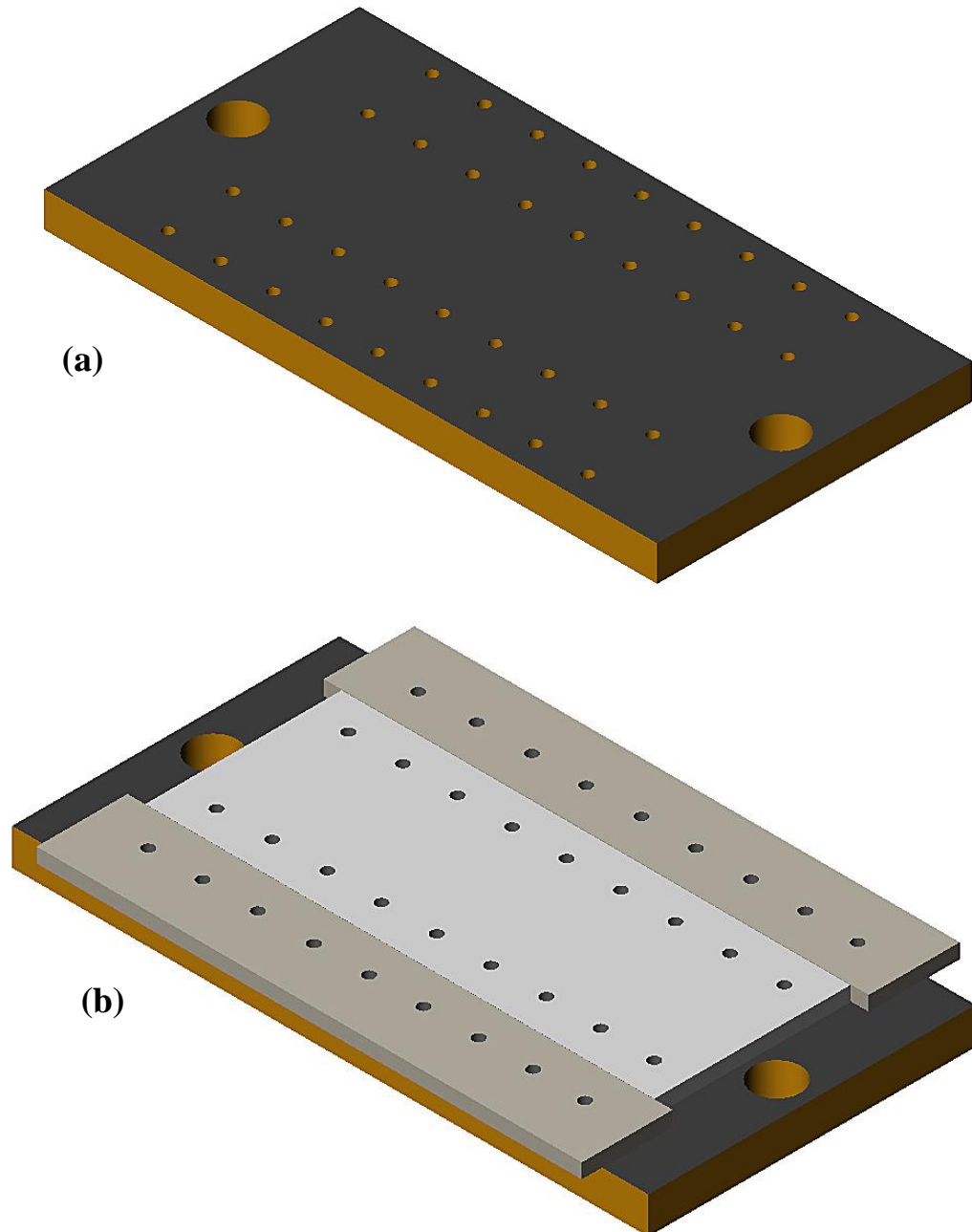
Figure 3-8   Assembly representation of final clamping system used. (a) backing plate with threaded clamping holes, and (b) the plates placed over backing plate

Backing plate are provided with two holes on either ends, to bolt it to the milling bed. The proper drilling of clearance holes on the plates, has alligned the entire clamping system, parallel to the traverse feed of milling bed.

Apart from the clamping screws, additional clamping was done with traditional Milling Machine Clamp Kit. This was done to assure more safety and protection of the milling machine bed.

Figure 3-9   Final clamping setup using additional milling machine clamping kit

The final clamping setup can be seen in Fig 3-9 which includes the Al 6060 plates which had been welded on before FSP the centre A356 casting.   The MP-FSP operation can also be seen in this image.

3.2 FSP Conditions

3.2.1 Tool Design

The tool pins made of H13 steel were used. As mentioned in chapter 1, the tool pin/shoulder design has a great role in determining the size and shape of the nugget region. The final design chosen was a flat-bottom cylindrical pin and a concave shoulder profile.

The tool was designed with concerns of ease of machining and to create a better quality processed zone. Depending on diameter of shoulder, diameter of pin and pin length, we have used two different batches of FS tools. Here, Tool 1 was used for initial MP-FSP runs; however, Tool 2 was used for the entire FS experiments carried in this proposed study. Engineering Drawings of the tool piece can be found in Appendix C.

Table 3-2   FSPTools used.

Tool Type	Tool 1	Tool 2
Pin profile		
Shoulder diameter	22mm	22mm
Pin diameter	6mm	7mm
Pin length	7mm	7mm
Pin Thread	M8 threaded, 1.25mm pitch	M8 threaded, 1.25mm pitch

Heat treatment was carried out at McGregor Furnace to make sure that, the tool pin would not deform while processing. This helped the tool pin to maintain its original shape during FSP. The following procedure was followed to attain a hardness value of HRC45.

- Here, the tools (wrapped in aluminium foils) were subjected to 1040^0 C for an hour followed by oil bath.
- The aluminium wraps were then taken off for tempering process, as the tools undergone tempering at a constant 650° C for an hour.
- It was followed by natural cooling. The hardness of the tool was tested before proceeding to FSP.

3.2.2 FSP Parameters

In this section, the purpose of each series of experiment is explained in detail. In order to achieve better mechanical properties, a systematic approach towards reporting the process parameters is vital. And hence, efforts were carried out towards the MP-FSP process parameters such as:

- Tool rotation speed ω (rpm)
- Tool traverse speed v (mm/min)
- Tilt angle θ^o
- Overlap distance (mm)
- Overlap direction (multipass direction)

During the course of this study, a number of preliminary series of FSP was carried out. Series 1 was carried out initially to study on the behaviour of cast alloy and tool performance on multipass conditions. Improvements in properties, in particular strain was obtained in this. Series 2 was undergone to study the flow mechanism and particle distribution along the SZ. Our latest attempt (Series 3) was conducted with 3 different tool rotation speeds, 2 overlap distances and 2 overlap directions, while keeping tool traverse speed and tilt angle, unaltered. Table 3-3 & Table 3-4 display the techniques and parameters used for Series 1 - Series 3 experiments.

Table 3-3   Process parameters used for various batch of Preliminary MP-FSP samples

Experiment Type	Series 1	Series 2
FS process	MP-FSP	Single pass FSP
Tool Type	Tool 2	Tool 3
Tool rotation, ω rpm	710 &1400	500,710,1000 & 1400
Traverse speed, v mm/min	56	56
Tilt angle, (^{o})	2.5	2.5
Overlap distance, mm	0	1
Overlap direction	Normal	Normal

Insufficient overlap (IO) between the passes was observed in the initial studies (Series 1). Although, sufficient pin overlap was provided, this feature was still evident. The particles at these locations were orientated along the overlapping end of the N+1th pass, in the form of a wedge. The observations on this phenomenon will be explained in the next chapter. However this has lead to Series 2 experiments to understand the flow mechanism and to define wedging. Since, these features observed were a factor of tool rpm, Series 3 experiments were carried out to evaluate wedging-effect caused at lower rpm(500 & 710rpm) and higher rpm(1000 rpm) as well as the different overlap conditions.

Table 3-4 *Process parameters used for various batch of current MP-FSP samples*

Experiment Type	Series 3
FS process	MP-FSP
Tool Type	Tool 3
Tool rotation, ω *rpm*	500,710 & 1000 (2 overlap directions for 1000 rpm)
Traverse speed, *v mm/min*	56
Tilt angle, *(^{o})*	2.5
Overlap distance, *mm*	1
Overlap direction	Normal & Reversed

Fig 3-10 is an illustration to demonstrate the position and direction of tool plunge and traversing. The spindle head of the milling machine was adjusted to 2.5^0 to provide tool tilt angle.
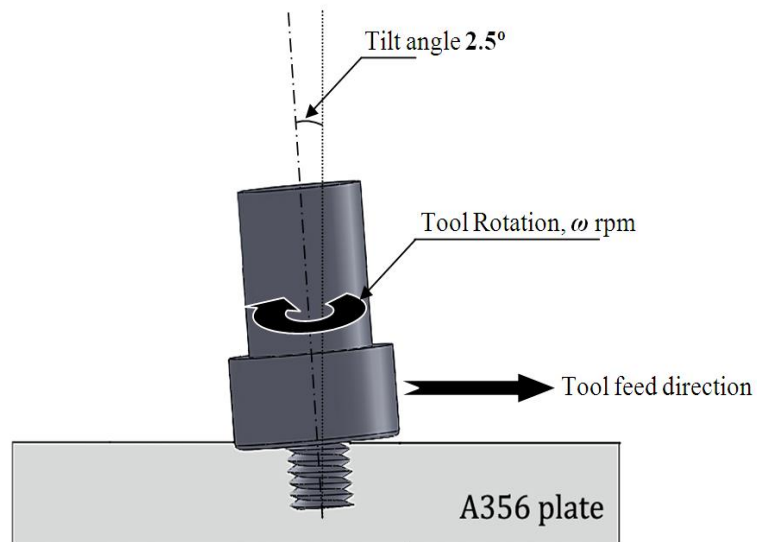
Figure 3-10   Schematic illustration of the process of tilting the tool, tool plunge and tool feed.

39

Methods of overlapping of passes are illustrated in Fig 3-11. Fig 3-11a demonstrates overlapping the passes with zero mm pin overlap, whereas, Fig 3-11b demonstrates the positions of tool pin from subsequent passes, thereby creating a pin overlap of say, 1mm.

(a)

(b)
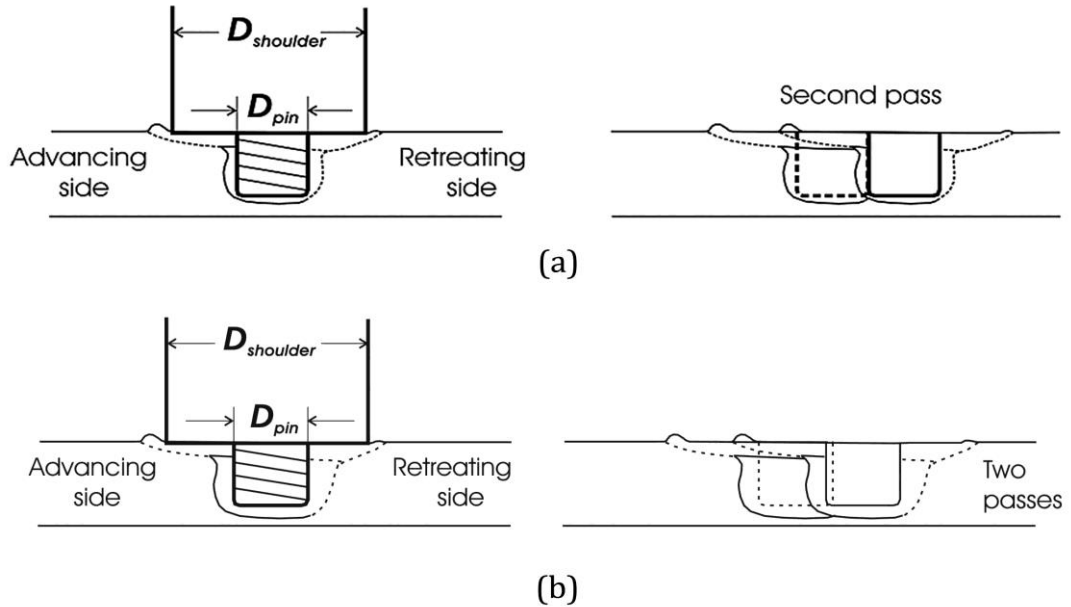
Figure 3-11   Illustration of FSPcrossection, two passes with (a) 0mm pin overlap and (b) 1mm pin overlap.

Series-3 has attempted to address the effect of change in overlap direction over the mechanical properties of the cast. As illustrated in Fig 1-9 (in Chapter.1), the drawing shows, how does the change in overlap direction works. The dotted pin profile denotes the first pass. For the ease of representing, the multipass overlap condition at Fig 1-9a is named as normal overlap direction and Fig 1-9b as reversed overlap direction.

3.2.3 MP-FSP Operation

The machine used to conduct FSP is a TOS FV20 turret milling machine as can be seen in Fig 3-12. This machine was selected because of its rigid milling bed, which can withstand the heavy loads during FSP. The machine has a bed locking system, which helps to prevent the bed from any form of shaking.

Figure 3-12   FSP machine (TOS FV20 turret milling machine)

As explained in section 3.1.4, the clamping system, was done. Series of experiments were carried out with several process parameters, as shown in Table 3-3 and Table 3-4. The sequences of experiments are as follows:

- Clamping of the plates which are welded together
- Tool spindle has activated with corresponding tool rotation and traverse speed was set.
- Downward plunge of the tool. Careful monitoring on the depth of plunge is needed. The tool was plunged till we see half of the tool shoulder (trailing end) plunged into the plate.
- Feed the milling machine bed (56mm/min), till the tool has reached the other end.
- Lift the tool from the plate and move it back to the starting location.
- Now feed the milling bed transversely, for the next overlapping pass.

The final processed plate can be seen in Fig 3-13, showing the welds on both sides (welding A356 to A6060 plates), clamping holes, and MP-FSPed region at the middle of the A356 plate. The system designed has provided a much rigid unit to withstand the forces from the rotating FS tool, leaving an effective 60mm for undergoing MP-FSP. 7 FS passes were overlapped with an overlap distance of 1mm.
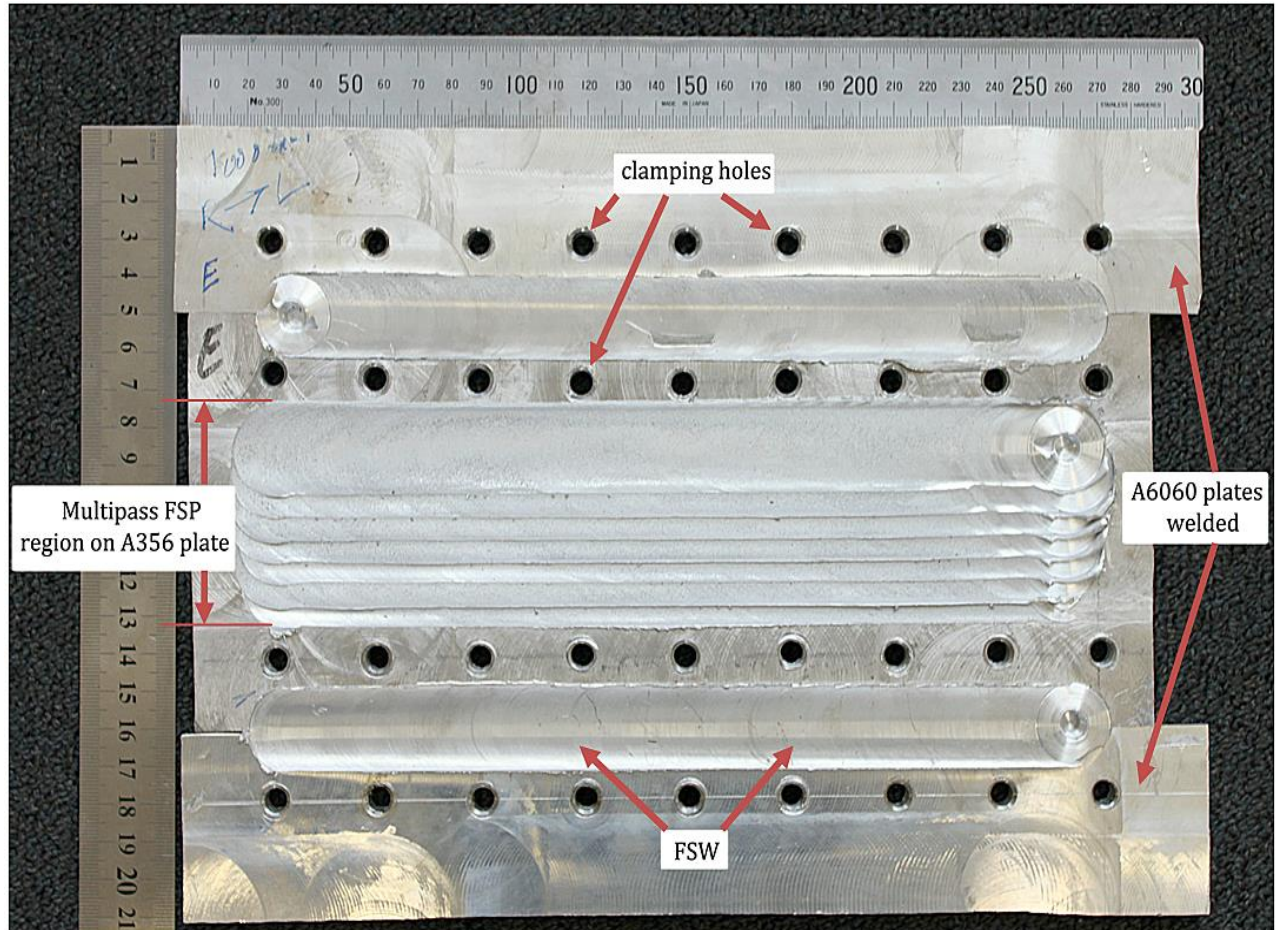
Figure 3-13   The final processed plate.

3.2   Sample preparation

3.3.1 Tensile Sampling

In order to machine the tensile samples from the FS processed plates; the plates were machined down to 3.5mm as shown in Fig 3-14. This is done to make sure that the as-cast regions are eliminated from the tensile samples, since the focus of the study is to report the mechanical behaviour of FS zone (particularly nugget

zone). The same milling machine (Pacific FU125 universal milling machine) which was used to machine the cast plate was employed to machine down 8mm processed plate to 3.5mm thickness plates. To produce an effective 3.5mm thickness, 2mm from the top and 2.5mm from the bottom were machined off.
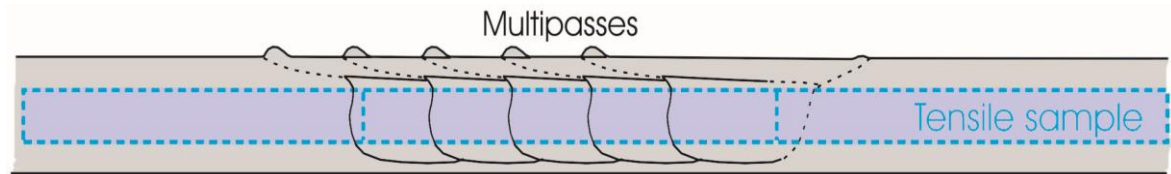
Figure 3-14   Illustration of the final thickness of tensile strips from the processed plate

 The tensile specimens were designed according to ASTM specifications. The tensile specimen engineering drawing can be seen in Appendix D. The machined FSPed plate is shown in Fig 3-15a. Fig 3-15b is a graphical demonstration of tensile sampling, showing the locations from the tensile strips are made. Thus, from every processed plate, 6 tensile strips were obtained. These batches are numbered from 1 to 6, where tensile strip No.1 is from the end of FS run on the plate, and 6 denotes the tensile strip from the location were FS run has started. The final tensile samples are shown in Fig 3-15c. Wire cutting was used to cut the tensile strips from the plates. Fig 3-15c shows the samples made from plate processed with ω = 500 rpm, v= 56mm/min, tilt angle = 2.5^0 and overlapping distance = 1mm.

Referring back to Fig 3-13, it can be seen that, an effective gauge length of 42mm (including the shoulders) was created at the narrowed section of the tensile sample. And careful consideration was taken to produce an effective space of MP-FSP ed zone covering the entire gauge length, thereby eliminating the chances for any tensile fracture to occur at the as-cast region of the tensile sample.
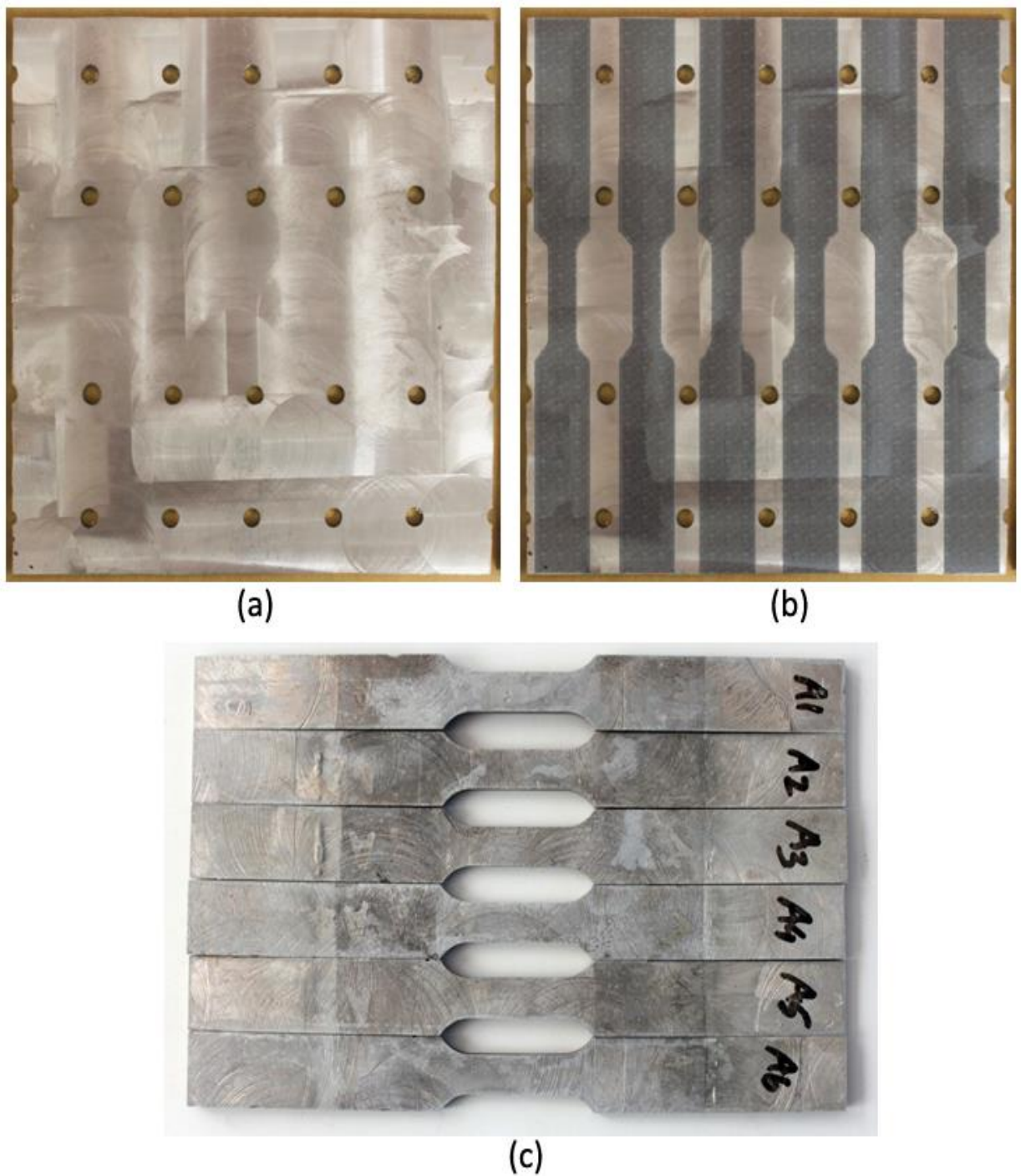
Figure 3-15   Photographs from: (a) machined plate of 3.5mm thickness (b)proposed locations from which the tensile specimens were obtained, and (c) final tensile samples machined from milled plates.

3.3.2 Heat treatment of samples (T6 condition)

All the tensile specimens were subjected to the processes of solutionizing and age hardening. Table 3-5 outlines the temperature and durations for solution heat treatment and age hardeneing.

Table 3-5   Heat treatment parameters to produce T6 conditions.

Process	Temperature	Duration	Cooling method
Solution heat treatment *(solutionizing)*	540°C	4 hours	Rapid water quenching
Age hardening	170°C	6 hours	Natural air cooling

3.3.3 Heat treatment Temperature Monitoring

A monitoring system was developed to provide a constant required temperature inside the furnace. Since the thermocouple is located towards the back of the containment unit, the temperature shown on the digital display of the furnace is not accurate. Several trials have been conducted, and realised that the display temperature on the furnace, was varying $\pm$ 8°C. On a metallographic point of view, it is not considered as a good practise, as any variation of $\pm$ 5°C can alter the internal microstructure and distribution. This has paved way for us to monitor the temperature within the furnace, while throughout the solutionizing and age hardening process. The heat treatment and age hardening setup can be seen in Fig 3-16.

Since this project outlines the mechanical behaviour of cast alloy subjected to MP-FSP with T6 heat treated condition, it is important to design a heat treatment system, with a well-controlled heating system. The components/equipments to serve the purpose are:

- McGregor Furnace

- Measurement computing USB-2416 data logger

- Type K thermocouple

- Lab View 7 interface
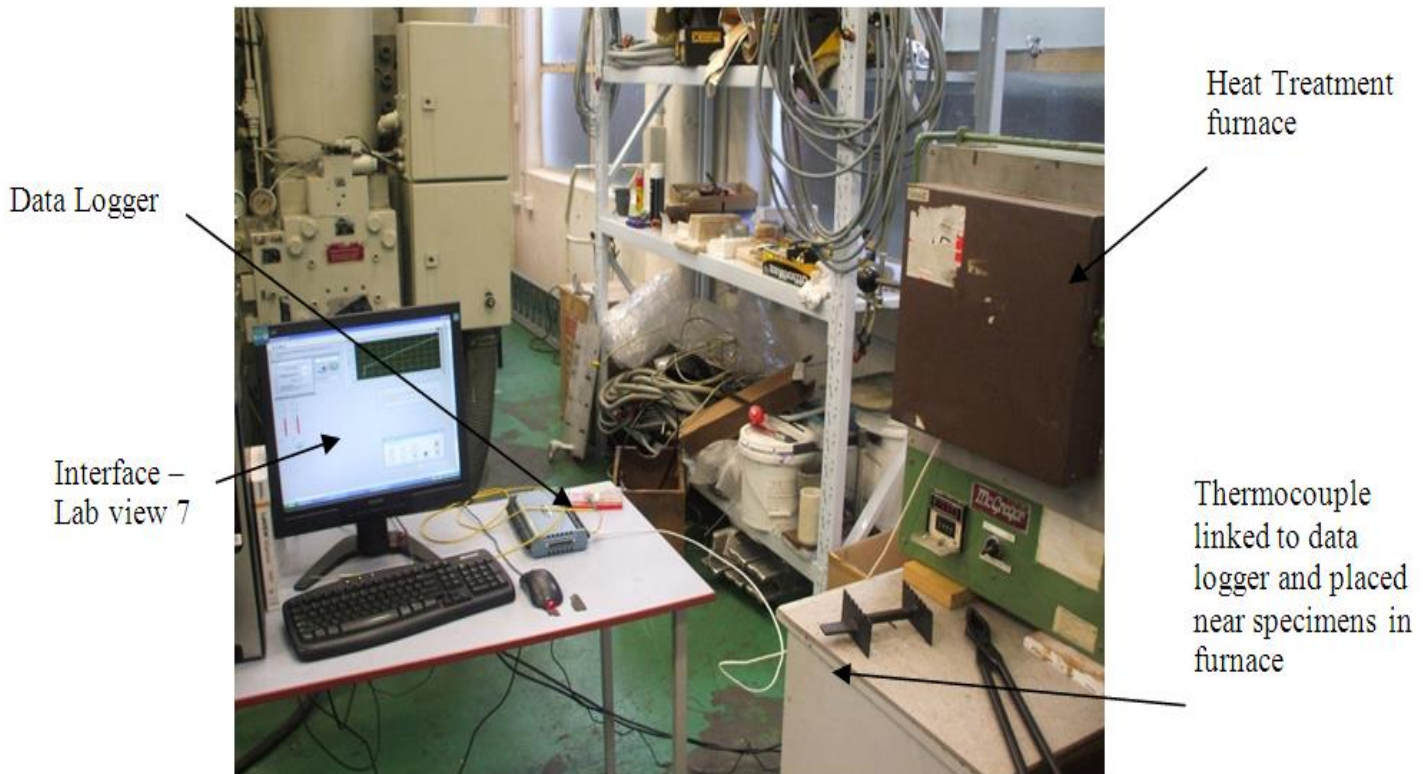
Figure 3-16   Heat treatment and Age hardening setup

To ensure that the temperature within the furnace a flexible Type K thermocouple was used so close to the processed samples. Lab View 7 interface along with Measurement computing USB-2416 data logger for logging of the temperature readings. One end of the thermocouple was connected to the data logger, while the other end was exposed to the high temperature inside the furnace. This system was tested several times and was proven more accurate than using the actual digital display temperature on the furnace.

3.3.4 Heat treatment calibration

For the solution heat treatment of tensile samples the following graph, Fig 3-17 was compiled from the data logged from the data logger. The following is an event log.

1. The temperature was kept constant at 540°C. The tensile specimens were then carefully placed.
2. The temperature was monitored in every 15min interval to make sure that, no variations were happening.
3. End of 4 hours, the samples were taken out from the furnace and rapidly quenched with water.

The same samples were then subjected to age hardening at a constant 170°C for duration of 6 hours. Aforementioned sequences were carried out, followed by natural air cooling. The graphs (Temperature Vs Duration) were plotted to ensure, that the specimens were heat treated according to the T6 standards, and no variation were reported. The age hardening graph shows the greater instability of the furnace at lower temperature. This has lead to the variability of temperature by ± 1°C throughout the age hardening process, which is well within the range of ± 5°C. Temperature variability is very low at elevated temperature (540°C), which means that use of the particular furnace at high temperature range is reasonably precise. Solution heat treatment graph shows a better smooth curve.
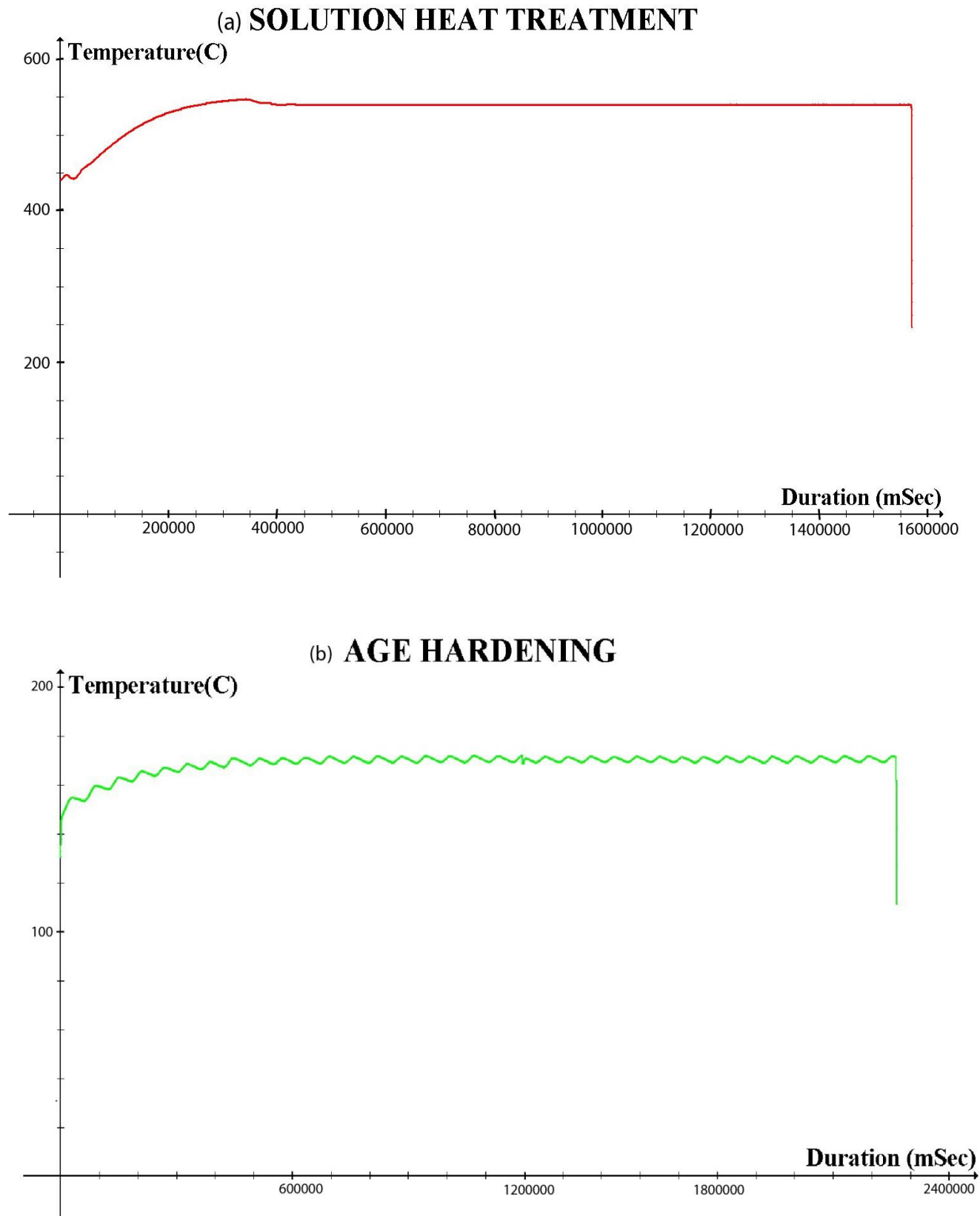
Figure 3-17   Heat treatment monitoring graphs of (a) Solution heat treatment and (b) Age hardening

The graphs show that T6 condition was well generated and controlled with the help of above mentioned monitoring system.

3.4 Tensile Testing Setup

The tensile testing was conducted on a Tinius Olsen H50KS tensile testing machine linked to Navigator software which logged the data obtained by the tensile testing machine. The tensile testing machine can be seen below in Fig 3-18 loaded with a tensile specimen. The MP-FSP zone is numbered from 1 to 7, showing the exact locations of 7 FSP passes carried out for this proposed study.
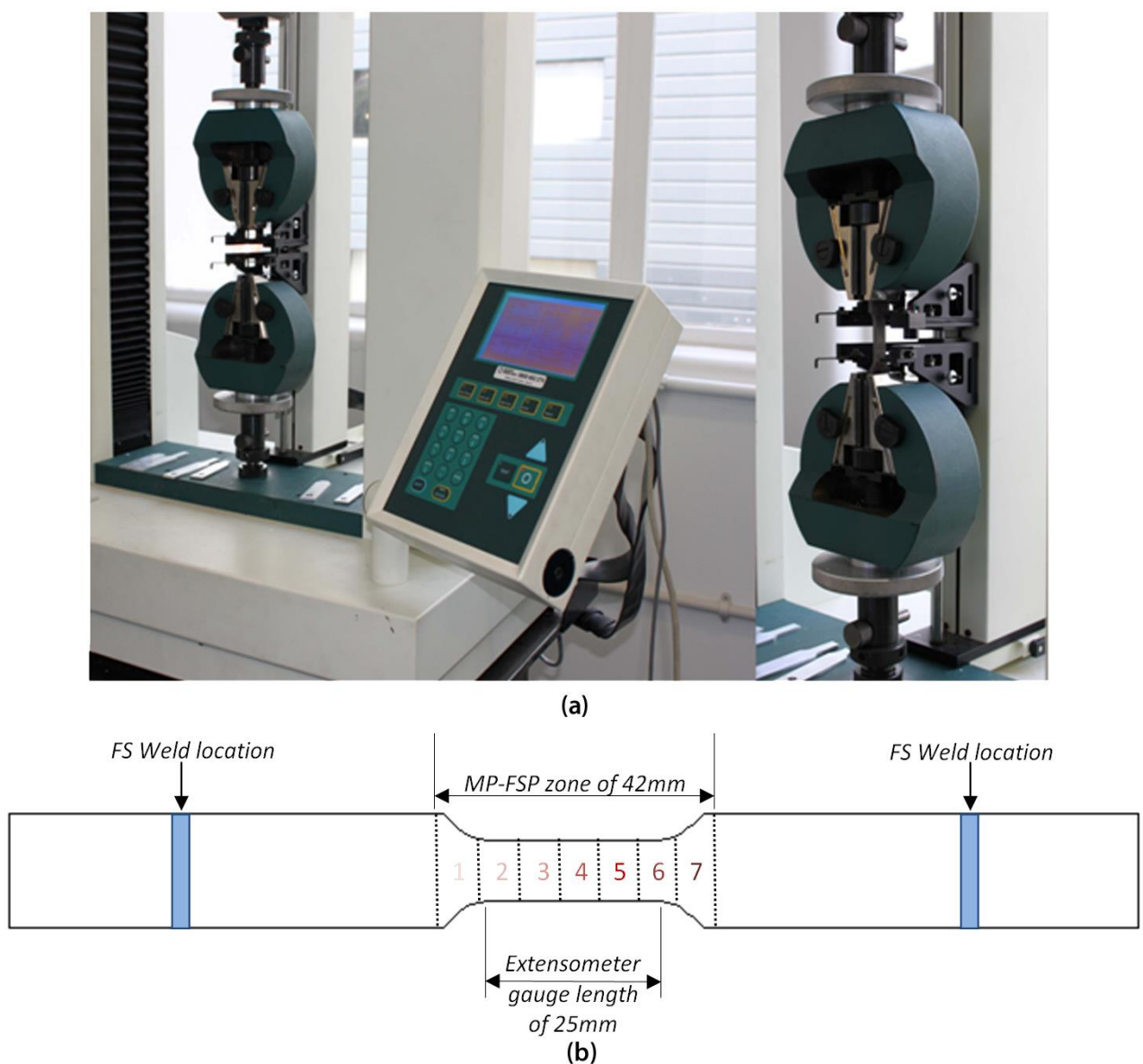
Figure 3-18   Tensile Testing setup: (a) Tensile Tester - Tinius Olsen H50KS, and (b) illustration of 7 passes (MP-FSP) on the tensile sample.

Tensile testing was carried out on all the specimens. Data was logged into an excel file for further analysis and graphing. The gauge length measured the extension of the reduced section zone of the tensile samples. As mentioned earlier, since the gauge length was made 42mm, there was enough space for the extensometer to feed in.

3.5 Metallurgical examinations

3.5.1 Pre- Testing:

A better understanding on the quality of the processed zone is required to evaluate. This presence of cracks, pores or FS defects needs to be evaluated before carrying out any analysis and hence X-ray radiography of the prepared plates were undergone. X-ray radiograph image of all the processed plates were taken and the tunnel defects are highly visible in the form of dark long strips.

The as-cast locations seen at the top and bottom of the FSP crossection should be avoided, due to its secondary brittle particles which will result in very poor mechanical properties. Hence, macro analysis was carried out along the crossection of the processed sample to get clearer picture on how much to be machined off from top and bottom of the plate and also to understand shape and size of SZ. The methods carried out are as follows:

- Few samples were cut from different locations to investigate the macro features of the flow.
- Samples were mounted using Struers LaboPress-3 hot mounting machine.
- Followed by polishing of the samples using Struers TegraPol-25
- Then the samples were macro-etched with Tuckers reagent.

The chemical composition of Tuckers reagent:
HCl - 45 ml, HF - 15ml, HNO3 - 15 ml, H2O - 25 ml

3.5.2 Post-Tensile Analysis

The fractured samples were prepared to carry out metallurgical examinations. The specimens were cut, mounted with Struers Labopress-3 hot mounting machine, and was polished to very high finish for micro analysis using Struers TegraPol-25. Nikon optical microscope (FX–35A) and Olympus stereomicroscope (SZX9) were used for macro/microstructure observations for low magnification range (up to 100 times). Scanning electron microscope used in the study was Hitachi SU-70 field emission type to observe the fracture surfaces and to produce EDS (Electron Dispersive Spectrometry) spectrum.

3.5.3 Quantitative examinations

Post processing and quantitative analysis was carried out in a typical sample using ImageJ, a java based image processing software. In this study the size, shape, orientation and distribution of the secondary Si particles in the Al matrix was studied to demonstrate the correlations. The next chapter details the results and further discussions on the results observed via tensile analysis, micro / macro analysis and finally quantitative analysis. A detailed analysis on all these features has demonstrated its correlations with the process parameters employed for FSP.

Chapter 4

RESULT AND DISCUSSION

In this chapter, findings from the initial study observing insufficient overlap (IO) given overlap distance being zero and the effect of tool rpm on this IO were presented. The effect of IO on tensile properties is also presented. The subsequent findings of material flows causing wedging and other features of the SZ (SZ) will be detailed. This is followed by presenting the results on the series of study relating macro/microstructure and mechanical properties to the effect of tool rpm and overlap direction.

4.1 Initial Study – evaluation using ω =710 rpm and 1400 rpm

4.1.1 Material Wedging

Cross sectional view of a MP-FSP sample made using the high ω value zero pin overlapping is shown in Fig. 4-1. The whole FS nugget of the last pass can readily be identified as outlined in the macrograph. When this outline is moved to the second to last pass it matches well except the size of the portion that the last pass has overlapped the second to last pass. Despite of the 0mm pin overlap between the FS passes, it is clear in Fig. 4-1 that there is a sufficient nugget overlap, meaning that the nugget is significantly wider than the pin.
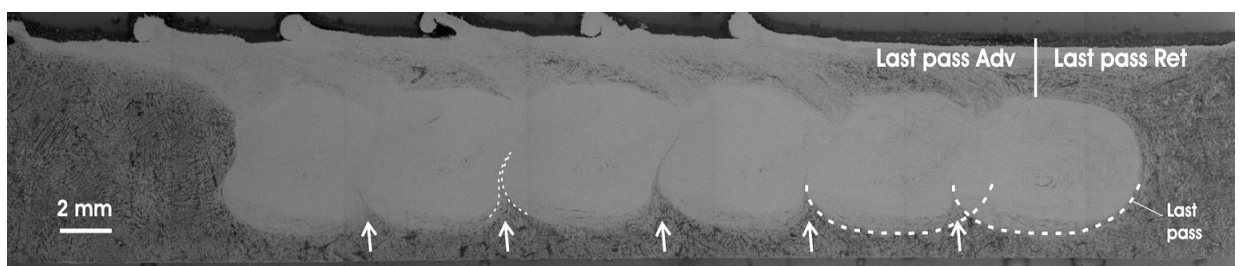
Figure 4-1.   Cross sectional views of a sample, after etching, taken from a MP-FSP plate made using ω = 1400 rpm and v = 56 mm/min. Arrows indicate material flow wedging up during FS.

A distinctive feature in Fig. 4-1 is observed between each pass along the MP-FSP region. Although, a zero pin overlap was used for this initial study, sufficient nugget overlap can be seen in Fig 4-1 in the last pass, highlighted by dotted curves. However, on a closer look, this region can be seen as dominant with upflow of coarse particles from the bottom of the SZ, orientating along the interpass location. On higher tool rotation of 1400 rpm, this feature can be observed in Fig 4-1, wedging from the bottom of the interpass location and stretching upwards, extending closer to the shoulder induced flow zone.

A clear panoramic view at the bottom of 1st and 2nd pass from Figure 4-1 is given in Appendix E. This material has wedged a long distance up and around SZ. The level of wedged upflow, demonstrated at every overlap location in fig 4-1, however changes as a function of ω value. Micrograph shown in Fig 4-2, is taken from the the lower part of wedge observed at the bottom of the interpass location, processed with with sufficient 1mm pin overlap. The deformed dendrite arms can be traced, indicated by the arrows. This wedging feature largely disappeared when the lower ω value was used. Despite of the positive pin overlap, the wedging feature is still evident in Fig 4.2a. However, wedging located at the bottom of plate processed at 710rpm is not intense like as in 1400 rpm.
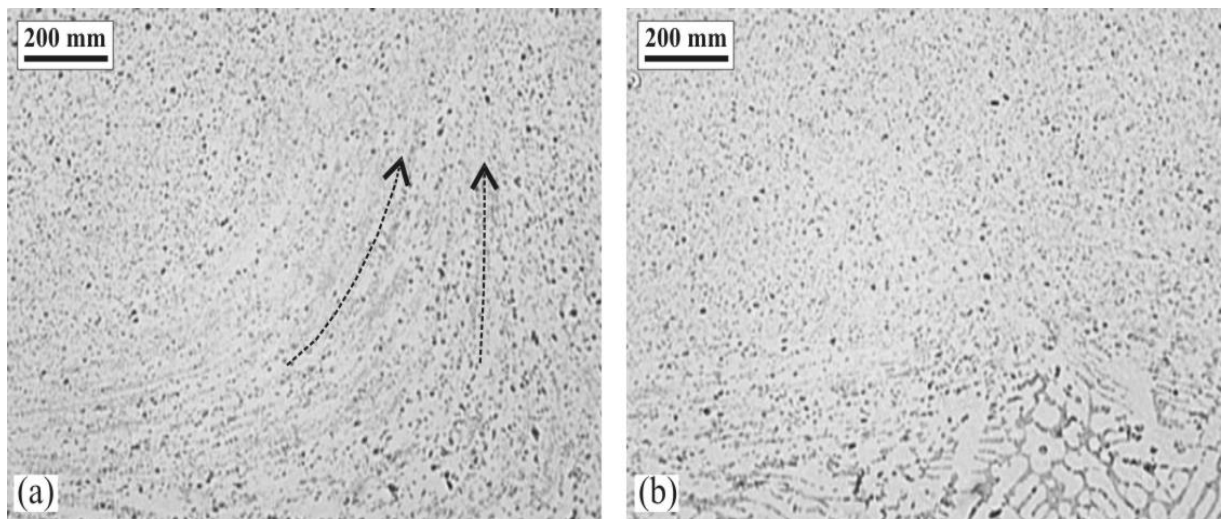
Figure 4-2.   *Microstructures in wedge locations samples made with v = 56*
               mm/min and (a) ω = 1,400 rpm and (b) 710 rpm and both with a pin
               overlap = 1mm. Arrows indicates the deformed dendrite arms
               thinning upwards.

4.1.2 The effect of wedging on tensile properties

The initial MP-FSP study conducted has focussed on studying the causes of the above mentioned Wedge formation and thus to eliminate these hassle. A very high tool rotation speed and slow travel speed *v* has produced highly refined nugget microstructure. But apparently, this high tool rotation speed has resulted in highly segregated layers at the overlap locations, showing no improvement in elongation (1-5%) over that of non-FS samples (demonstrated with red curves). The effect of low tool rotation (710 rpm) has almost disappeared the Wedge formation, and hence resulted in better tensile properties, %elongation in particular ranging from 10-13% (Fig 4-3). In the graph, stress-strain curves for 1400 rpm are illustrated in blue lines. Furthermore, the samples processed (1400 rpm) with 0mm and 1mm pin overlap shows almost the same tensile properties, showing no improvements.
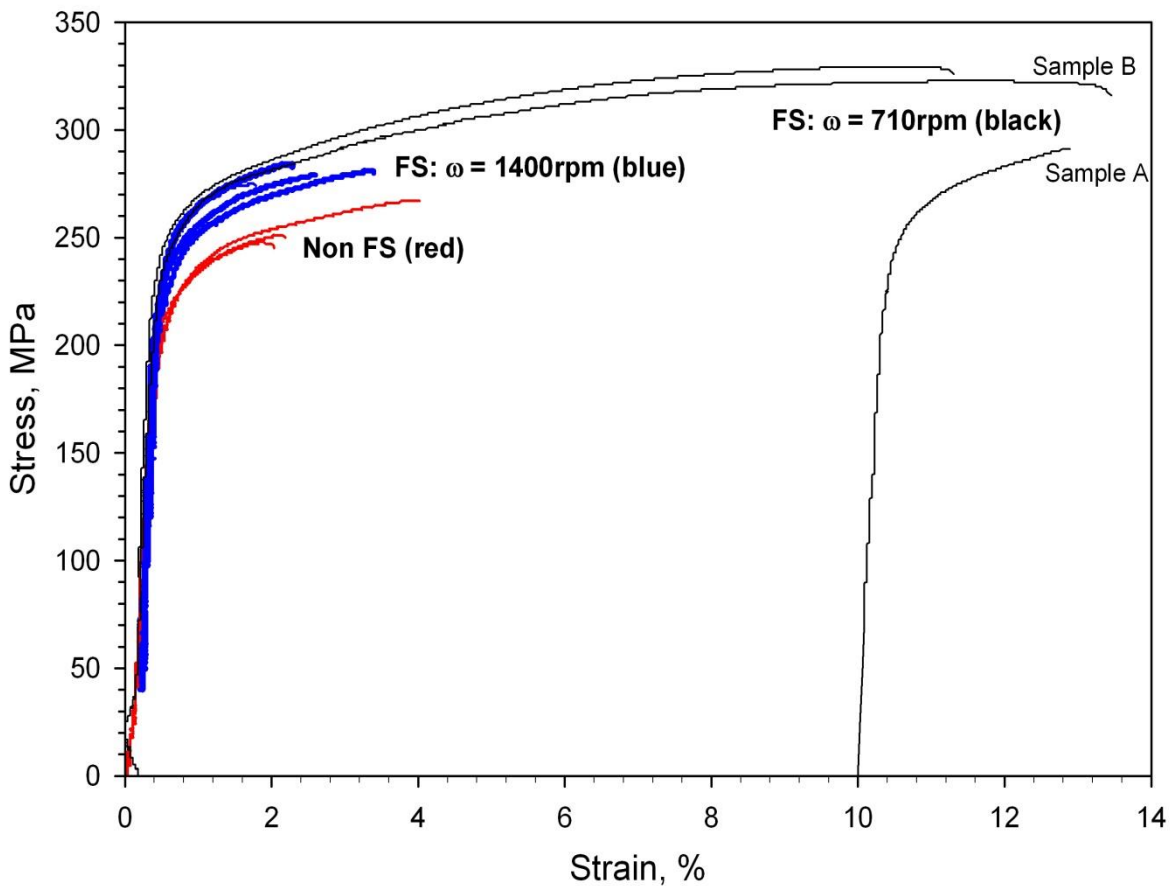
Figure 4-3.   Selected engineering stress-strain curves of T6 non-FS and FS samples.

However, the change in wedge flow observed at lower and higher ω value, is evident in the tensile testing data plotted in Fig 4-3. For non-FS samples, 0.2% proof strength ($\sigma_{0.2}$) was ~ 210 MPa and elongation (ε) values ranged from 2 to 4% and UTS from 245 to 265 MPa. These low ε and the relatively low UTS values are typical of this cast alloy in the presence of pores and oxide films which can be readily identified on fracture surfaces. For all FS samples $\sigma_{0.2}$ is 240-250 MPa, higher than that of non-FS samples. However, for all FS samples made using the high ω value, ε values are below 4%, showing no improvement over those of non-FS samples. Subsequent improvement in the elongation and UTS values were observed by nullifying the wedged formation through 1mm overlapping of the FS passes.

(a)   (b)
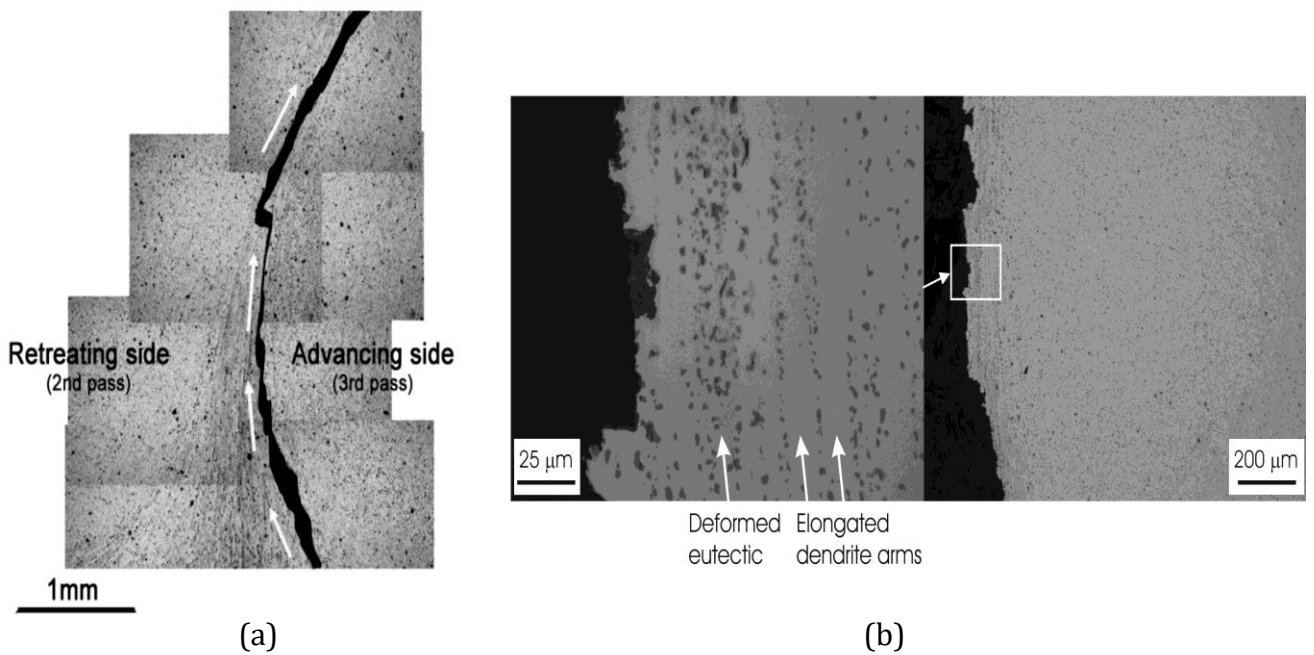
Figure 4-4   Cross sectional images and micrographs of tested samples (a) a Tool 2 sample in low magnification and (b) mid height location in a Tool 1 sample in higher magnifications.

The crack has been observed propagating through the overlap region, following the path set by the wedge. At higher *tool rotation speed*, the upflow has leaded the deformed eutectic and elongated dendritic arm to line all the way up to half of the SZ. Fig 4-4a, the crack propagation can be traced with the arrows shown. On a

higher magnification Fig 4-4b, the density of particle distribution and deformation direction can be seen. The quantitative analysis has given us better sketch of the density and the morphology of the Si particle distributed across the cross section of the overlapped nuggets. Large variation of Si particle size and density in the overlap regions were identified using Image-J analysis software and the variations are plotted in Figure 4-5. The large variation of Si particle density (Number of particles / 10 x 10 μm^2) in the wedge location is the result of severe segregation of Si particles. The region between 1700 – 1900 μm in the graph was the location of overlap, where the higher rate scatter of quantities was analysed. On a close look, the regions of zero Si particles or totally α-Al matrix were observed are clearly, the result of insufficient amount of deformation and mixing of the originally highly segregated cast α-Al and Al-Si eutectic, orientated perpendicular to the axis of tensile loading. This indeed has provided promising path for the microcrack initiation and propagation.
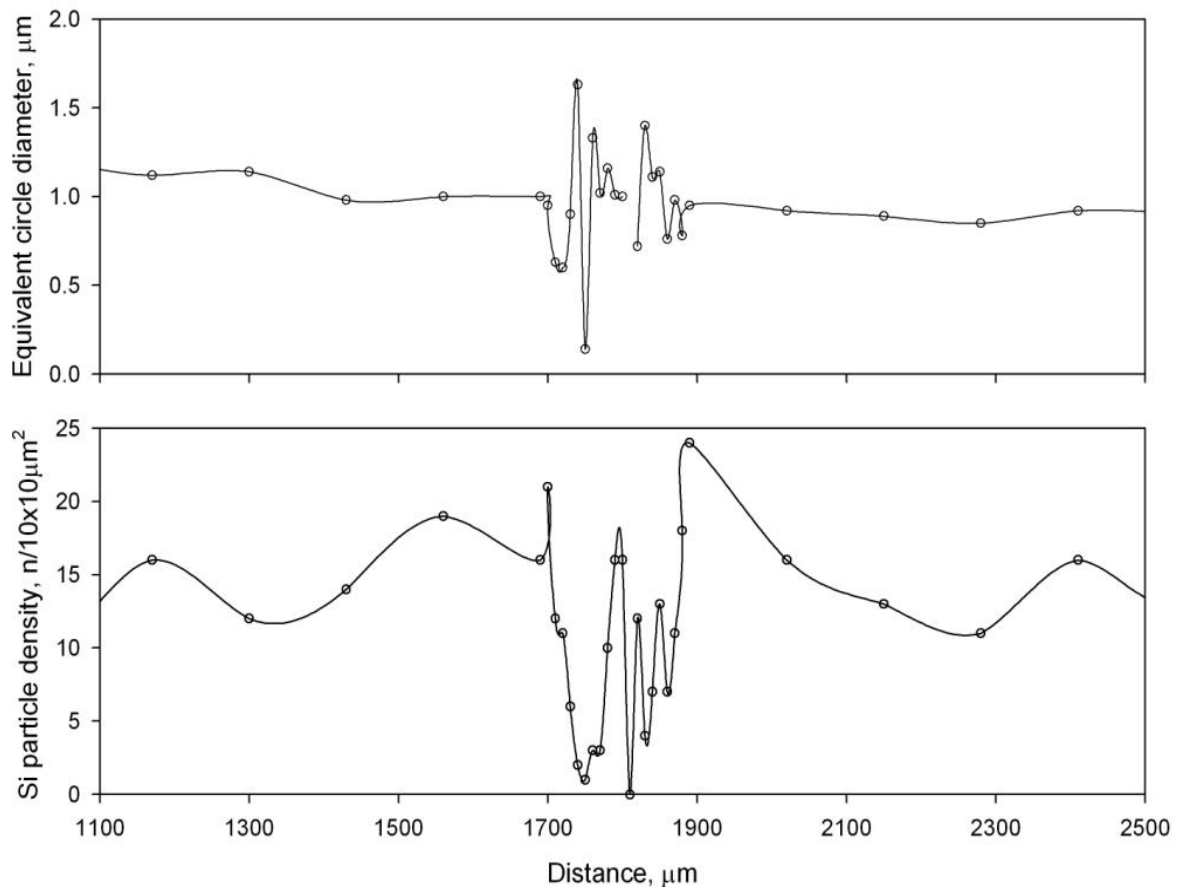

Figure 4-5.   Initial quantitative analysis done on samples processed at ω = 1400 rpm, v=56 mm/min & tilt angleθ=2.5⁰.

4.2   Subsequent study – material flow in single pass.

4.2.1 SZ macro/microstructures and their relationships to ω

Macro feature varieties as a function of tool rotation speed are presented in Fig 4-6. The region outlined by the solid lins is the total friction SZ. Within the SZ, as will be explained, two regions can be broadly recognised. The region of extensive deformation is called as Rotational Shear Material (RSM), the rest of the SZ has regions of coarse,fine and porous microsturcture. For the ease of use, this region is called as RFM. The details of why they are named RSM and RFM, which indicate their flow features during Friction Stir, will be explained in the rest of this section and next section.

In the present study, cross section of FS samples obtained at various tool rotation speeds were observed as shown in Fig 4-6. This macrograph was taken using a stereo-microscope. The Al dendrites appear black while the Al-Si eutectic appears light grey. As can be seen, the total SZ, which includes material that has gone through less deformation material within the SZ (RFM), is outlined by the dotted curve. The shape and area of the nugget is illustrated by white lines.

As explained by Song, the volume of RSM material within the SZ increases on increasing tool rotation rpm. Here, at lower rpm (500 rpm), the RSM material is observed to be deposited at the advancing end of the SZ. However, on a slight increase in tool rpm, the RSM material has started to extend towards the retreating side, as shown in Fig 4-6b. At this same tool rpm, the RFM started to extend more towards the advancing end, at the bottom of SZ. And on further increase in tool rotation speed (ω= 1000 rpm), the SZ is observed to be dominated by RSM, thereby the volume of RFM has decreased. Here again, a thin layer of region is visible at the bottom of nugget, stretching towards the advancing side, showing tendency to flow up along the advancing side. This layer of swirl observed at the bottom of the nugget, shows the FS flow characteristics resulting in stretching of RFM towards the advancing end, and further-up, thereby forming wedged formation.
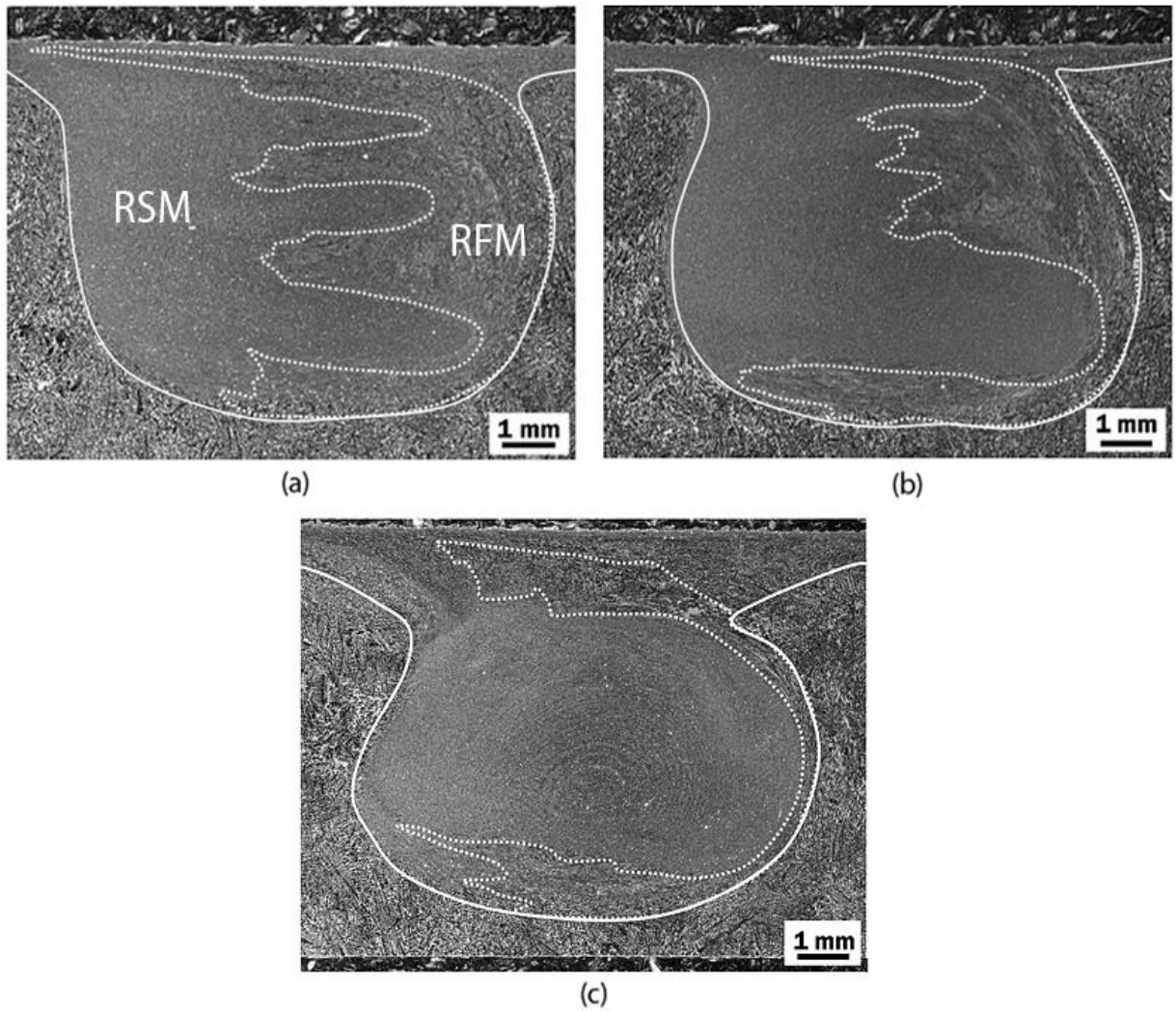
Figure 4-6.   *Cross sections of A356 FS single pass samples at constant traverse speed v = 56mm/min, tilt angle θ = 2.5⁰ and (a) ω = 500 rpm, (b) ω = 710 rpm, and (c) ω = 1000 rpm*

Fig 4-7, illustrates the macro/micrographic mapping on the cross section of single pass FSP sample at lower rpm. Locations A1, A2 and A3 highlight the particle distribution in the RFM region. Here the regions of less deformed particles are visible occupying the better half of the entire nugget region. On a micro analysis, fine (A1) and long coarse particles (A2) and tiny pores of size 1 - 3μm (A3) were also observed in these locations, thereby creating a poor processed zone in terms of its mechanical properties. A region of extensive refinement (B) can be seen in the SZ, extending from TMAZ (C) on the left towards the centre half of the SZ.
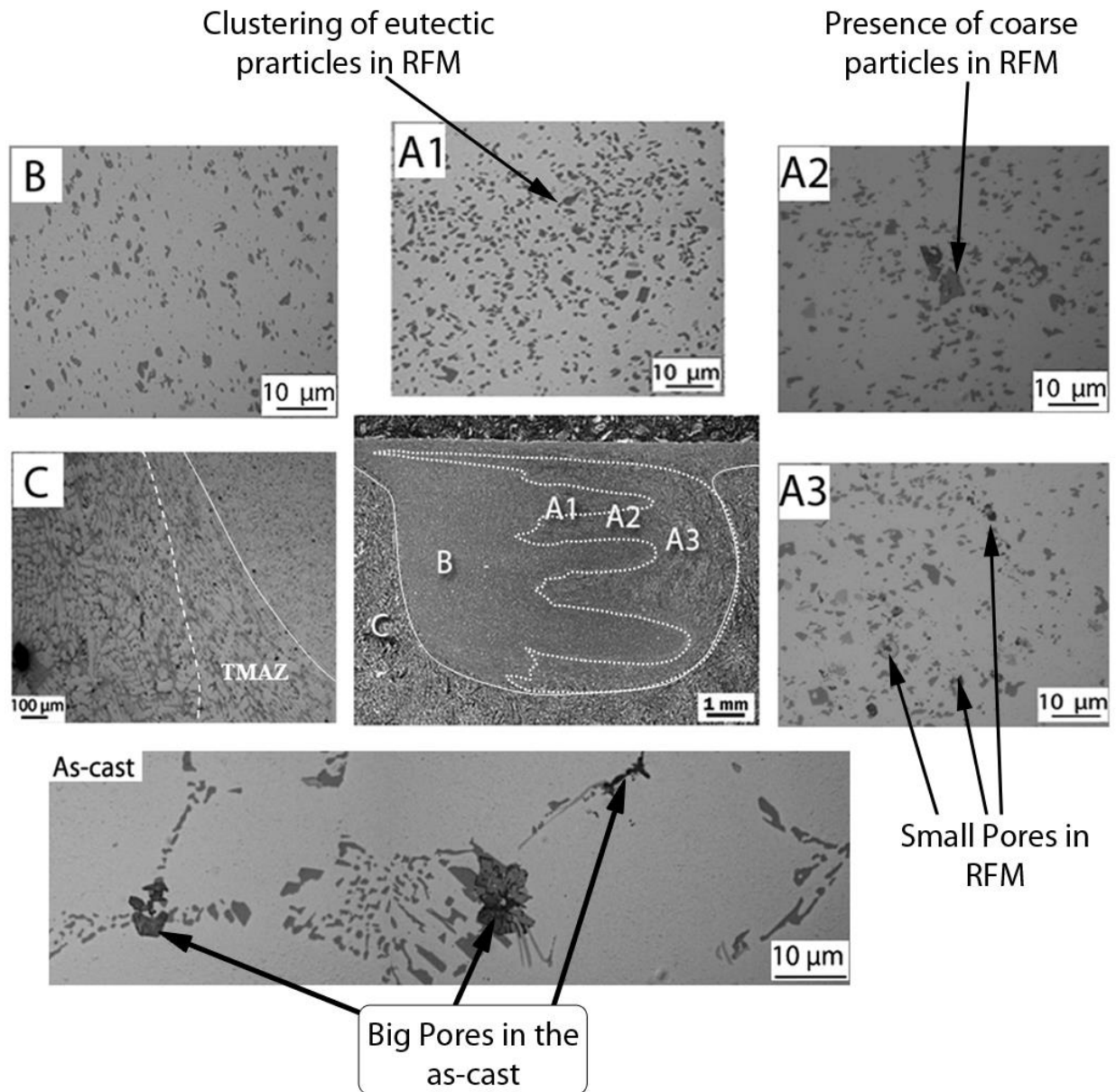
Figure 4-7.   Micrographic map of crossection of FSP at 500 rpm.

In the as-cast state, coarse Si particles are visible in the interdendritic region and also coarse α-Al dendrites are also present in the micrograph shown in Fig 4-7. Porosities ranging from 10 - 15μm were observed within the as-cast structure and no large size pores are visible within the microstructure of friction SZ. However locations of small pores, less fine particles and some clustering were observed within the RFM zone. On the other hand, RSM location is characterised by quite evenly distributed Si particles in the α-Al matrix.

4.2.2 Summary of flow mechanisms and deformation

The FS flow and macro/microstructure formations reported in the previous section have been explained by Cui [24]. Referring back to pin-breaking technique done here at AUT University, flow segregation, between Rotation Shear Material (RSM) and the rest of the nugget, can be clearly observed in FSP on A356. This segregation is common in all the samples although the relative portions vary as rotation speed changes. A high level of microstructural refinement was reported by Cui, at the advancing half of the nugget, which is in agreement to this current study. Fig 4-8 shows the crossection of a broken pin embedded within the workpiece which was obtained by a specifically designed sudden stop FS experiment. The RFM region within the FS zone can be observed towards the retreating half of the nugget.
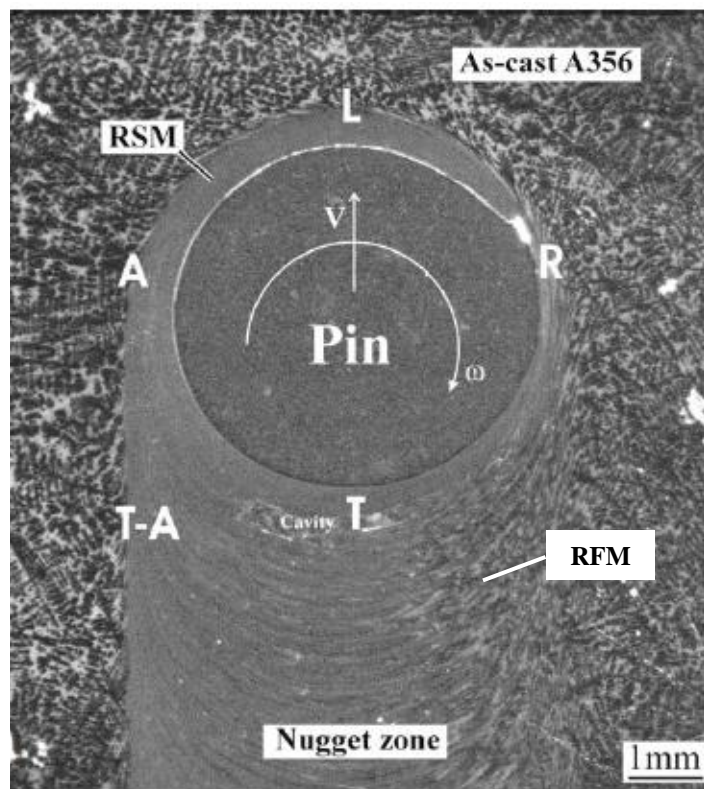

Figure 4-8   Cross sections of FS samples made using θ = 0°, v = 160 mm/min and
ω = 710 rpm: (b) a broken pin embedded sectioned longitudinally
along the plane ~ 4 mm from the surface. [24]

As explained by Cui, as the rotating tool moves forward, a portion of the workpiece material in the front is forced (sheared) into thread spaces and then becomes RSM. The further movement of this RSM in thread space is referred to as RSM flow. In the trailing half, for mass balance, RSM needs to detach from thread spaces. For a better illustration, the pin-workpiece couple in Figure 4-8 is schematically represented in Figure 4-9.
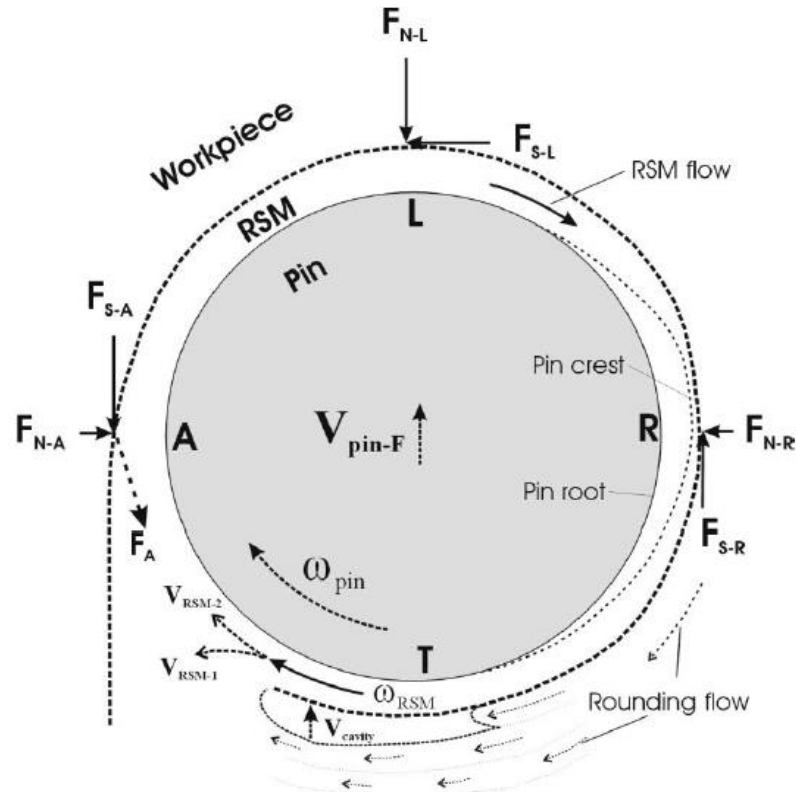
Figure 4-9   *Schematic illustration of RSM around the pin, forces acting on the periphery of RSM, and various material flow directions. For generality, RSM has been drawn continuously around the pin with the pin crest in a particular location is also indicated.* [24]

In this figure, forces and features of material flow are suggested. Each pair of forces (normal force FN and shear force FS) represents the forces acting on the edge of the RSM from outside material. And material outside RSM imparts resistance to its flow. Therefore, there will be an opposite (reactive) force of these forces which shears and compresses the material outside RSM. This reactive force within regions L to R generally shears the workpiece material outside RSM to R–T regions. This shear flow is referred to as rounding flow. Thus, phenomenon of rounding

flow explains the formation of locations of distinct microscopic features within the same nugget as RFM.

The feature of deformation and flow induced by the pin along the TMAZ location is studied in fig 4-10. To do this, a primary dendrite trunk or a secondary dendrite arm was traced and drawn as a curve. One end of this trunk is in the low deformation side of the transitional zone. Along the trunk, the amount of deformation increases, elongating towards the nugget. However, when the tracing approaches RSM, there is a region where dendrites have been deformed to such an extent that they appear as fine α(Al) layers wrapped around RSM. A dendrite trunk (or an arm) can be traced from the outside flowing into this most heavily deformed region but where it ends cannot be identified.
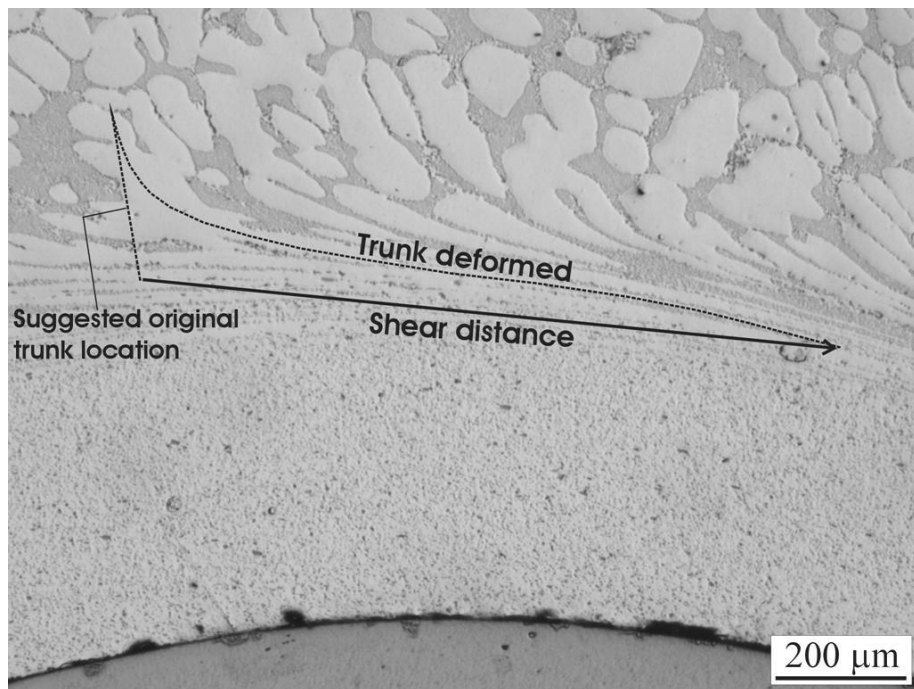
Figure 4-10.   The high magnification micrograph obtained with pin-breaking technique at the leading edge of the tool pin. [24]

Since Cui's study focused on FS single pass flow mechanism, the occurrences at the bottom of the SZ was not studied. In this present study, the major focus is to correlate the flow features at the bottom of SZ, which causes the wedging of coarse particles into the interpass location during subsequent FS passes. Hence, in agreement to the aforementioned study, the trunk deformation at the bottom of the SZ, at the location of wedged upflow is shown in Fig 4-11.

*Figure 4-11.   The high magnification micrograph obtained at the TMAZ location
for FS condition at higher ω = 1000rpm*

Even though a trunk deformation is visible, the location looks more of compressed
by the combined effect of Normal and Shear resistances. Unlike, the shear reported
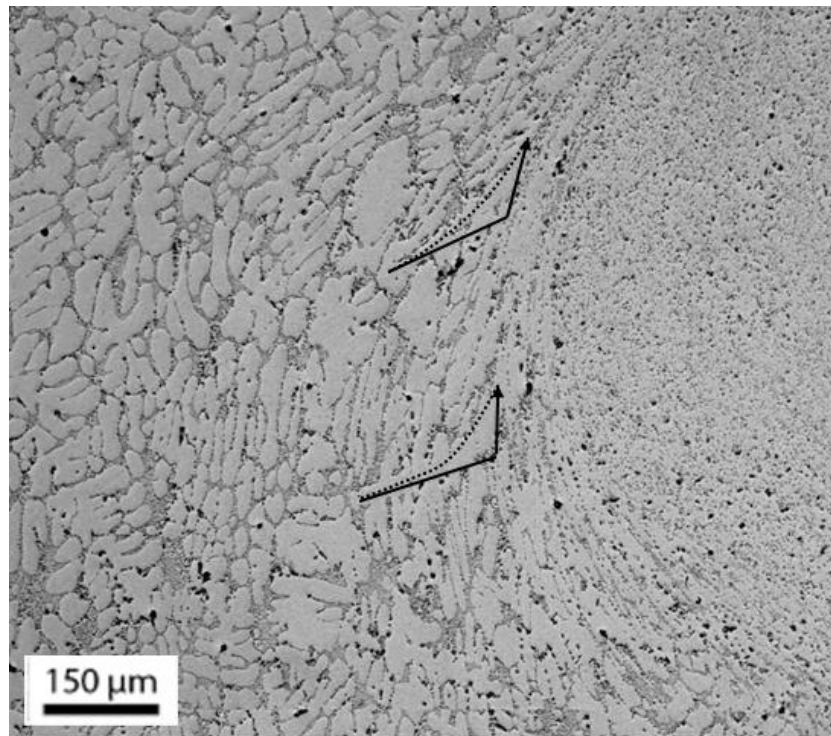initially at the leading end of the tool pin, the shear observed at these locations is
not seen vigorous. On a closer look the flow can be seen coming from the region of
as-cast, from the bottom of the SZ. The shear observed on the trunk is not intense.
Particles far away from the SZ can also be seen flowing upwards, induced by the
stirring action of tool pin, however rather than upflow, primary and secondary
dendritic arms in this region has been compressed by the normal and shear forces
excerted by the pin.

These analyses have paved way to better understanding towards the major
reasons for low tensile properties of MP-FSP conditions on A356 Al alloys.
Elimination of Wedged Upflow and better distribution of refined particles in the Al
matrix can somehow create difference to the current poor tensile properties
reported. However, in the current study (Series 3), a selection of process
parameters ranging from 500 to 1000 rpm has been selected.

Analysis on TMAZ location on the advancing side produces a better indication on the overlapping conditions (multipass) as it can be seen in Fig 4-12. The width of the TMAZ location and the size of elongated Al-Si particles changes with varying the tool rotation rpm. In agreement to the explanation given above (on wedging at higher rpm), the flow mechanism at TMAZ has been seen acting like extrusion of particles from the bottom of the nugget. This region displays compressed Si particles along the width of TMAZ. The shape and flow mechanism at TMAZ, varies; however Fig 4-12 demonstrates how does it physically changes with changing tool rpm.
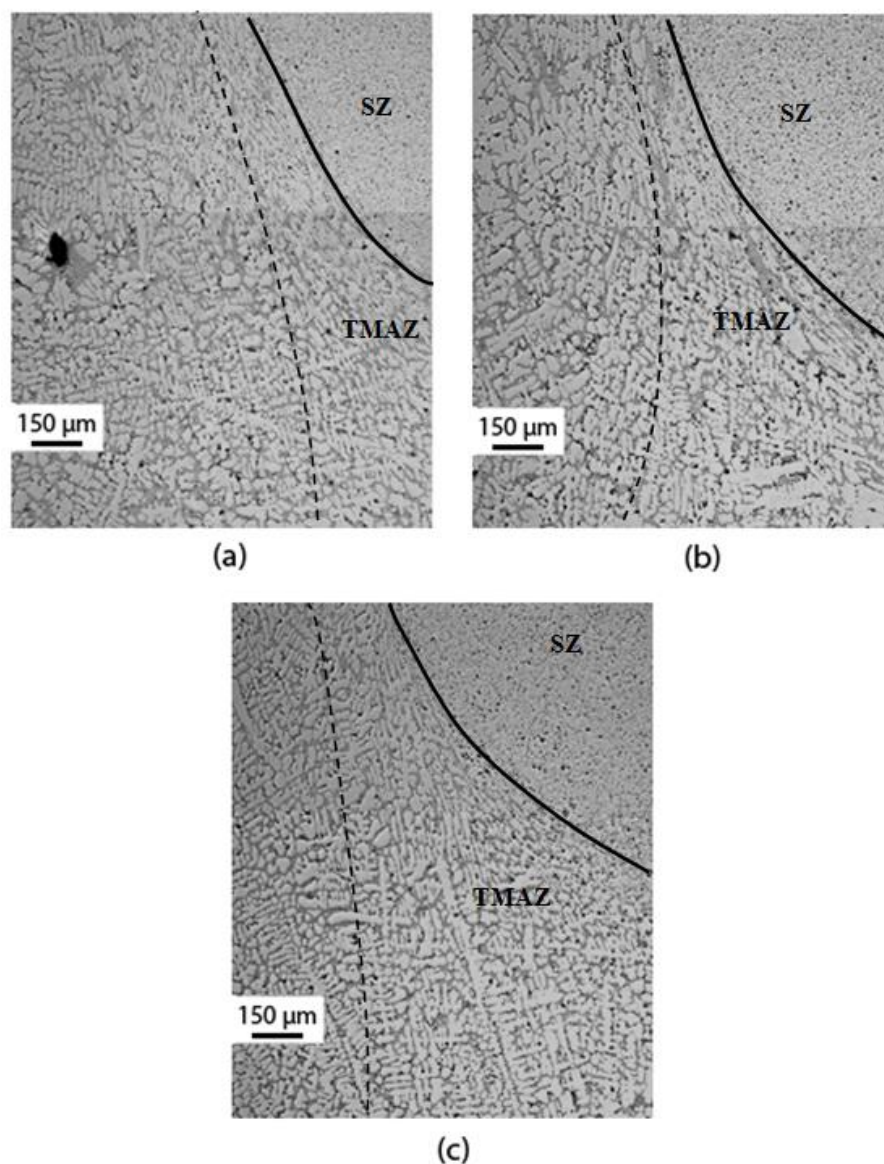

Figure 4-12.   *Low magnification micrograph showing the orientation and shape of TMAZ region at: (a) 500 rpm, (b) 710 rpm & (c) 1000 rpm*

Fig 4-12, shows the low magnification micrographs at the TMAZ locations of various FS sample. The as-cast microstructure, slightly away from the TMAZ region seems unaltered by the stirring action of FS tool at lower rpm. Despite of the change in tool rpm (Fig 4-12 b&c), the intensity of upflow remains fairly similar to the low rpm. A slight widening of the TMAZ location has been observed in 710 rpm and 1000 rpm respectively. As explained in the previous section, the extrusion of as-cast microstructure along the TMAZ, thereby lining up the coarse and less deformed Al-Si formation are visible. The high intense upward force from the bottom of the tool pin has lead to the extrusion of coarse particles, which initially lies away from the SZ. Hence, the growth and propagation of upflow are induced and controlled by the tool rotation rpm selected. In this study, the changes in Upflow feature is studies at tool rotations of 500, 710 and 1000 rpm in correlation to the severe upflow reported at 1400 rpm (in the preliminary results). Figure 4-13 summarizes the suggested flow mechanism happening at the bottom of the rotating tool pin during FSP.
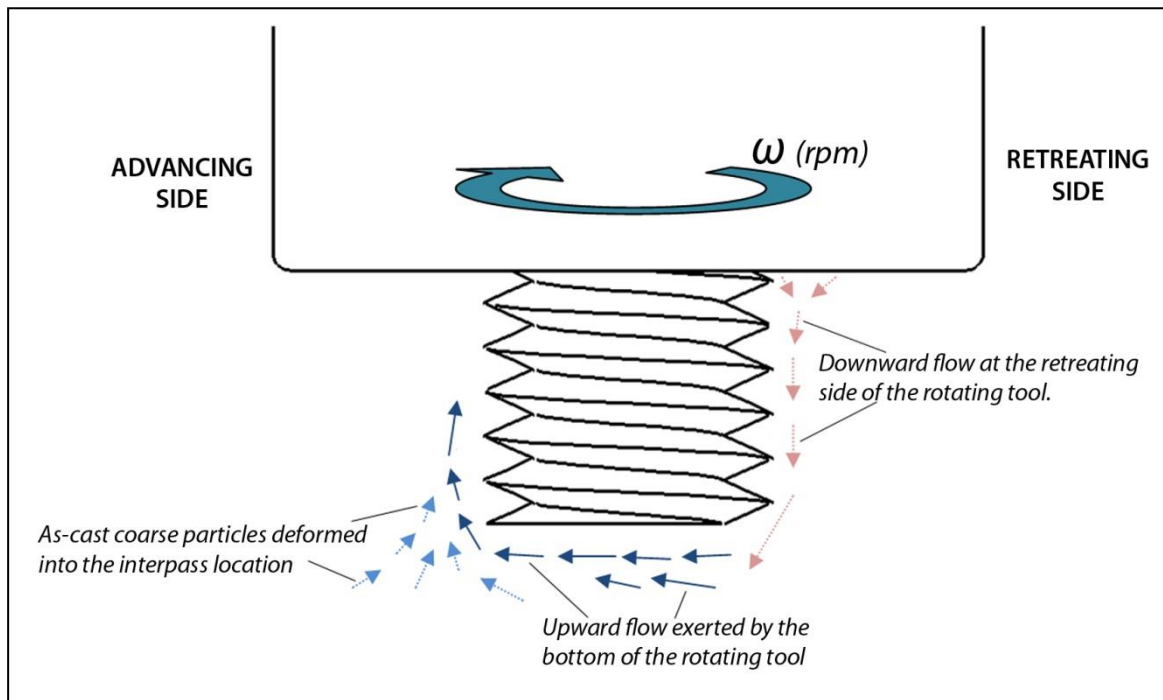

Figure 4-13   *Schematic representation of the flow mechanism at the bottom of the rotating tool.*

As mentioned in Section 4.2.1, the processed zone comprises of various zones of highly refined and less extensive deformation regions. The presence of RFM

observed towards the retreating side and at the bottom of the SZ, is illustrated schematically in Fig 4-13. The flow lines with red dotted curves demonstrates the downward flow observed from locations closer to the shoulder induced zone and propagates along the retreating side towards the bottom of the pin. However, the flow induced by the rotation and traversing of tool pin is shown with dark blue lines. This flow line has been seen nucleating at the bottom of the retreating end of the pin, and later it extends towards the advancing side. The extrusion of as-cast coarse particles is highlighted in dotted curves at the bottom of the advancing side, which is extruded into the interpass location due to the stirring force exerted by the tool pin bottom. The intensity of these flow-fields (both downward and upward flows & extruded as-cast particles) is observed to be highly sensitive to tool rotation speed, than traverse speed (v), and tilt angle (θ).

4.3 Subsequent study – Analysis of MP-FSP

Aforementioned mechanisms and features of single pass are controllable to an extent by varying the process parameters, but it has distinct effects on the processed zone, especially when the flow is overlapped by another pass. In this section, the various correlations between those mechanism and features with the process parameters are addressed.

4.3.1 X-ray radiographic analysis on multipass defects

It is good to mention, the tunnel defects that are prone to occur during FSP, in particular MP-FSP. Insufficient clamping and insufficient depth of tool plunge may lead to the presence of tunnel defects in the processed zone (normally observed at the advancing side of the SZ for a cylindrical tool with threaded pin). These defects are highly sensitive to the rigidity of the clamping technique used. When a narrow gap is left between the A356 plate and the backing plate, the material flow will be disrupted by pushing more material to the gap (forming a bulging at the bottom of the plate) and thereby causing insufficient upward flow of material from the tool pin. In some conditions with better clamping, this can be avoided by providing enough tilt-angle to the tool. Hence, the extended plunging of tool shoulder will close these tunnels by pushing the material to the voids.

A better understanding on this phenomenon is crucial to address and hence X-ray of the prepared plates were undergone. Fig 4-14 shows the X-ray radiograph film illustrating possible tunnel defects in the last passes in 500 rpm and 1000 rpm processed plates. In the X-ray radiographs, dark areas are the possible empty spaces internally. High magnification radiographs are also provided in Fig 4-14, illustrating the presence of empty spaces within the processed zone. These long strips can be present in two different ways;

- Tunnels within the processed plate
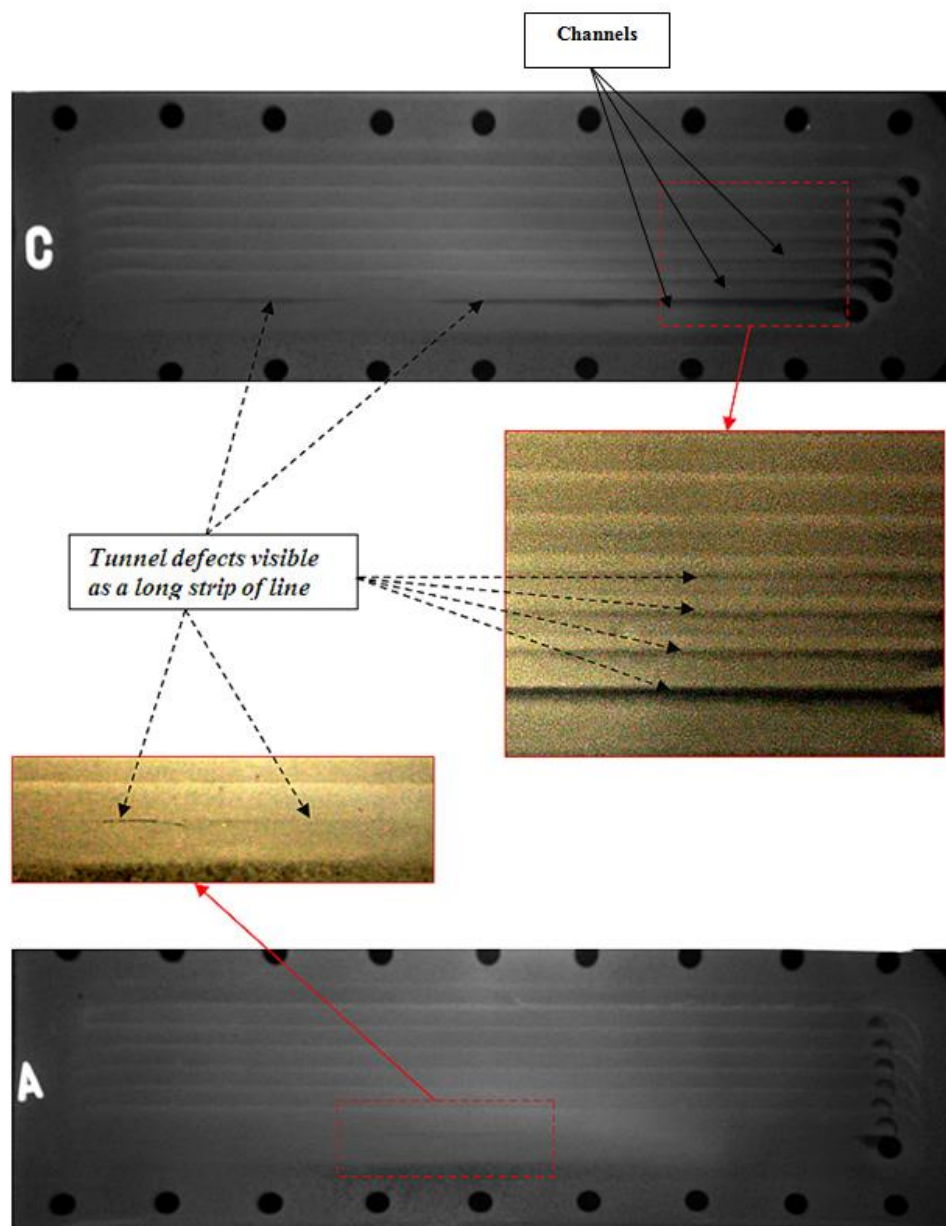- Extended tunnels to the top of the plate, forming a long channel of voids.

Figure 4-14   X-ray images showing the presence of tunnel defects within the processed zone at ω=500 rpm (A), and ω=1000 rpm(C)

The macrograph shows the formation of tunnels within the processed zone, just underneath the shoulder induced flow region. These tunnel grows, depending on the rigidity that clamping system and tilt angle, hence forming channels, which can be observed on the top of the processed plates as seen in figure 4-15.
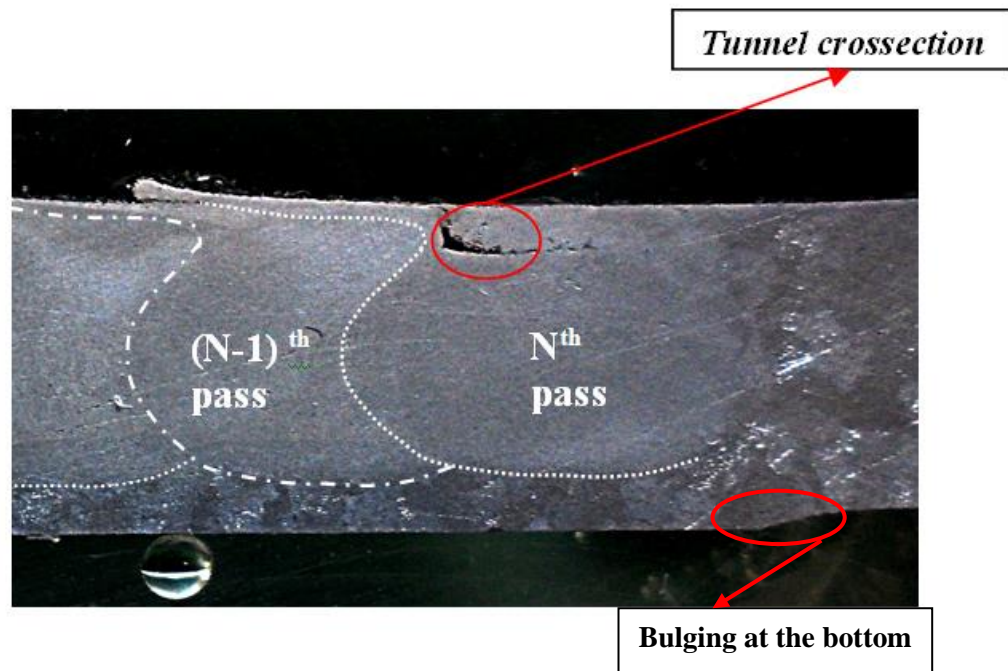

Figure 4-15   *Macro Image highlighting the multipasses and tunnel formation within the processed zone at ω=710 rpm*

In normal conditions of MP-FSP, the tunnel formation in the previous pass will lead to much bigger tunnel in the next pass. We have observed that, the material flow during FS passes has a tendency to fill the void left by the previous passes, and hence when it comes to the final FS pass, a channel formation was left over. The X-ray image of plate C in figure 4-14 shows how the tunnel grows with the passes. Macro image observed from another plate is shown in figure 4-15 showing the presence of void close to the shoulder induced flow region. Macro analysis was carried out before the tensile sampling, to investigate on the size, shape and tunnel defect in the processed zone. These defect formations were later on nullified by providing better clamping and tilt angle.

4.3.2 Macro analysis

It is good to define the area of RFM and TMAZ region, in order to define the pin overlapping distance. Aforementioned, RFM region at lower tool rpm, has been observed of occupying half of the nugget. In the present study, an overlap distance of 1mm was selected, in agreement to the previous observations on SZ overlap characteristics. Series 1 experiement was carried out with an overlap of 0mm, which even created sufficient SZ overlap (Fig 4-1).

Fig 4-16, shows the macrographs of FS-multipass samples under various process conditions. All the samples were processed at constant traverse speed *(v =56 mm/min)* and tilt angle *(θ = 2.5⁰)* under varying tool rotation speeds. Fig 4-17a to 4-16c, shows the cross section of FS-multipass conditions with normal overlapping conditions, where the advancing side of the N+1th pass (next pass) is overlapped over the Nth pass(previous), thereby creating a processssed zone which is dominated by the advancing side flow features. The above mentioned RFM region and upflow features are visible along the cross section (Fig 4-16a to 4-16c). Apart from the upflow, considerable bulging-down of the plates were observed at lower rpm, which results in tunnel defect close to the shoulder induced flow region (Fig4-16a&b).

The width and height of the wedge can be seen increasing with increase in tool rotation speed. The upflow at lower rpm is very low, comparing with higher tool rpm. The upflow highlighted in Fig 4-16a – 4-16c are from FS processed zone with normal overlapping conditions, where the advancing side of the next pass overlaps with the retreating side of previous pass. In Fig 4-16c, red dotted curves demonstrates the upflow between 1st and 2nd passes at ω= 1000 rpm. However, the intensity of this upflow is not as severe on comparison with the wedging observed in the initial studies, processed with ω =1400 rpm. This clearly displays the effect of tool rpm on wedging formation, which results in the appearance of Insufficient Overlap (IO). Fig 4-16d is the crossection of plates processed with reversed overlap direction. And hence, the flow feature highlighted with yellow dotted curve, has different flow mechanism.

In this study, attempt was created in finding the effect of change in overlap direction to investigate on the resultant flow mechanism and its effects on mechanical behavior of the processed zone (Fig 4-16d). This *Reversed MP direction*, was carried out at 1000 rpm. Here the interpass location has features corresponding to the retreating side of the nugget, which look-alike the upflow in the normal multipass overlaps. Unlike the Upflow along the advancing side, this flow has downward direction, with Al-Si particles orientating downwards and hence the mechanical characteristics and fracture behavior also varies.
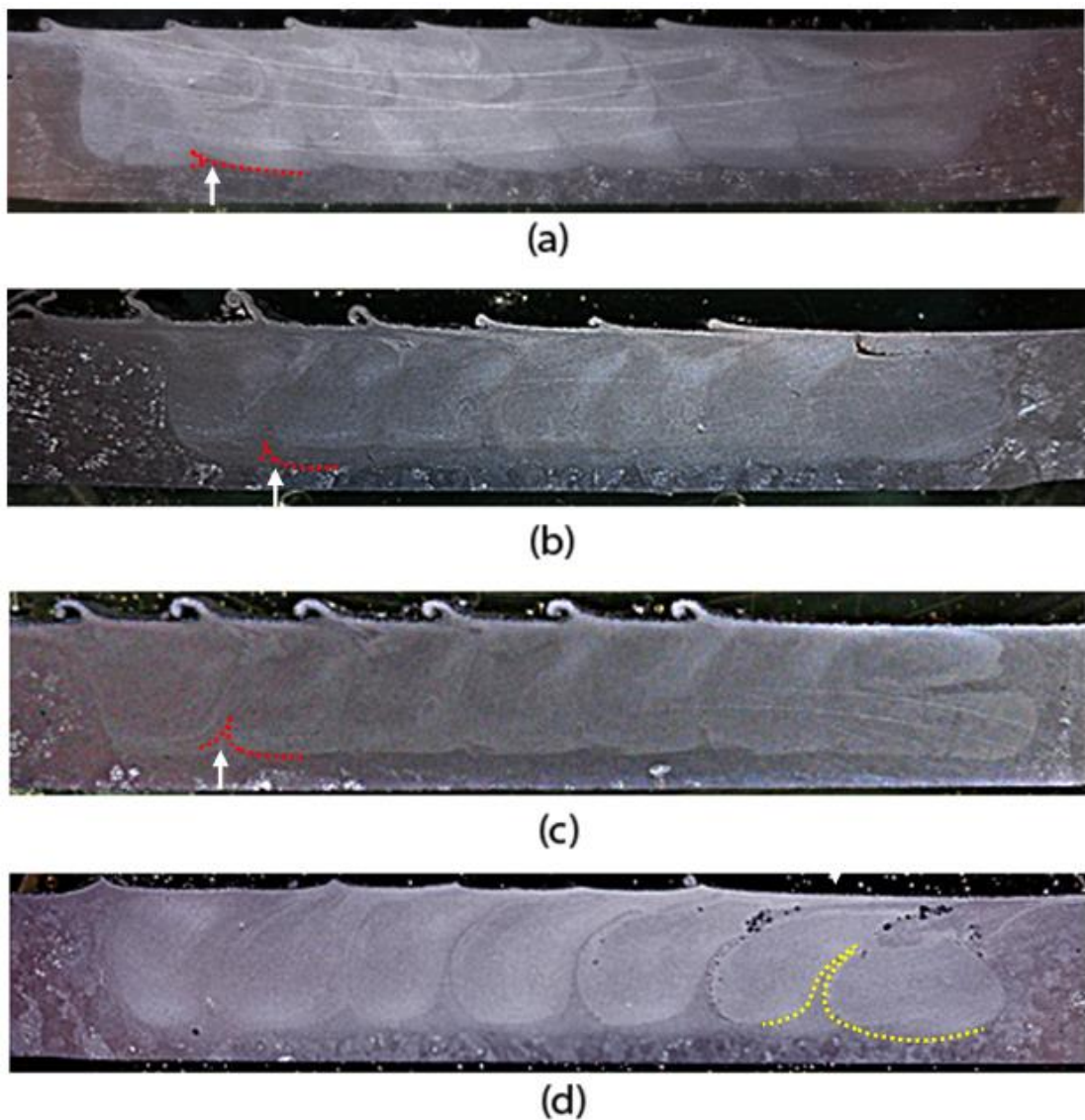

(a)

(b)

(c)

(d)

Figure 4-16. *Macro photographs of FS-Multipass samples; (a) 500 rpm and 56 mm/min, (b) 710 rpm and 56 mm/min, (c) 1000 rpm and 56 mm/min, and (d) 1000 rpm and 56 mm/min at Reversed MP direction*

Furthermore, in MP-FSP the less deformed region (formed by Rotational Flow Material, RFM) has secondary stirring action exerted by the next pass, thereby altering the microstructural features. This leads to closing of pores and further breaking of coarse eutectic particles, hence resulting in better mechanical properties.

Fig 4-17 is a graphical representation of 3 passes with lower tool rotation speed of 500 rpm illustrated to demonstrate the secondary stirring effect. Location marked as **1** in the 1st pass, which is initially the location of cluster of particles and porosity, was subjected to stirring action caused by the 2nd pass thereby depositing the particles at the retreating side of 2nd pass, which is marked as **2**. This process is repeated, creating a processed zone, which gets better mechanical properties from 1st to the last FS pass. The level of refinement caused by these repeated stirring action is a function of overlap distance. Hence raising the overlap distance from 0mm to 2mm could reduce the volume of RFM in the multipass cross section. This indeed will affect the mechanical behaviour of the processed zone.
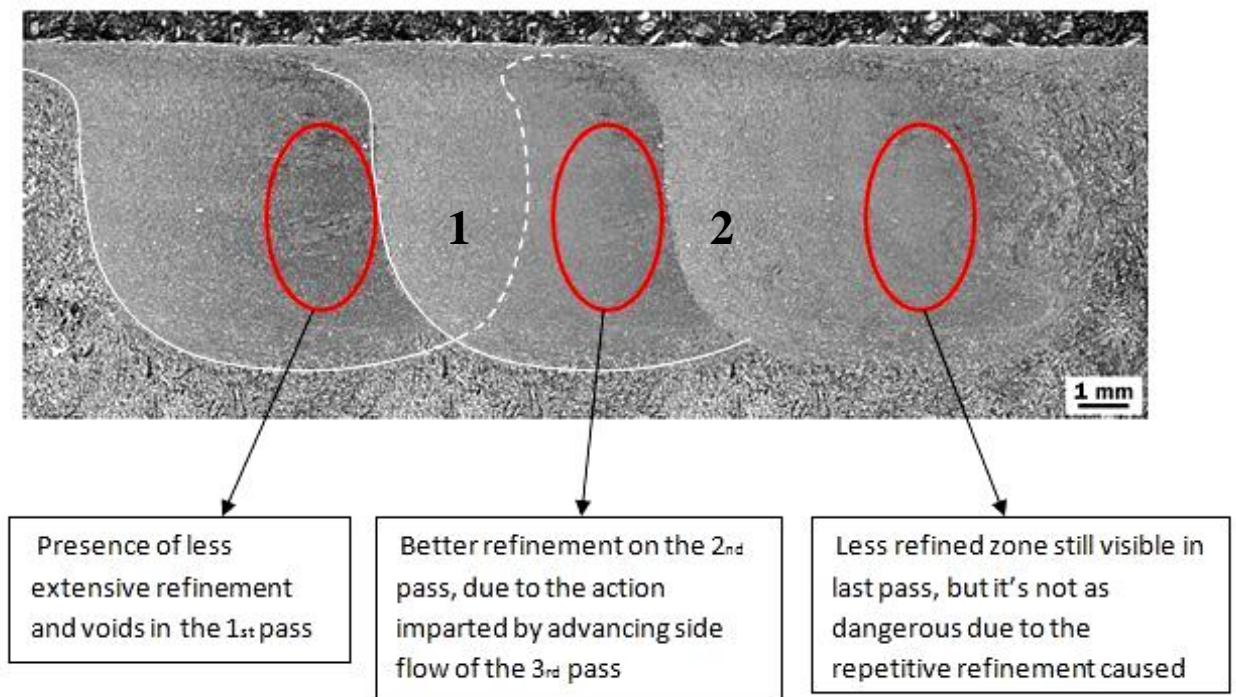

| Presence of less extensive refinement and voids in the 1st pass | Better refinement on the 2nd pass, due to the action imparted by advancing side flow of the 3rd pass | Less refined zone still visible in last pass, but it's not as dangerous due to the repetitive refinement caused |

Figure 4-17.   Graphical demonstration on how the repetitive passes contributed towards the micro/macro features of RFM using ω=500rpm.

4.4 Subsequent study – Mechanical Behaviour of Multipass FSPed materials

Although, some tunnels (empty spaces) were observed in the X-ray radiograph, it does not affect the mechanical properties evaluated of the main FS zone, as the tensile sampling was done from the nugget material for mechanical testing (Refer Section 3.3.1). Referring to the preliminary results, MP-FSP with 0mm overlap and higher tool rotation speed has shown poor elongation due to the intensity of wedged upflow. FS experiments were carried out with 1mm overlap conditions, focussing to eliminate the upflow feature at the interpass locations. Thus under sufficient overlap of 1mm, samples at lower tool rotation speed has been reported with significant improvement in elongation values. Batches of 6 tensile samples from each FS conditions were prepared to carry out the tensile analysis, as described in section 3.2. Due to the poor cast quality, few samples were broken well outside the FS zone and hence these samples with %elongation ≤ 0.2% are opted out of the graph, since the focus of this study is to investigate the tensile features of FS zone.
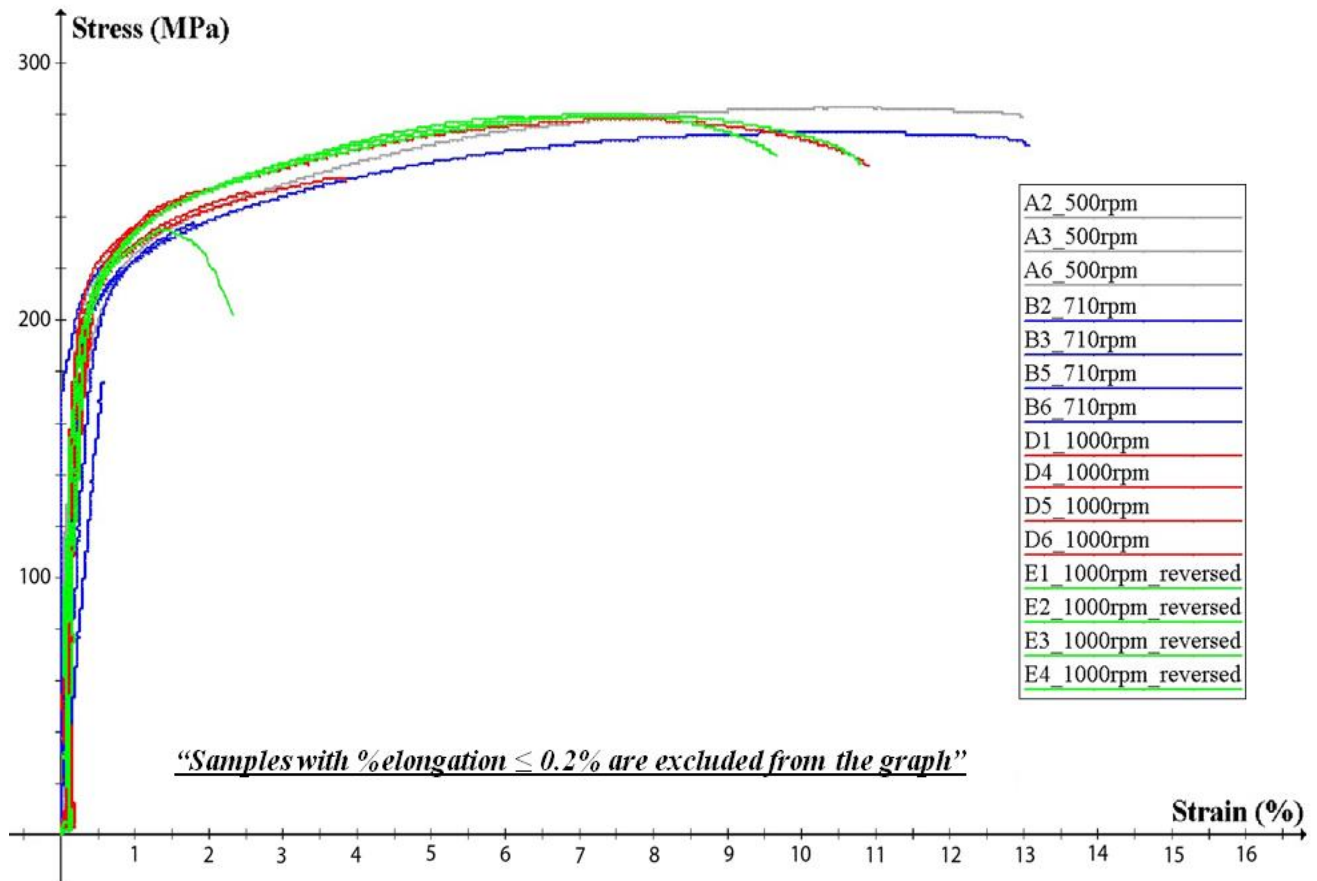

Figure 4-18 Engineering Stress Vs Strain graph

Engineering stress and strain curves of both normal MP-FSP and reversed MP-FSP sample after T6 heat treatment are shown in Fig 4-18. For A356- T6 heat treated samples, the 0.2% proof strength ($\sigma_{0.2}$) is ~210 MPa and elongation values ranges from 2 to 4 and UTS from 245 to 265 MPa. However, the cast plate used here for the present study has been observed with very poor mechanical UTS values of ~180 MPa and elongation of less than 1%. Despite of the poor mechanical behaviour of these cast plates, while FS processed, has shown significant advancement in the UTS (250-285 MPa) and elongation (3–13%) values. Considering the interest of the current research, based on location of tensile fracture, the samples broken outside of FS processed zone (broke in the as-cast material) are opted out of the graph and chart.

4.4.1 Tensile Properties affected by tool rotation speed

Fig 4-19 displays the fracture strain of all the processed samples. As can be seen, 6 batches of samples were undergone tensile analysis from each processed plates, where batch 6 is from beginning of FS run on the plate and batch 1 is from locations, at the end of FS run (Refer Section 3.3.1). FS samples at normal multipass direction conditions either with lower rpm (500 rpm & 710 rpm) or with a higher rpm (1000 rpm) has shown higher level of scatter, with elongation values obtained.

Either 1 or 2 samples among the 6 batches has given the highest elongation values, however the remaining samples failed to show the consistency in elongation and UTS values. The intensity of scatter and average elongation can be observed in Fig 4-19. For, samples processed at 500 and 710 rpm are showing highest scatter (5.1 and 5.2), and the average elongation is very low for 500 rpm. However, on increasing rpm to 1000 rpm, the scatter can be observed to be reduced (3.9) and a slight increase in average elongation from the low rpm can be seen. On reversed MP-FSP, the scatter observed is very low (3.2) and there is a better stability to the The strain gauge –extensometer did not provide accurate measurement in the initial largely elastic range. For samples fractured with low strain value position - strain curves are used and the initial elastic strain of 0.3% has been given (Appendix F).
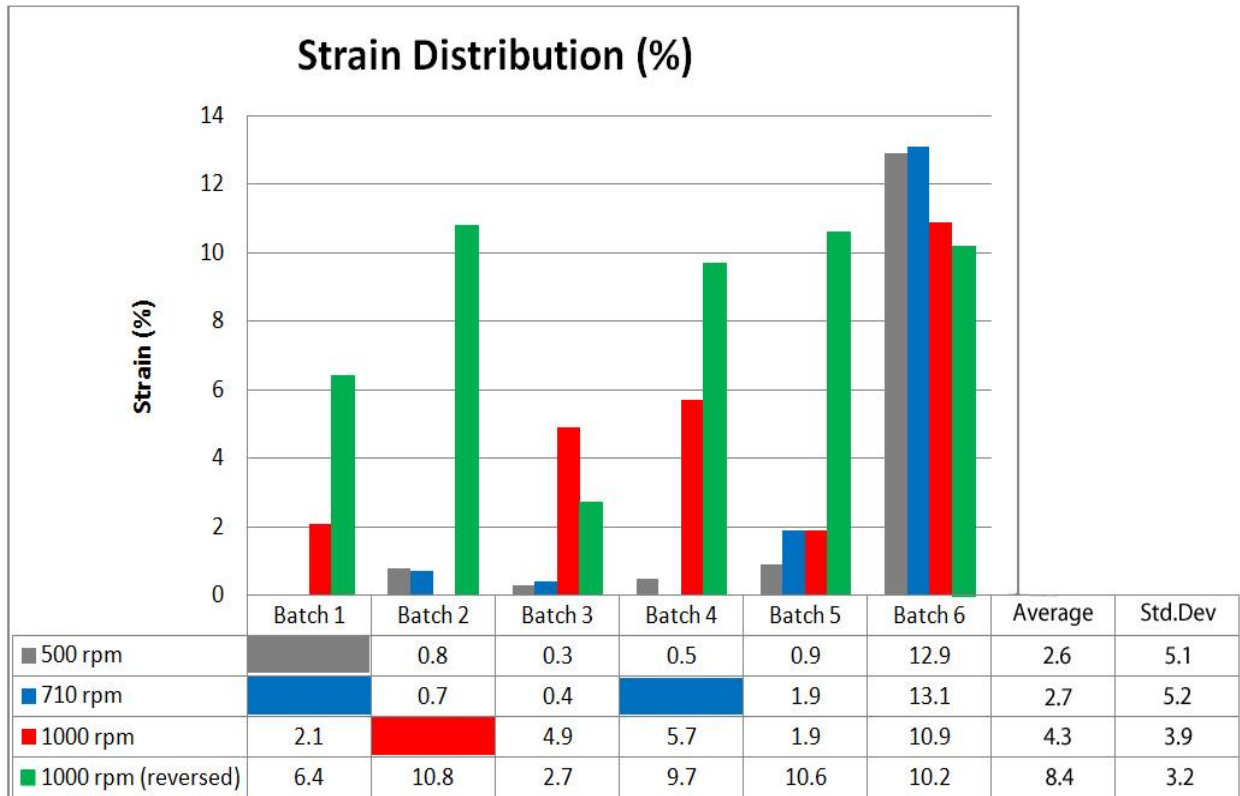
Figure 4-19. Engineering strain distribution.

However, the FS samples with reversed multipass direction have produced better consistent elongation and UTS values, as can be seen in the chart (highlighted with green bars). The scatter is reduced to 3.2 with an average elongation of 8.4%, which is comparatively much better than the samples processed under normal direction.

4.4.2 Reasons for the Scatter; from failure analysis

The improved FSP parameters, has produced better cross sections of multipass MP-FSP samples in Series 3 exeperiments. The upflow reported in the previous experiements were eliminated via 1mm pin overlap and tool rpm. Despite of this improvement, fracture has still been spotted at the interpass region or closer to interpass region, between the passes. And the reason for this phenomenon is comprised of several FS flow related mechanisms. Tables 4-1 to 4-4 show the results of failure analysis on the MP-FSPed samples.

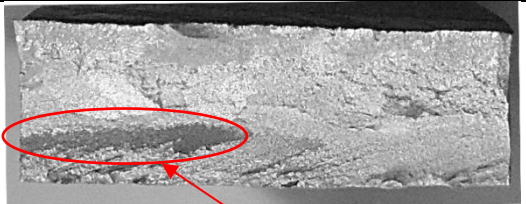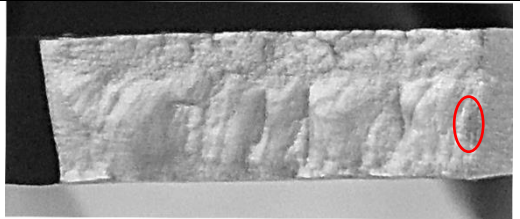***Table 4-1.*** *Fracture analysis on FS sample with ω= 500 rpm, v= 56 mm/min and θ=2.5º.*
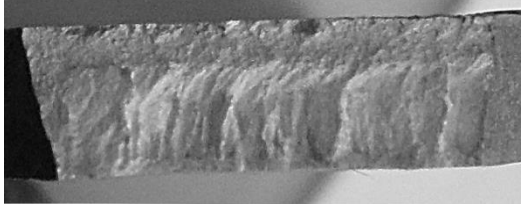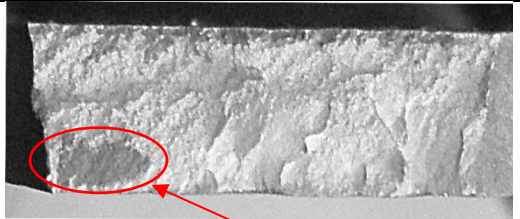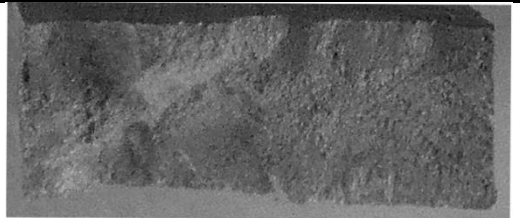
Sample A-500	Fracture (multipass location)	Strain	Macro
A1			BROKEN OUTISE THE PROCESSED ZONE
A2	1	0.8	
A3	6-7	0.3	*IH oxide film*
A4	1	0.7	
A5	1-2	0.4	*IH oxide film*
A6	4-5	12.9	

Table 4-2. *Fracture analysis on FS sample with ω= 710 rpm, v= 56 mm/min and θ=2.5º.*
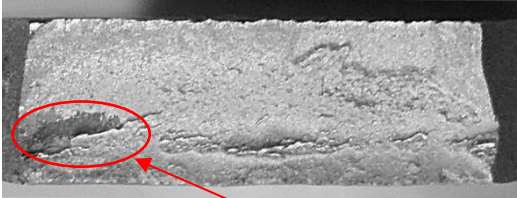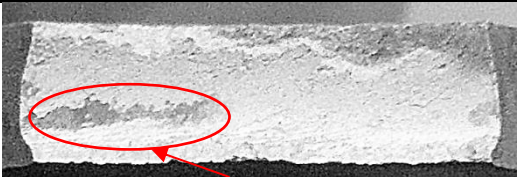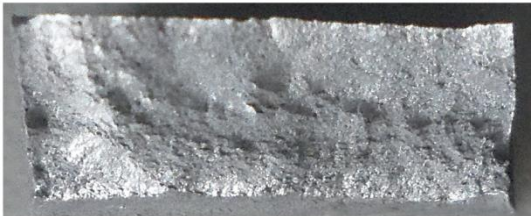
Sample B-710	Fracture (multipass location)	Strain	Macro
B1			BROKEN OUTISE THE PROCESSED ZONE
B2	1-2	0.7	 *IH oxide film*
B3	1-2	0.5	 *IH oxide film*
B4			BROKEN OUTISE THE PROCESSED ZONE
B5	1-2	1.7	 *IH oxide film*
B6		13.1	

Table 4-3. *Fracture analysis on FS sample with ω =1000 rpm, v =56mm/min and θ=2.5°.*
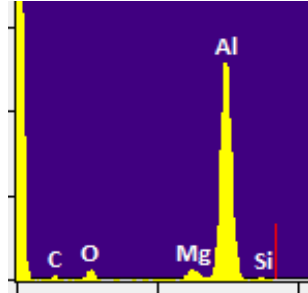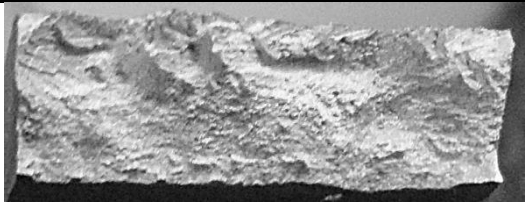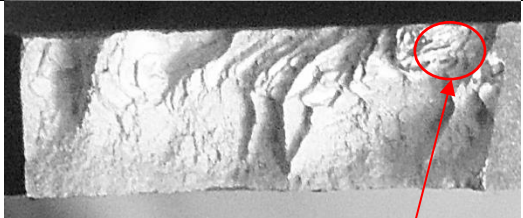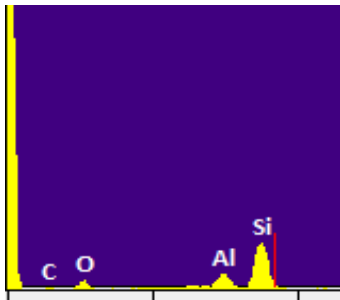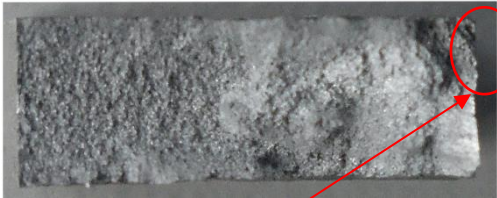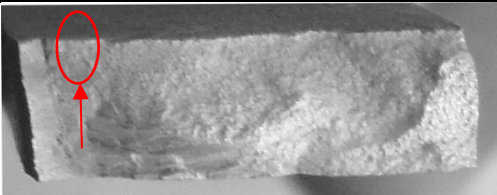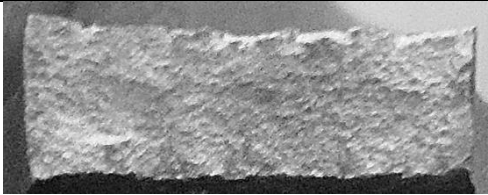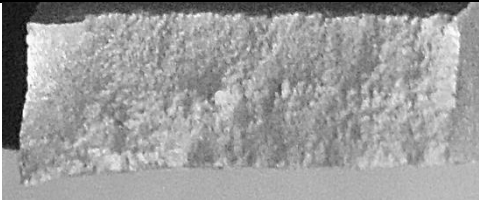
Sample D-1000	Fracture (multipass location)	Strain	Macro
D1		2.1	*Internal Oxide Films*
D2			**BROKEN OUTISE THE PROCESSED ZONE**
D3	3-4	4.9	
D4	4-5	5.7	
D5	1	1.9	*Internal Oxide Films*
D6	2-3	10.9	

Table 4-4. *Fracture analysis on Reversed multipass direction FS sample with ω= 1000 rpm, v= 56 mm/min and θ=2.5º.*

Sample E-1000	Fracture (multipass location)	Strain	Macro
E1		6.4	*Casting rubbish*
E2	5&6	10.8	
E3	3-4	2.7	
E4	5&6	9.7	
E5	6	10.6	
E6	3	10.2	*Casting rubbish*

As in the Tables 4-1 to 4-4, the fracture surface observed are different from one another and various flow and process mechanisms are contributing these fracture surfaces. The analysis on the fracture surface produces 4 major findings, which are explained below.

4.4.2a Incomplete Healing of Oxide Films

Among the entire batch of samples, A3 and A5 (processed at 500 rpm) produced the least elongation. On a closer observation, oxide peaks are observed as detailed using SEM/EDS in these samples resulting in very low elongation of ≤0.4%. The thermomechanical reason for this failure is illustrated in Fig 4-20.

Consider the tool rotation speed = 0 rpm, which means no stirring action is taking place forward motion of tool would leave a large tunnel behind. However, once when tool rotates (inducing stirring action), the material flows around the tool pin and gets deposited behind the pin towards the advancing side of the SZ. However at lower tool speed (ω = 500 rpm), due to the smaller stirring volume and less stirring action the oxide which is initially present on the tunnel wall surface, will not be broken down to smaller particles and finally it gets deposited along the advancing side of the nugget, which is in agreement to the explanation given in Section 4.2. For the ease of reference, this phenomenon will be named as Incomplete Healing (IH). The size of IH oxide film varies with tool rpm. These oxide films are broken down to microns at higher tool speeds due to higher degree of disruption and even distribution around the SZ. And hence, higher tool speed causes complete healing of oxide films. The deformation and temperature at higher tool speed is sufficient enough to break the oxide films to undetectable sizes.

Later, on exposed to high constant temperatures during heat treatment (which has been performed to create T6 conditions), the oxide films trapped (locally along the "tunnel") within the nugget, changes its appearance and looks black. These Incompletely Healed (IH) oxide films were observed closer to any of the 4 faces of solid sample. Despite of the presence of IH oxide films on the fractured samples processed at 710 rpm, its impact on elongation is reduced slightly. The samples were analysed to be broken at elongation ≤0.6 to 1.7%.
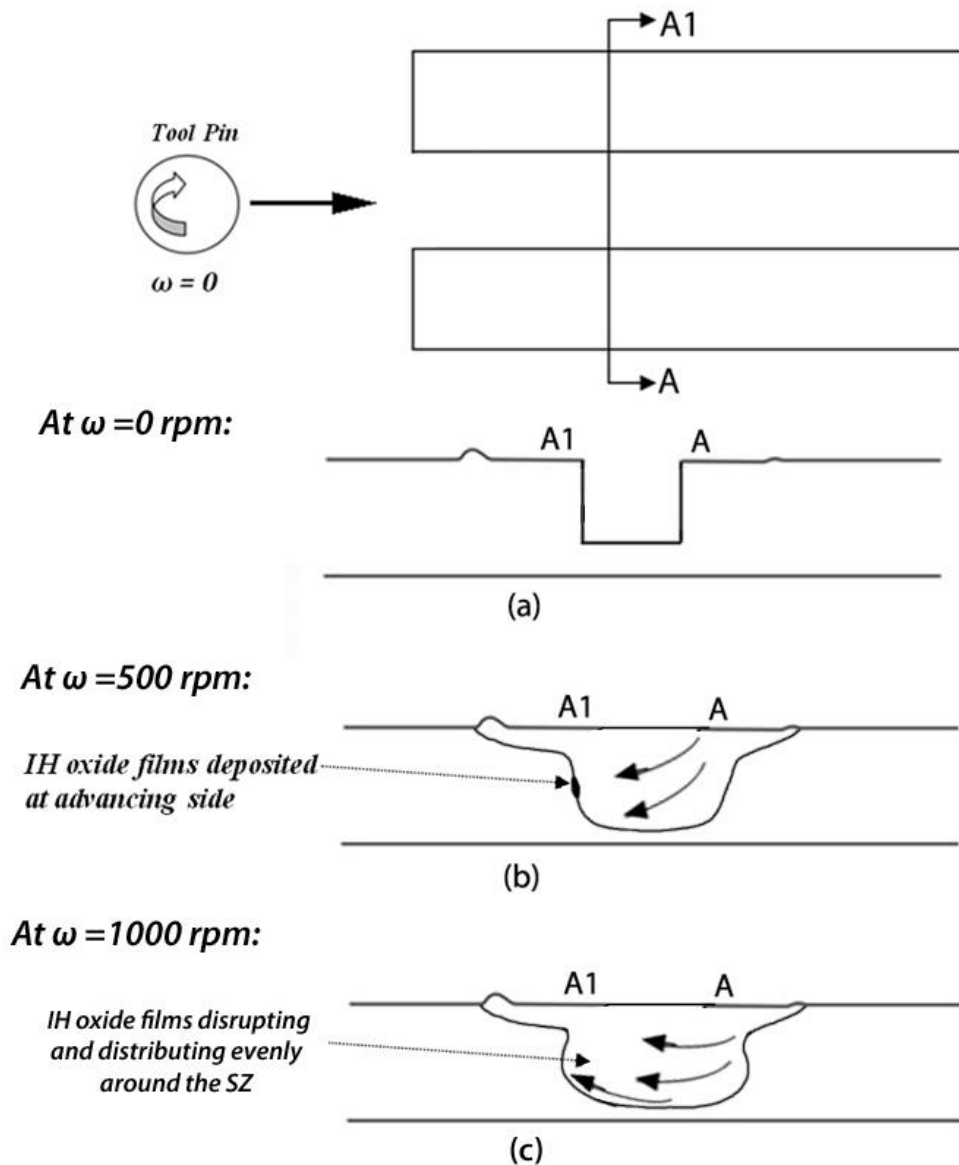
Figure 4-20 *Graphical Illustration explaining IH oxide films: (a) Top View and crossection showing the pin profile at ω=0 rpm leaving an empty channel on the plate. (b) at ω=500 rpm, the empty space is occupied by the stirring action of the tool and (c) at ω=1000 rpm, a better deformation which leads to complete healing of oxide films.*

The size of IH oxide film ranges from 1 to 4mm within the tensile strips for lower tool rotation speeds and it is almost to nothing at higher tool rotation speeds. Figure 4-21 defines the extent of IH oxide film observed, which varies with tool rotation speeds. Hence it is clear that the increase in tool rpm (higher stirring action) has disrupted and completely healed the initial oxide films obtained within the material.

Figure 4-21. *Macrograph showing the effect of tool rpm on breaking up of IH oxide film at lower rpm, observed towards the advancing end of the nugget.*

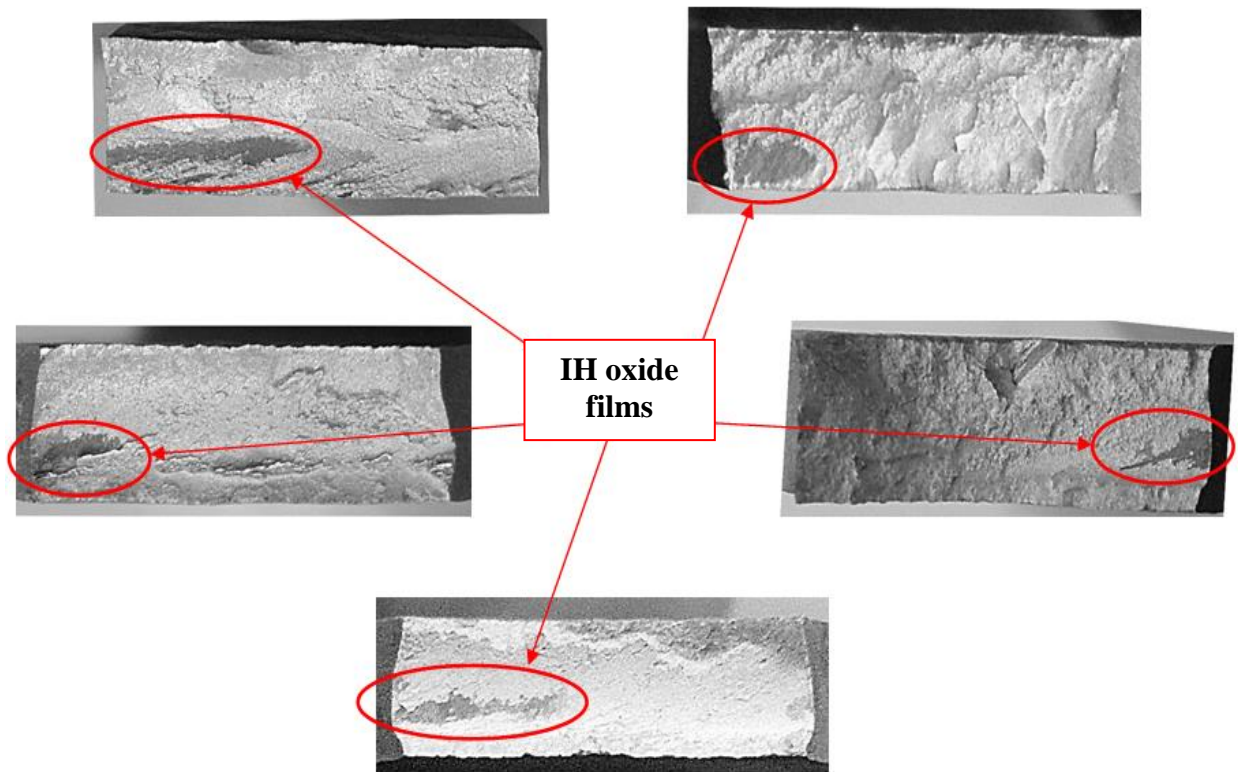On micro analysis, few cracks were found to be initiated from the pores visible within this region. Fig 4-23 shows the pores observed at the locations of RFM from the plate processed with ω = 500rpm. These defects are spotted at locations of RFM, at bottom, mid region of nugget and towards the shoulder flow region. The orientations of particles are observed to be following along the thin layer of Swirl reported in Section 4.2 at the bottom of nugget, towards the advancing side. In the Fig 4-23, the particles orientated close to the pores, can be seen extending towards the left hand side (which is the advancing side), and showing a tendency to orientate upwards. In agreement to the behavior of these locations from Section 4.2, the flow patterns visible on the macro image can be summarized as the result of clustering of fine, coarse particles and porosities observed within the nugget at lower rpm conditions.
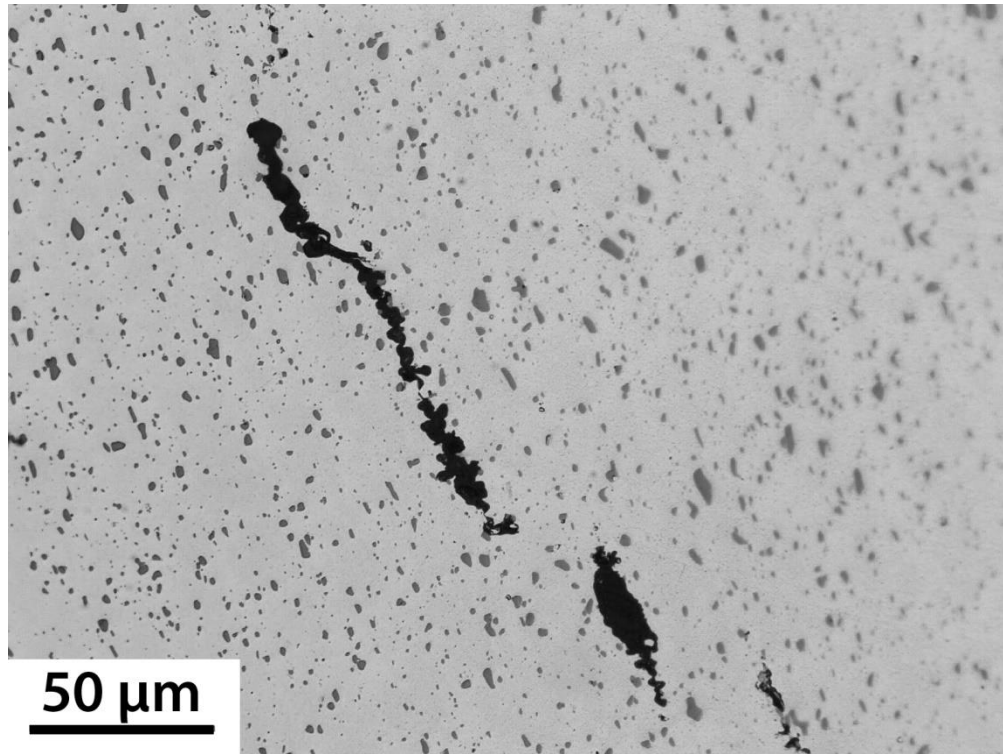
Figure 4-23.   *The micrograph from RFM region showing the crack originating from the pores at ω =500 rpm*

As can be seen in Table 4-3, samples with higher tool rotation speed of 1000 rpm, has highly homogeneous fracture surface and hence has shown distinct features in comparison with lower tool rotation speed. The major reason for this is the IH oxide films in microstructure at lower tool rotation speed (section 4.4.2a). The fracture surfaces show a clean profile, and the IH oxide films were observed to be broken down into few microns. Figure 4-24 shows the Scanning Electron Microscopy images from the fractured surface demonstrating highly ductile profile obtained at high tool speed and brittle patches observed at the IH oxide film at lower tool rotation speed.
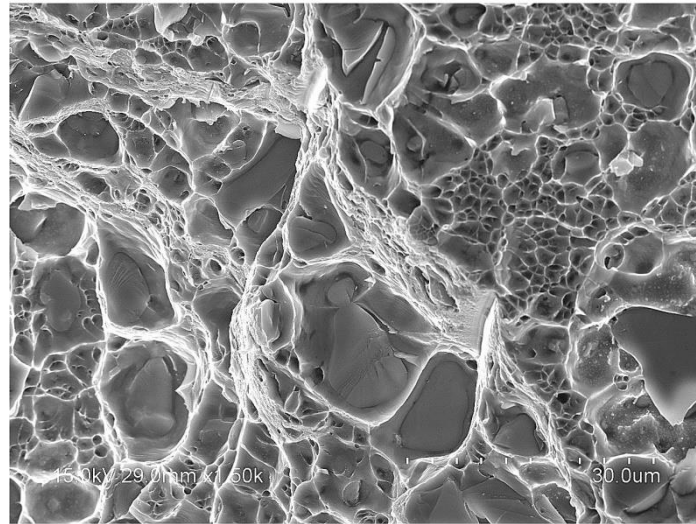
(a)
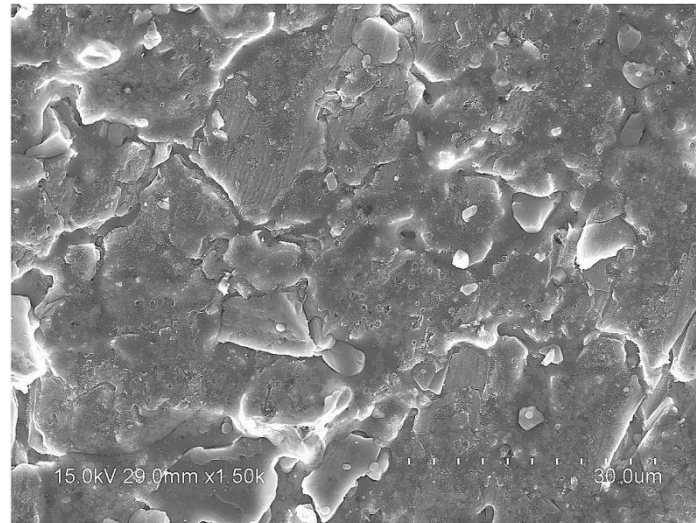
(b)

Figure 4-24.   *SEM images: (a) Highly ductile fracture surface from A356 plate processed with ω=1000 rpm, (b) IH oxide films observed at the location of FS defect from a sample processed at ω=500 rpm.*

4.4.2b Flexible Vertical Bands

Again with samples processed at 500 rpm, comparatively different fractured surface was observed. In Table 4-1, the fracture surface on A2 and A4 can be seen as flexible vertical bands, bended at the top region along the flow travel direction. And these samples were observed to be of poor elongation of ≈ 0.7 to 0.8%. Referring back to Fig 4-8 the fracture path can be defined, as a function of RFM region explained. The vertical flexible bands are observed at mid nugget regions

and the bended band along the travel direction is observed at locations, close to shoulder induced flow. Despite of the 1mm overlap, a portion of RFM region is still exposed in the MP-FSP crossection, which forms this flexible vertical banded fracture path. The clustering and orientation of coarse, fine and pores observed at this location thus forms the banded structure. And this feature was not observed in any of the samples processed at higher tool rpm, as the volume of RFM region reduces towards the retreating end of the nugget. Although, the presence of very small IH oxide films are also visible for samples A2 and A4, the crack has been induced by the flexible vertical bands observed.

4.4.2c Internal Oxide films

As explained before, the presence of IH oxide films were not visible at processed zones, obtained with 1000 rpm. However, EDS analysis on 2 of the samples (D1 and D5, which has produced low elongation of ≈ 2%), a slight peak of oxide content has observed (Table 4-3). This is in agreement to the explanation given for IH oxide films, where at higher tool rpm; the oxide films are broken into fine fragments and are deposited internally. The presence of internal oxide films are also spotted on sample E3 (with reversed overlapping direction) which results in elongation of 2.7%.

4.4.2d Mould wash Impurities

As observed in the fracture surface (Table 4-4) of reversed MP-FSP condition, the presence of casting defects within the SZ is illustrated in the figure. Figure 4-22, shows the macro/micro mapping of casting defects found within the nugget and across the fractured surface. These might have trapped into the A356 plate while coating the mould with Mould wash. And later the large chunks were fragmented by the stirring action of tool and desposited along the shoulder zone at the retreating side. This feature appears as shining dirt particles in the fractured surface fig 4-22a.
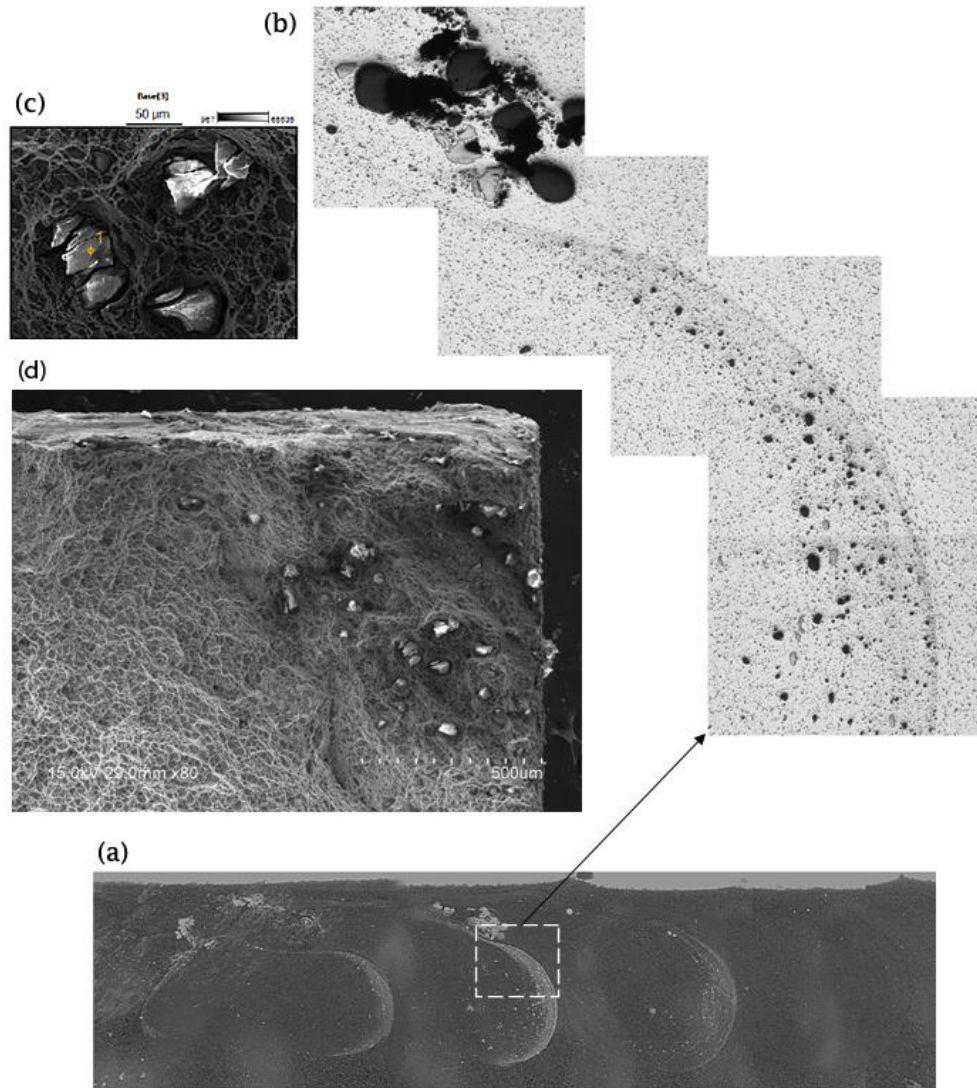
Figure 4-22.   Presence of impurities at the interpass location of reversed multipass direction : (a) macrograph of multipass, (b) Panoramic image investigating the distribution of impurities along the retreating side, (c) & (d) high magnification images captured using Scanning Electron Microscope.

This was observed only in the samples processed at higher tool rotation speed, with reversed multipass direction. Even though, large chunks of foreign particles, Fig 4-22c & 4-22d are present in the fracture zone; the samples show better stability in the tensile properties. Apart from this feature, on a scanning electron microscopy image, the surfaces look highly ductile (Fig 4-22d). And again, this phenomenon clearly demonstrates how the flow mechanism behaves at the

retreating side of the nugget, in agreement to the RSM and RFM flow, defining the FS flow mechanism.

Chapter 5

CONCLUSIONS

MP-FSP experiments have been conducted successfully and the initial objectives introduced in Chapter 2 have been achieved with the following conclusions:

1. At high tool rotation speed (1400 rpm), less deformed cast material with a degree of Si particle aligned vertically up has been identified in the interpass region, despite of both zero and sufficient pin overlap. This is the result of a severe cast material wedging up from below the pin on the advancing side. This wedging and thus Si particles alignment provided as easy path for fracture during tensile testing, thus resulting in low fracture strain.

2. Wedging decreases with decrease of rotation speed and at 500 rpm, wedging was basically eliminated, due to the elimination of the upward flow during FSP. The Si particles along the previously stirred structure at the interpass locations in reversed overlapping condition, was orientated downward and results in improved mechanical properties.

3. The various flow regions within the SZ, in a single pass FSP have been identified. Region of rounding flow material (RFM) was identified along the retreating side and extending downward towards the advancing side of the SZ. Clustering of coarse and fine eutectic particles along with porosities was seen at these locations. The area of RFM decreases with increasing tool rotation speed.

4. The RFM persist in the MP-FSP because RSM cannot overlap completely the RFM from previous pass. Thus micro pores from RFM aligned slightly upward resulting in poor fracture strain during tensile testing.
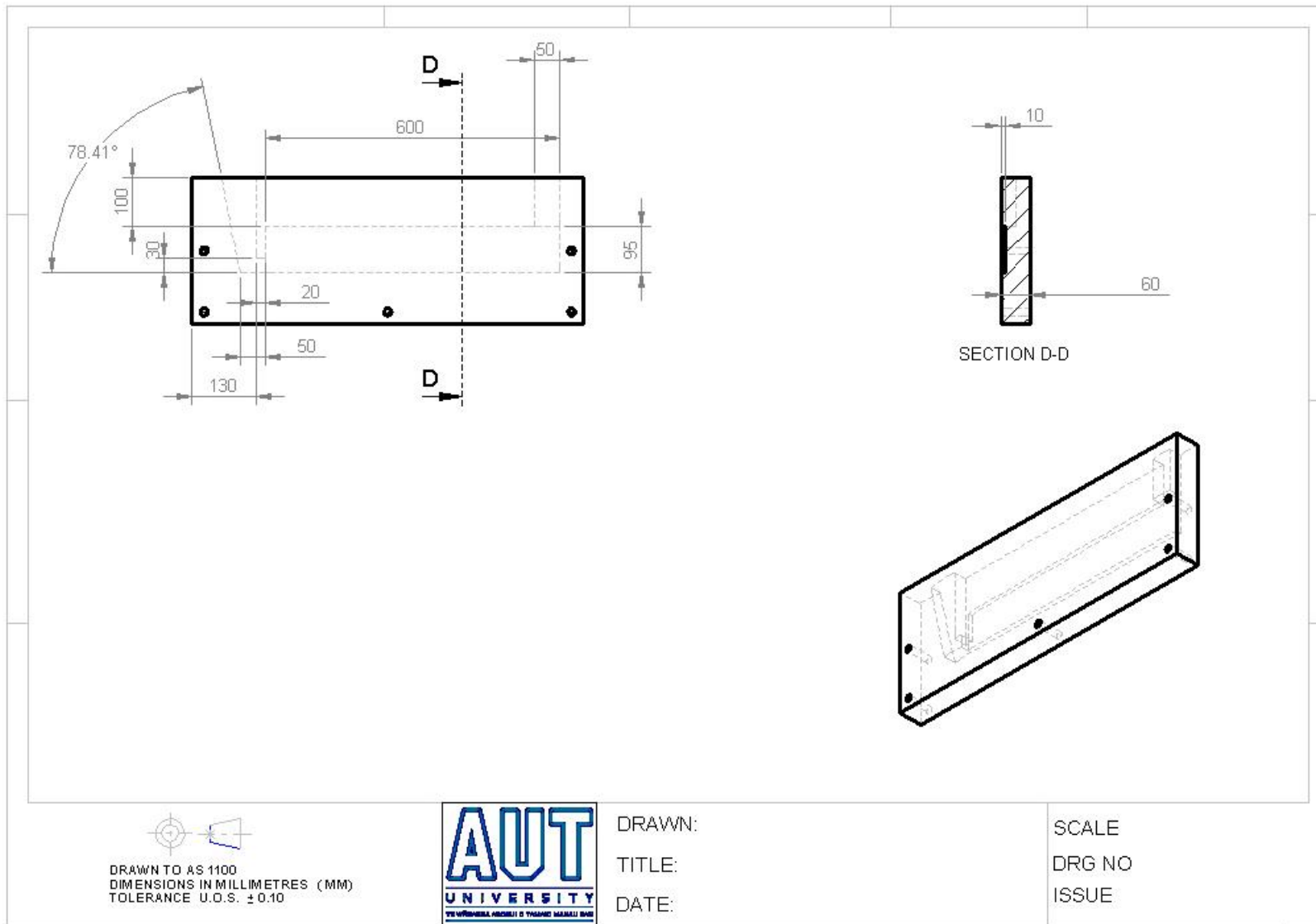
5. Detrimental effect of lower ω on oxide films within the SZ, towards the advancing side was observed. Less disruption and even distribution of oxide films were analysed due to the smaller stirring volume and less stirring action at lower ω rpm.

6. Considering the features of wedging, persisting RFM, oxide film, tool rotation speed, ω =1000 rpm have been found to be optimum resulting in the mostly elimination of these defects. Thus resulting in high fracture strain.

7. The reversed MP-FSP has been reported with better mechanical chracteristics and the scatter observed was comparatively very low in comparison with the normal MP-FSP conditions. Hence the technique of reversed MP-FSP is recommended over normal MP-FSP.
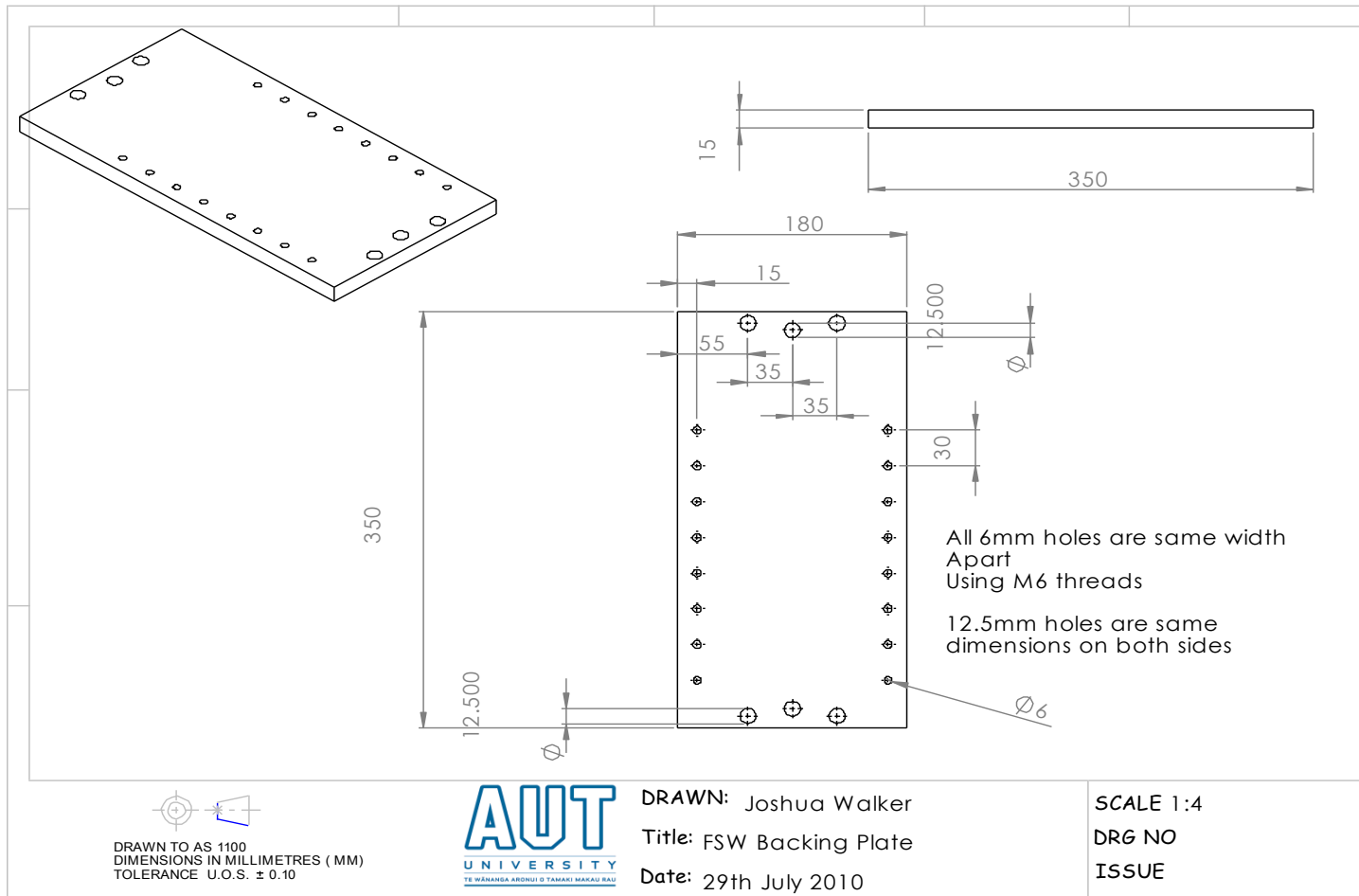
REFERENCE

1. Tiryakioglu, M. (2008). *Materials Science and Engineering A 497*, 512-514.

2. Ammar, H. R., Samuel, A. M., & Samuel, F. H. (2008). *International Journal of Fatigue 30*, 1024-1035.

3. Wang, Q. G., Davidson, C. J., Griffiths, J. R., & Creoeau, P. N. (2006). *Metallurgical and Material Transactions 37B*, 887-895.

4. De-Feng, M., Guo-Qiu, H., & Zheng-Fei, H. (2008). *International journals of Fatigue 30*, 1843-1850.

5. Sonsino, C. M., & Zeise, J. (1993). *International Journal of Fatigue 15*, 75-84.

6. Mishra, R. S., & Ma, Z. Y. (2005). *Materials Science and Engineering R 50,* 1–78.

7. Mishra, R. S., Ma, Z. Y., & Sharma, S. R. (2006). *Materials Science and Engineering A 433*, 269-278.

8. Ma, Z. Y. (2008). *Metallurgical and Materials Transactions A39*, 642-658.

9. Sharma, S. R., Ma, Z. Y., & Mishra, R. S. (2004). *Scripta Materialia 51*, 237-241.

10. Dabayeh, A. A., Xu, R. X., Du, B. P., & Topper, T. H. (1995). *International Journal of Fatigue, Volume 18, Issue 2*, 95-104.

11. Sabau, A. S., & Viswanathan, S. (2006). *POROSITY PREDICTION IN ALUMINUM A356 ALLOY CASTINGS*. Tennessee: Metals and Ceramics Division Oak Ridge National Laboratory.

12. Chen, Z., S, C., Gao, W., & Zhu, T. (2010). *Materials Science Forum 654 - 656,* 962-965.

13. MA, Z. Y., Sharma, S. R., & Mishra, R. S. (2006). *Metallurgical and materials transactions 37A*, 3323-3335.

14. Chen, Z. W., & Cui, S. (2009). *IOP Conf. Series: Materials Science and Engineering 4 012026.*

15. Lee, K., Kwon, Y. N., & Lee, S. (2008). *Engineering Fracture Mechanics 75,* 4200-4216.

16. Ni, D. R., Wang, D., Feng, A. H., Yao, G., & Ma, Z. Y. (2009). *Scripta Materialia 61*, 568-571.

17. Jana, S., Mishra, R. S., Baumann, J. B., & Grant, G. (2009). *Acta Materialia 58, Issue 3*, 989-1003.

18. Uematsu, Y., Tokaji, K., Fujiwara, K., Tozaki, Y., & Shibata, H. (2009). *Fatigue and fracture of Eningeering Materials & Structures,* 541-551

19. Wang, D. A., & Chen, C. H. (2009). *Journal of material processing technology 209*, 367-375.

20. Sato, Y.S., Kokawa, H., Enmoto, M., Jogan, S. (1999). *Metallurgical and Material Transactions A30,* 2429*.*

21. Mahoney, M.W., Rhodes, C.G., Flintoff, J.G., Spurling, R.A., Bingel, W.H. (1998). *Metallurgical and Material Transactions A29,* 1955*.*

22. Ma, Z.Y., Mishra, R.S., Mahoney, M.W., in: Jata, K.V., Mahoney, M.W., Mishra, R.S., Semiatin, S.L., Lienert, T. (Eds.), 2003. *FSW and Processing II, TMS,* 221–230.

23. A.P. Reynolds. (2000). *Science and Technology of Welding and Joining Volume 5, Issue 2,* 120-124

24. S. Cui. (2011). "Thermomechanics, material flow and microstructure evolution during friction stir processing of light cast alloys", Ph.D Thesis, AUT university.

25. Sun, J., Nelson, T., Sterling, C. (2005). *Scripta Materialia 52*, 135-140.

26. Johannes, L. B., Mishra, R. S. (2007). *Material Science and Engineering A 464*, 255-260.

27. Ma, Z. Y., Mishra, R. S., Mahoney, M. W. (2004). *Scripta Materialia., 50*, 931.

28. Ma, Z. Y., Mishra, R. S., Sharma, S. R. (2006). *Material Science and Engineering. A 433*, 269.

29. Jana, S., Mishra, R.S., Baumann, J. B., Grant, G. (2010). *Metallurgical and Materials Transactions A 41*, 257.

30. Nakata, K., kim, Y. G., Fujji, H., Tsumura, T., & Komazaki, T. (2006). *Material Science and Engineering A 437*, 274.

31. Santella, M. L., Engstrom, T., Storjoham, D. & Pan, T. Y. (2004). *Scripta Materialia. 51*, 237

32. Nascimento, F., Santos, T., Vilaca, P., Miranda, R. M. & Quintino, L. (2009). *Material Science and Engineering A 506*, 16-22.

33. Gandra, J., Miranda, R. M. & Vilaca, P. (2011). *Material Science and Engineering A 528*, 5592-5599
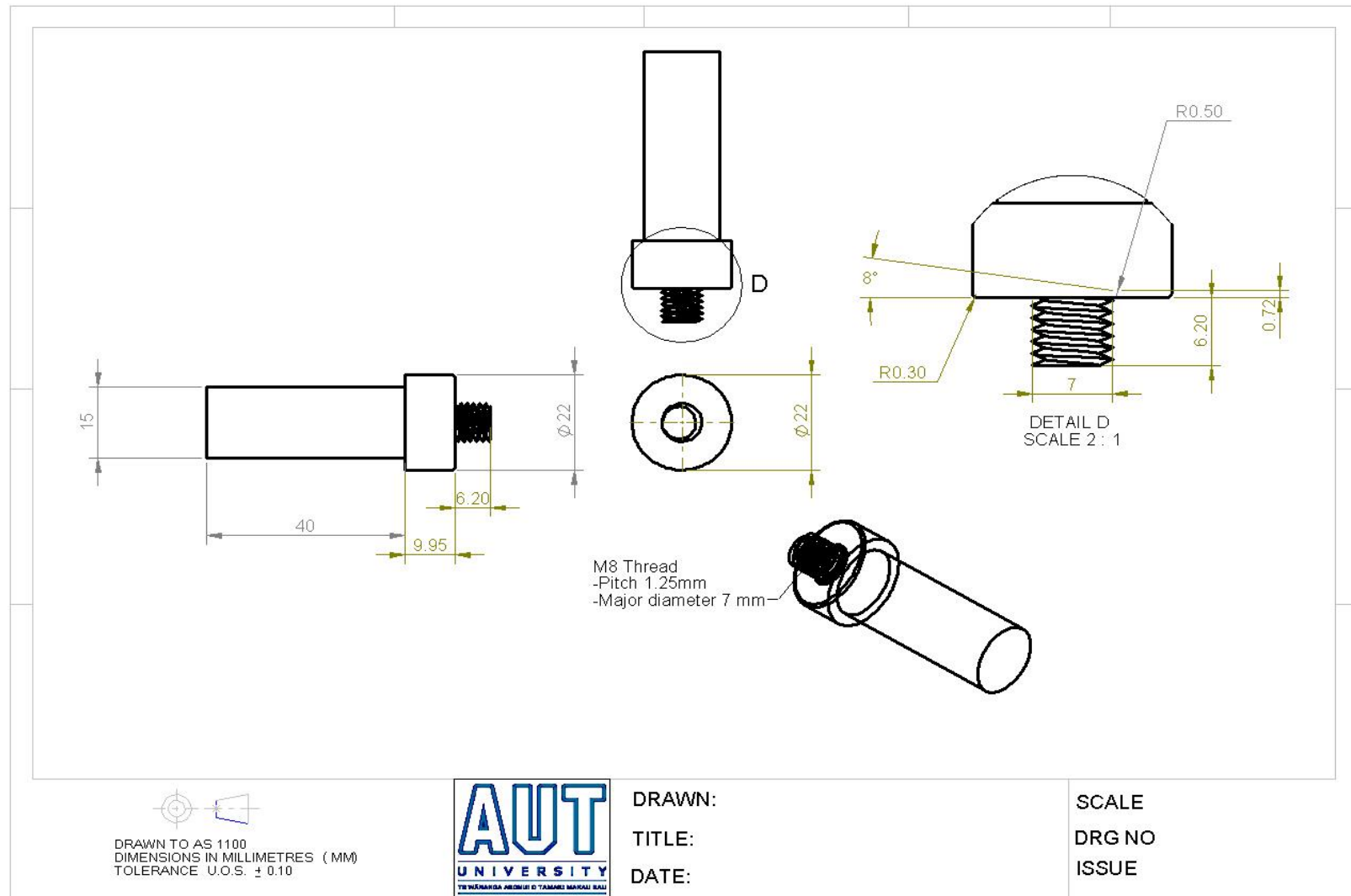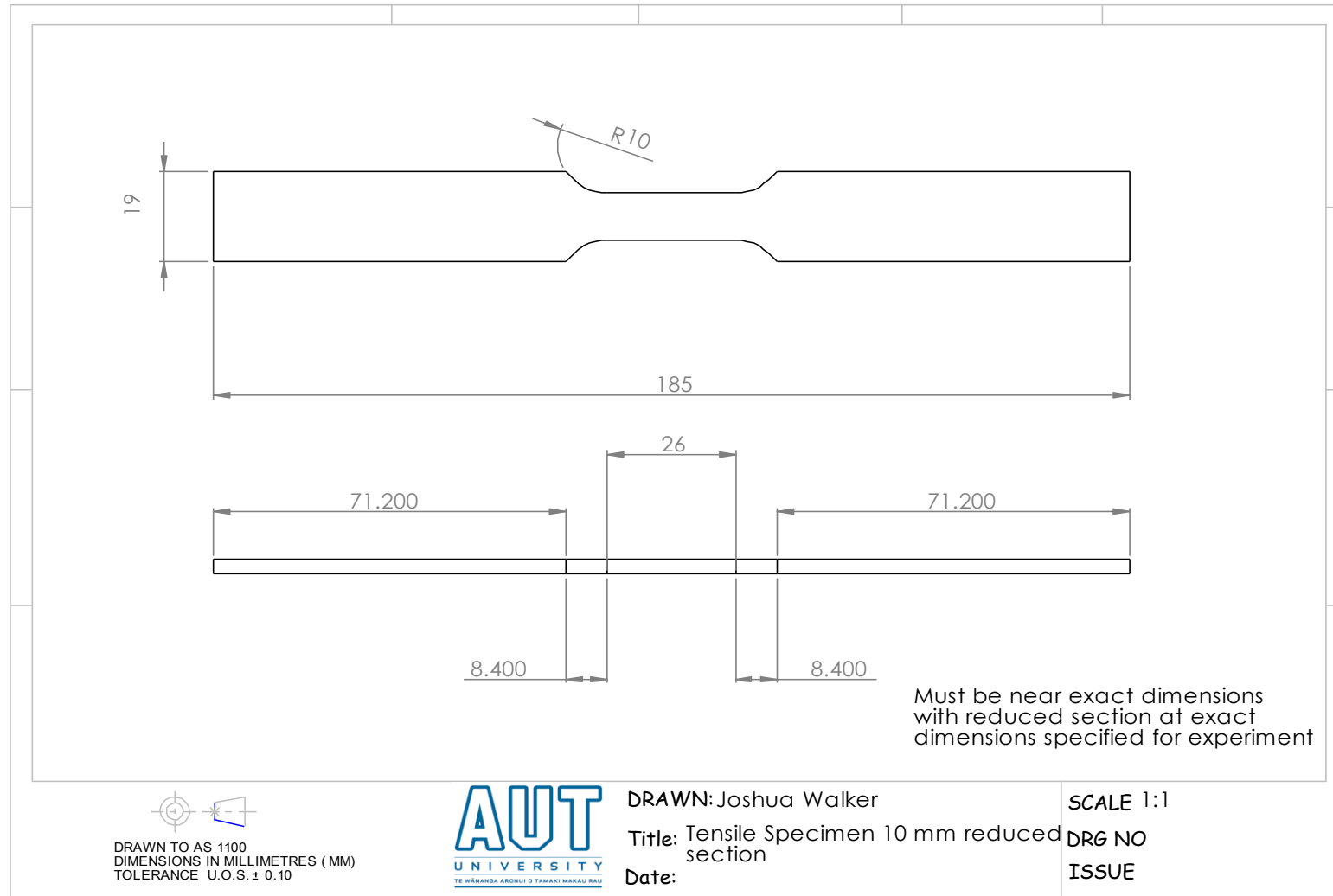
APPENDIX A – Casting Mold
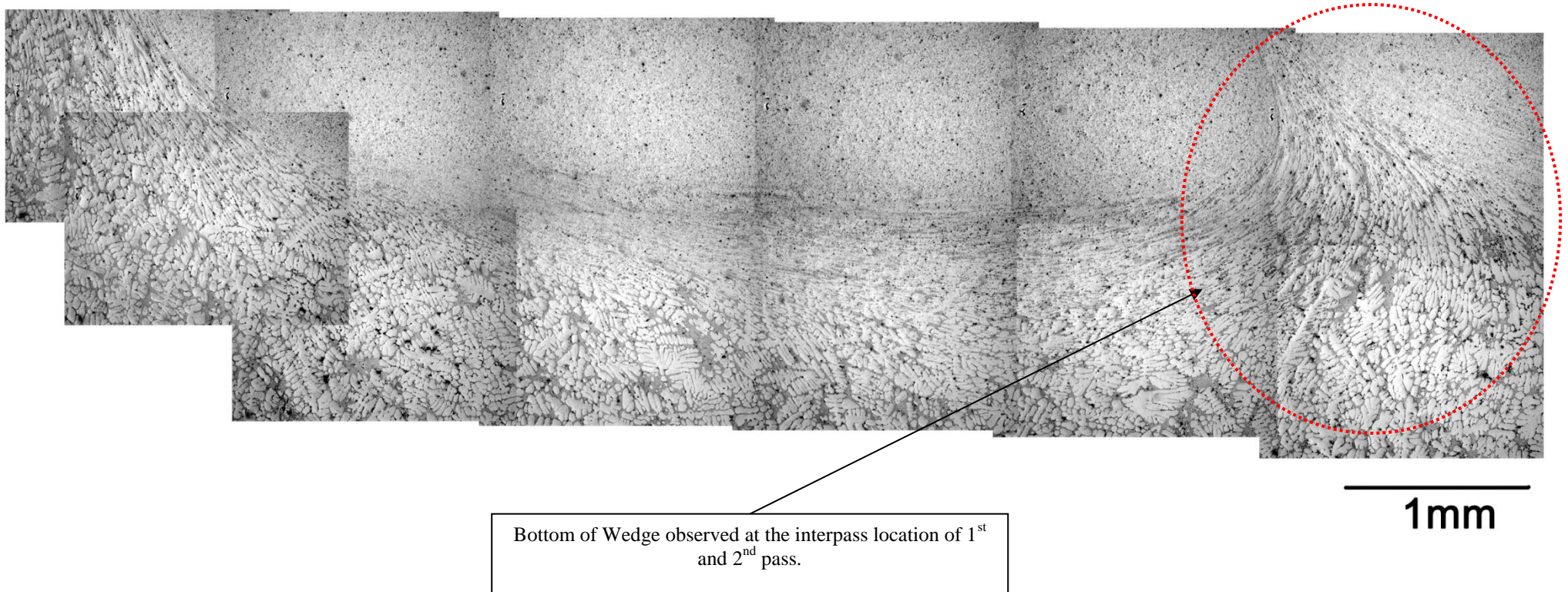
APPENDIX B – FSP Backing Plate with clamping holes

All 6mm holes are same width Apart
Using M6 threads

12.5mm holes are same dimensions on both sides

350

180

15

55

35

35

15

12.500

30

350

12.500

Ø6

DRAWN TO AS 1100
DIMENSIONS IN MILLIMETRES (MM)
TOLERANCE U.O.S. ± 0.10

AUT UNIVERSITY
TE WĀNANGA ARONUI O TAMAKI MAKAU RAU

DRAWN: Joshua Walker

Title: FSW Backing Plate

Date: 29th July 2010

SCALE 1:4

DRG NO

ISSUE

APPENDIX C – FSP/FSW Tool

R0.50

8°

R0.30

6.20

0.72

7

DETAIL D
SCALE 2 : 1

15

⌀22

⌀22

40

6.20

9.95

M8 Thread
-Pitch 1.25mm
-Major diameter 7 mm

D

DRAWN TO AS 1100
DIMENSIONS IN MILLIMETRES (MM)
TOLERANCE U.O.S. ± 0.10

AUT
UNIVERSITY
TE WĀNANGA ARONUI O TAMAKI MAKAU RAU

DRAWN:

TITLE:

DATE:

SCALE

DRG NO

ISSUE

APPENDIX D – Tensile Sample

19

R10

185

26

71.200

71.200

8.400

8.400

Must be near exact dimensions
with reduced section at exact
dimensions specified for experiment

DRAWN TO AS 1100
DIMENSIONS IN MILLIMETRES (MM)
TOLERANCE U.O.S. ± 0.10

DRAWN: Joshua Walker

Title: Tensile Specimen 10 mm reduced section

Date:

SCALE 1:1

DRG NO

ISSUE

AUT
UNIVERSITY
TE WĀNANGA ARONUI O TAMAKI MAKAU RAU

APPENDIX E – Panoramic Image on "Wedging"

Bottom of Wedge observed at the interpass location of 1st and 2nd pass.

Panoramic image formed from the bottom of the SZ, displaying the wedging of coarse particles at the locations of overlap, using very high tool rotation speed of 1400 rpm.

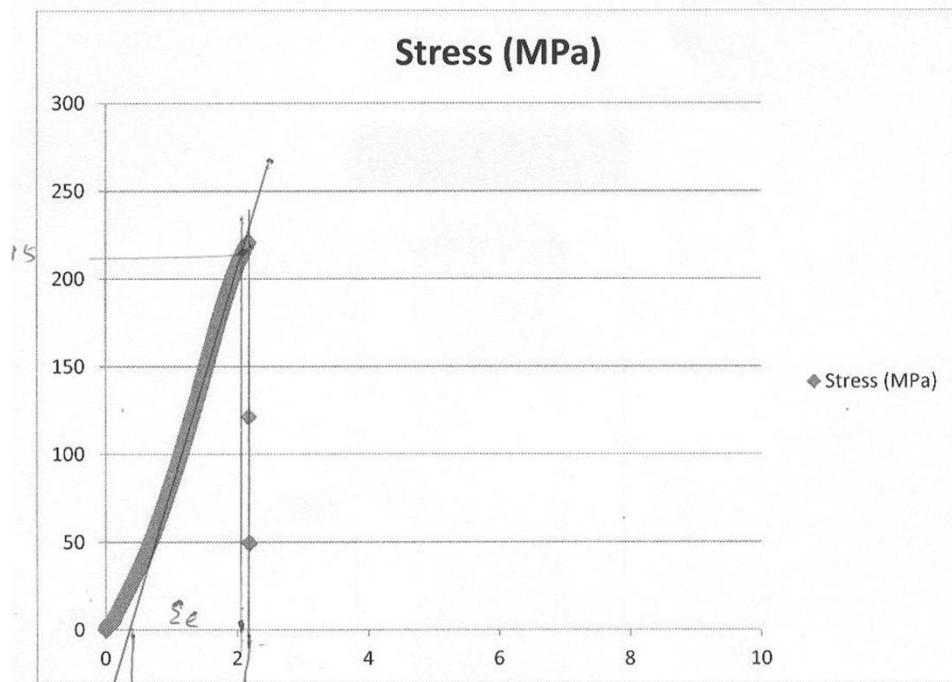## APPENDIX F – Position Vs Strain Curves

"Due to technical error in the extensometer, few strain values were obtained by plotting Position Vs Strain graphs, and by calibrating it with the known values."
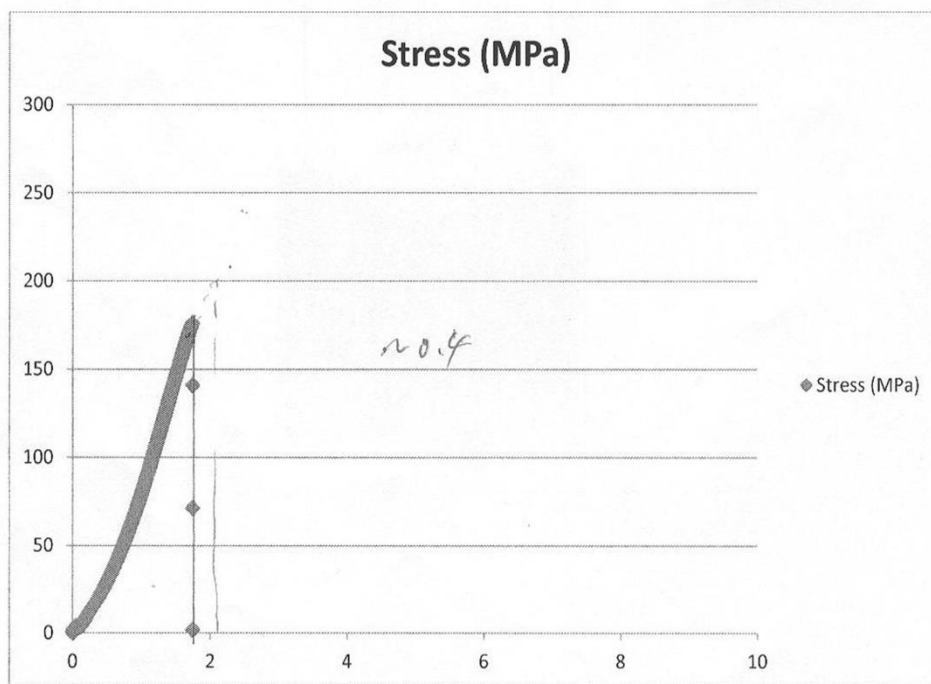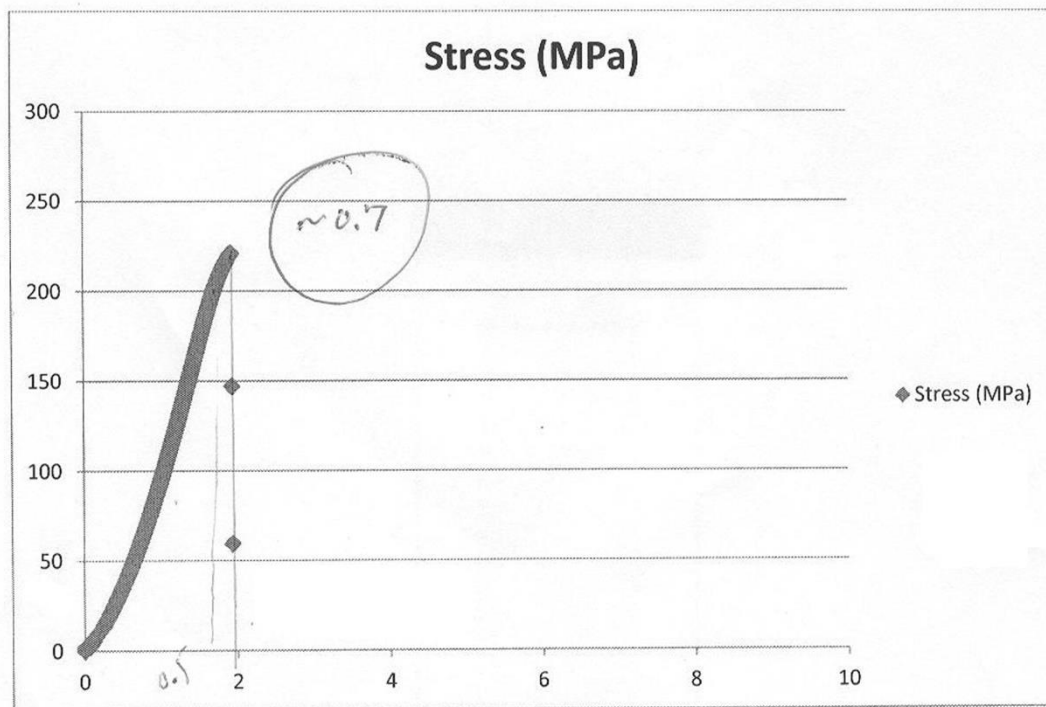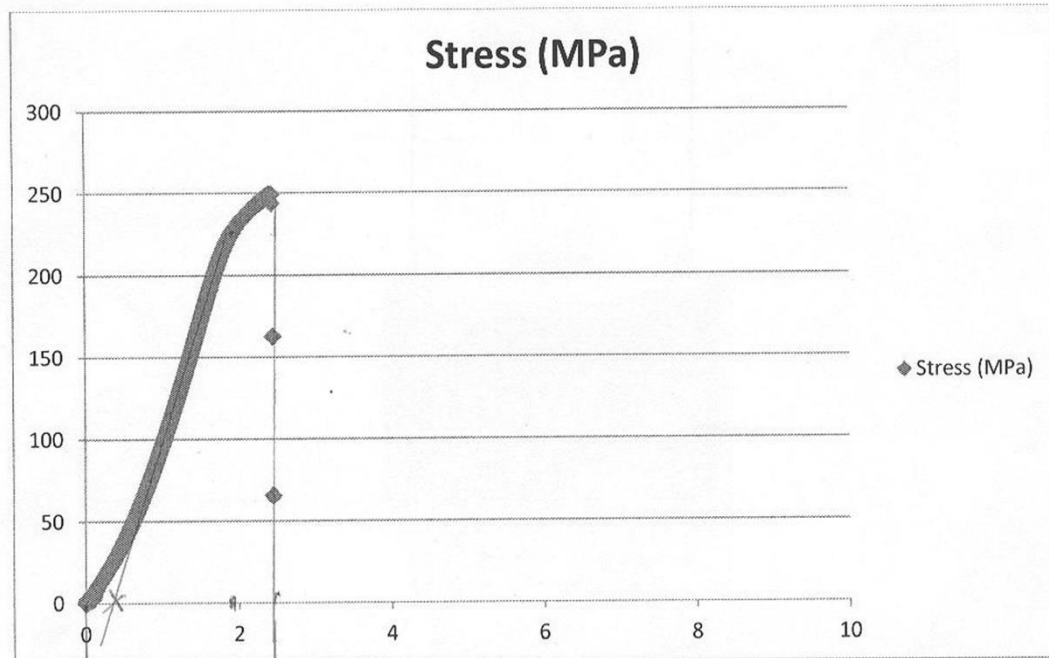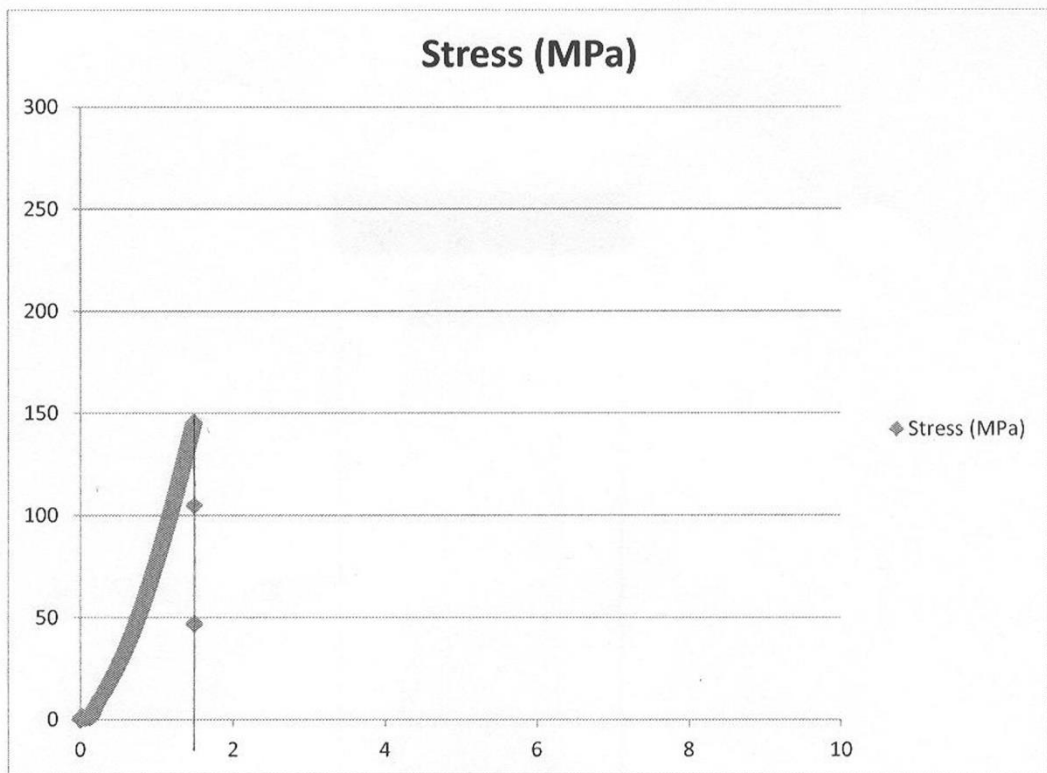

D3

D4

A4

B3

B2

D1

A3

B2